ABSTRACT

Title of Dissertation:	VIMENTIN AND CYTOKERATIN INTERMEDIATE FILAMENTS IN THE MECHANOBIOLOGY AND MALIGNANT BEHAVIORS OF CHORDOMA CELLS
	Lauren Resutek, Doctor of Philosophy, 2018
Dissertation directed by:	Associate Professor Dr. Adam H. Hsieh, Fischell Department of Bioengineering

Chordoma, an aggressive tumor derived from notochordal remnants, is difficult to treat due to its proximity to the spinal cord and brain stem and its resistance to conventional treatments, such as radiation and chemotherapy. The development of effective treatments requires research at the molecular level, which presumably due to its rare diagnosis, is lacking for chordoma. Recent studies have identified potential targets for systemic therapy; however, there are currently no drugs approved by the Food and Drug Administration (FDA) to treat chordoma. One promising approach is to target the cytoskeleton, in order to stall progression and sensitize cells to chemotherapeutics. Similar to other cancers, chordoma cells co-express vimentin and cytokeratin intermediate filaments (IFs), which have both been found to play roles in cell mechanical properties and behaviors and their expression has been associated with cancer metastasis, chemoresistance, and poor prognosis. Therefore, we investigated the

functional roles of vimentin and cytokeratin IFs in chordoma cells using RNA interference (RNAi).

First, we examined whether cytoskeletal disruption by siRNA-mediated silencing of vimentin or cytokeratin-8 altered the chordoma phenotype. We determined that the vacuolated cytoplasm, a distinguishing feature of chordoma, was dependent on cytokeratin-8 IFs. Next, we examined the effects of vimentin and cytokeratin-8 knockdown on chordoma cell mechanics. We found that chordoma cell stiffness, traction forces, and mechanosensitivity to substrate stiffness were all dependent on vimentin IFs. These results suggest that vimentin, rather than cytokeratin, IFs play a predominant role in chordoma cell mechanobiology. Finally, we analyzed the roles of vimentin and cytokeratin-8 IFs in cellular behaviors associated with cancer progression. We demonstrated that chordoma cell invasion and expression of the biomarker sonic hedgehog were dependent on vimentin. Further, we found that decreasing vimentin expression in chordoma cells may increase their sensitivity to chemotherapeutics. Because mechanical cues are important determinants of cell function, we hypothesize this correlation is in part due to the newly discovered role of vimentin IFs in chordoma cell mechanobiology. These results elucidate novel roles of vimentin and cytokeratin-8 IFs in chordoma cells, which may assist in the development of effective treatments for chordoma.

VIMENTIN AND CYTOKERATIN INTERMEDIATE FILAMENTS IN THE MECHANOBIOLOGY AND MALIGNANT BEHAVIORS OF CHORDOMA CELLS

By

Lauren Marie Resutek

Dissertation submitted to the Faculty of the Graduate School of the
University of Maryland, College Park, in partial fulfillment
of the requirements for the degree of
Doctor of Philosophy
2018

Advisory Committee:
Associate Professor Dr. Adam H. Hsieh, Chair
Professor Dr. William Bentley
Assistant Professor Dr. Giuliano Scarcelli
Assistant Professor Dr. Kimberly Stroka
Professor Dr. Wenxia Song, Dean's Representative

Acknowledgements

First, I would like to thank my advisor, Dr. Adam Hsieh, for welcoming me into his lab and for his guidance, encouragement, and support. I would also like to thank my committee members for their insight and helpful advice in the completion of this work.

Thank you to all of the members of the Orthopaedic Mechanobiology Laboratory that I had the pleasure of learning from and working with. I would especially like to thank Dr. Poonam Sharma, Dr. Carlos Luna, and Hyunchul Kim for their endless help and support. Thank you to the undergraduate researchers, Sara Kwon and Matthew Le, for their hard work and assistance in the lab. I would also like to acknowledge Christina Conrad, who completed the Brillouin microscopy analysis presented in this work. Thank you to Dr. John Fisher and his Tissue Engineering and Biomaterials Laboratory for welcoming me into their new lab space and all of their support during my last year at UMD. Finally, thank you to my family and friends for their continuous support and encouragement.

Table of Contents

List of Tables

List of Figures

List of Abbreviations

AFM- Atomic force microscopy

BME- Basement membrane extract

CMCF- Corrected mean cellular fluorescence

Col-PA- Polyacrylamide gel coated with collagen

CTCF- Corrected total cellular fluorescence

CTF- Collagen thin film

DMA- Dynamic mechanical analysis

dsRNA- Double stranded RNA

ECM- Extracellular matrix

EHS- Engelbreth-Holm-Swarm

EMT- Epithelial-to-mesenchymal transition

FBS- Fetal bovine serum

FDA- Food and Drug Administration

hMSC- Human mesenchymal stem cell

IF- Intermediate filament

IVD- Intervertebral disc

LAMP1- Lysosomal-associated membrane protein 1

Lam-PA- Polyacrylamide gel coated with laminin

LOX- Lysyl oxidase

NC- Notochordal cell

NGS- Normal goat serum

NP- Nucleus pulposus

PA- Polyacrylamide

PBS- Phosphate buffered saline

PET- Polyethylene Terephtalate

PFA- Paraformaldehyde

qRT-PCR- Quantitative reverse-transcriptase polymerase chain reaction

RFU- Relative fluorescence unit

RISC- RNA-inducing silencing complex

RNAi- RNA interference

RNase- Ribonuclease

shRNA- Short hairpin RNA

SHH- Sonic hedgehog

siKRT8- Cytokeratin-8 knockdown cells

siNEG- Cells transfected with negative control siRNA

siRNA- Small interfering RNA

siVIM- Vimentin knockdown cells

TCTP- Tissue-culture treated polystyrene

TEMED- N,N,N',N'-Tetramethylethylenediamine

Chapter 1: Introduction

Chordomas are rare, but aggressive, malignant bone tumors that arise from remnants of the embryonic notochord and occur along the length of the spine. Because chordomas are resistant to traditional radiation and chemotherapies, the prognosis of chordoma generally depends on the success of surgical resection. However, complete surgical resection is difficult to accomplish due to the proximity of chordomas to vital structures, such as the brain stem and spinal cord. As a result, chordomas are associated with high recurrence rates and the median survival time with chordoma is only approximately 6 years [1]. In order to develop effective treatments for patients living with chordoma, we need to improve our understanding of chordoma at the molecular level.

Many cellular behaviors associated with cancer progression, such as cell invasion, are dependent on the cytoskeleton. Therefore, the cytoskeleton may serve as a potential target to mitigate malignancy and metastasis. Cancer cells tend to co-express vimentin and cytokeratin IFs, indicating a hybrid phenotype that has partially gone through the epithelial-to-mesenchymal transition (EMT) or vice versa [2]. Individually, vimentin and cytokeratin IFs have been found to play roles in cell mechanical properties and processes. For instance, studies of other cell types have shown that both vimentin and cytokeratin IFs contribute to cell stiffness [3], [4], and play roles in cell traction forces [5], [6], response to mechanical stimuli [7], [8], and migration [9]–[12]. These cellular processes are also influenced by the mechanical properties of the

extracellular matrix (ECM). Consequently, the increased ECM stiffness characteristic of tumors is connected to a malignant cell phenotype [13], [14]. In addition to their involvement in cell mechanics, both vimentin and cytokeratin expression have been associated with cancer metastasis [15]–[19] and chemoresistance [11], [20]–[22], and their co-expression may indicate a more aggressive malignancy [23]. However, the functional roles of vimentin and cytokeratin IFs in chordoma cells have not yet been reported. **The overall goal of this dissertation was to examine the roles of vimentin and cytokeratin-8 IFs in the mechanobiology and malignant behaviors of chordoma cells using RNA interference (RNAi).**

To accomplish this, our first objective was to investigate whether knockdown of vimentin and cytokeratin-8 IFs altered the chordoma cell phenotype. We found that optimal knockdown, as measured by qRT-PCR, western blotting, and immunofluorescence, was achieved in human chordoma cells derived from the MUG-Chor1 cell line six days after transfection with siRNA. We discovered that the presence of characteristic cytosolic vacuoles, often used to differentiate chordoma from other cancers, was dependent on cytokeratin-8 IFs (Chapter 3). Insight into factors that function to maintain the chordoma cell phenotype is critical for assisting in the development of targeted therapies for chordoma.

Our second objective was to examine how vimentin and cytokeratin-8 knockdown, and resulting changes to the vacuolated cytoplasm, affect the biophysical interplay between chordoma cells and their surroundings. Specifically, we measured their roles in chordoma cell mechanics, traction forces, and mechanosensitivity to substrate stiffness. We show that vimentin, but not cytokeratin-8, IFs significantly

contribute to chordoma cell stiffness and are involved in generating cell traction forces and mechanosensing substrate stiffness (Chapter 4). Because abnormal changes in cell and tissue mechanics can lead to disease, determining the involvement of vimentin and cytokeratin IFs in chordoma cell mechanobiology may provide insight into chordoma progression.

We ultimately wanted to determine how these mechanical changes affect cellular processes and qualities associated with cancer progression. Therefore, our third and final objective was to examine the effects of vimentin and cytokeratin-8 knockdown on chordoma cell migration, invasion, gene expression, and resistance to chemotherapy drugs. We found that chordoma cell invasion and the expression of the cancer biomarker sonic hedgehog (SHH) were both dependent on vimentin expression (Chapter 5). Additionally, our results suggest that decreasing vimentin expression may increase the sensitivity of chordoma cells to the chemotherapy drugs cisplatin and paclitaxel (Chapter 5). Elucidating biological factors that encourage chordoma progression and chemoresistance is essential for the development of effective treatments.

These results identify, for the first time, functional roles of vimentin and cytokeratin-8 IFs in chordoma cells and indicate a potential association between vimentin expression and chordoma progression. Based on these results, vimentin may serve as a potential therapeutic target that could be used in combination with conventional chemotherapy to increase cell sensitivity and mitigate metastasis in residual cells. Future studies should further investigate the dependence of aggressive chordoma cell behaviors on vimentin expression.

Chapter 2: Background

2.1 Embryonic Notochord

The notochord, a midline structure which serves essential structural and signaling roles for embryonic development, is composed of large, vacuolated notochordal cells (NCs) that are surrounded by a basement membrane sheath [24]–[26] (Figure 2.1a, b, c). Radial constriction provided by the outer membrane sheath on osmotically swelling vacuoles of the inner cells is essential for embryonic axis elongation and spine morphogenesis [24], [26], [27]. Notochord development is also dependent on various molecules. The transcription factors brachyury (T), Sox-5, and Sox-6 are required for NC cell survival and differentiation [28], [29]. Additionally, the secreted factors SHH and noggin play critical roles in patterning of the axial cytoskeleton and neural tube [30], [31]. With embryonic development of the vertebral column, notochordal remnants become segmented between vertebral bodies and form the immature nucleus pulposus (NP) (Figure 2.1d) [32], [33]. Located at the center of the intervertebral disc (IVD), the immature NP is a proteoglycan-rich tissue that contains residual NCs.

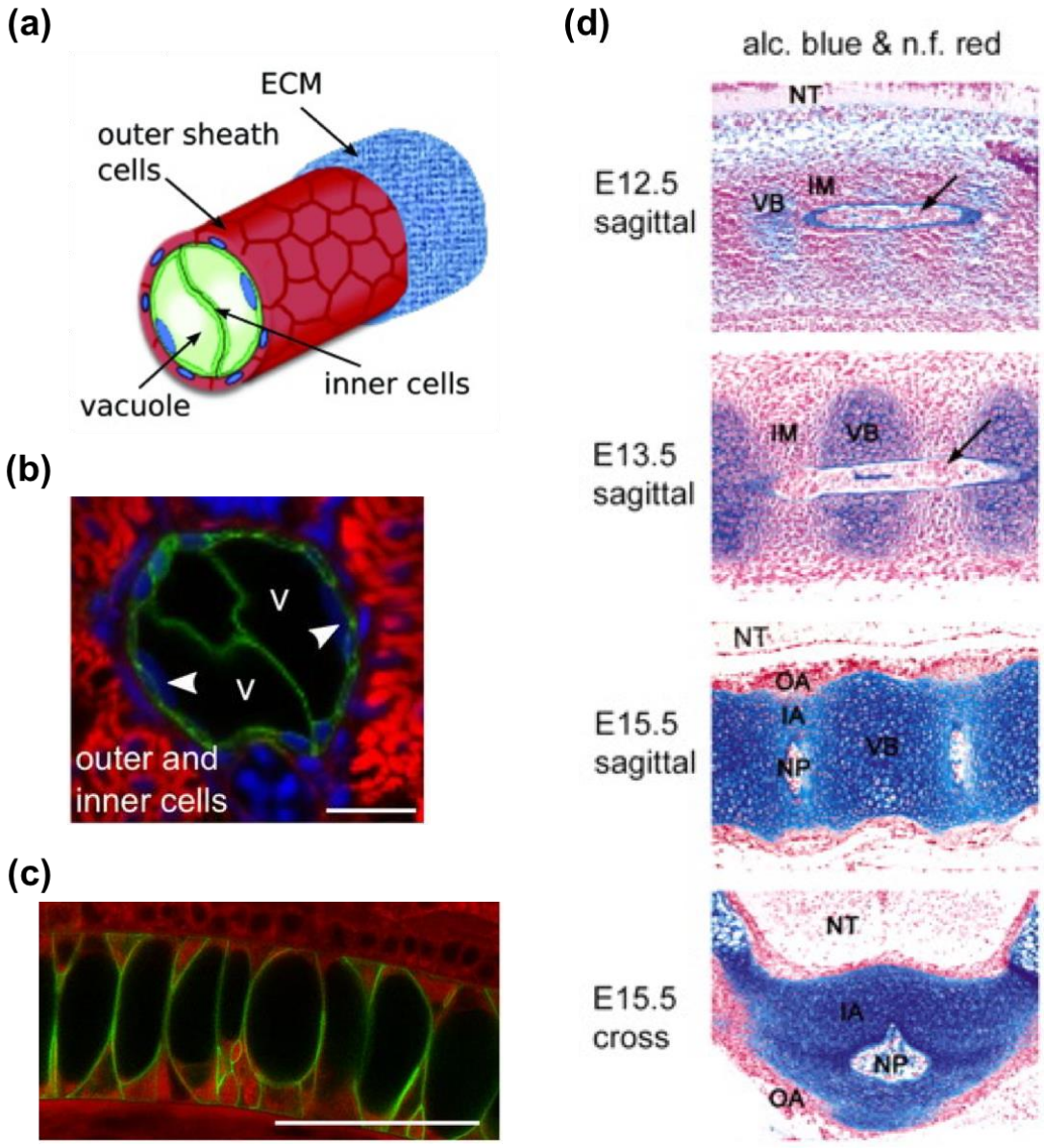

Figure 2.1: Anatomy and development of the embryonic notochord. (a) Schematic of the embryonic notochord illustrating the organization of large, vacuolated cells; (b) Confocal image of a cross section of a zebrafish embryo labeled with membrane GFP in the outer and inner cells of the notochord. Cross sections were stained with Phalloidin (red) and DAPI (blue). V, vacuole; arrowheads show inner cell nuclei. Scale bar: 20 µm; (c) Live confocal image of a transgenic membrane GFP (green) zebrafish embryo stained with MED (red) to visualize internal membranes. Scale bar: 50 µm; (d) Mid-sagittal sections made in the lumbar vertebral column of mouse embryos (E12.5-E15.5). Sections were stained with Alcian Blue and nuclear Fast Red to identify the neural tube (NT), notochord (arrows), intervertebral mesenchyme (IM),

inner annulus (IA), outer annuls (OA), nucleus pulposus (NP), and vertebral bodies (VB). (a, b, and c: Adapted from Ellis, K, 2013 [24]; d: Adapted from Smits, P, 2003 [29]).

2.2 Immature and Mature Nucleus Pulposus Cell Phenotypes

In some vertebrates such as pigs, rabbits, rats, mice, and non-chondrodystrophoid dogs, cells of presumed notochordal origin remain in the NP throughout life [33], [34]. However, as humans age, the majority of NCs give way to smaller, more chondrocyte-like, mature NP cells [35]–[37]. NCs are commonly distinguished from mature NP cells by their cytosolic vacuoles (Figure 2.2a, b), larger size (25-85μm compared to 17-23μm), and organization in isolated cell clusters (Figure 2.2c) [38]–[41]. In addition to their distinct morphology, NCs express phenotypic markers such as T brachyury, SHH, N-cadherin, and cytokeratin-8, -18, and -19 [42], [40], [43]–[47]. NCs are one of the unique cell types that co-express cytokeratin and vimentin IFs (Figure 2.2c) [44], [48]. In contrast, mature NP cells tend to express only vimentin IFs [44]. Because cells of the NP are responsible for the synthesis of a functional ECM, the cellular transition observed with aging is believed to be involved in the progression of disc degeneration [49], [50].

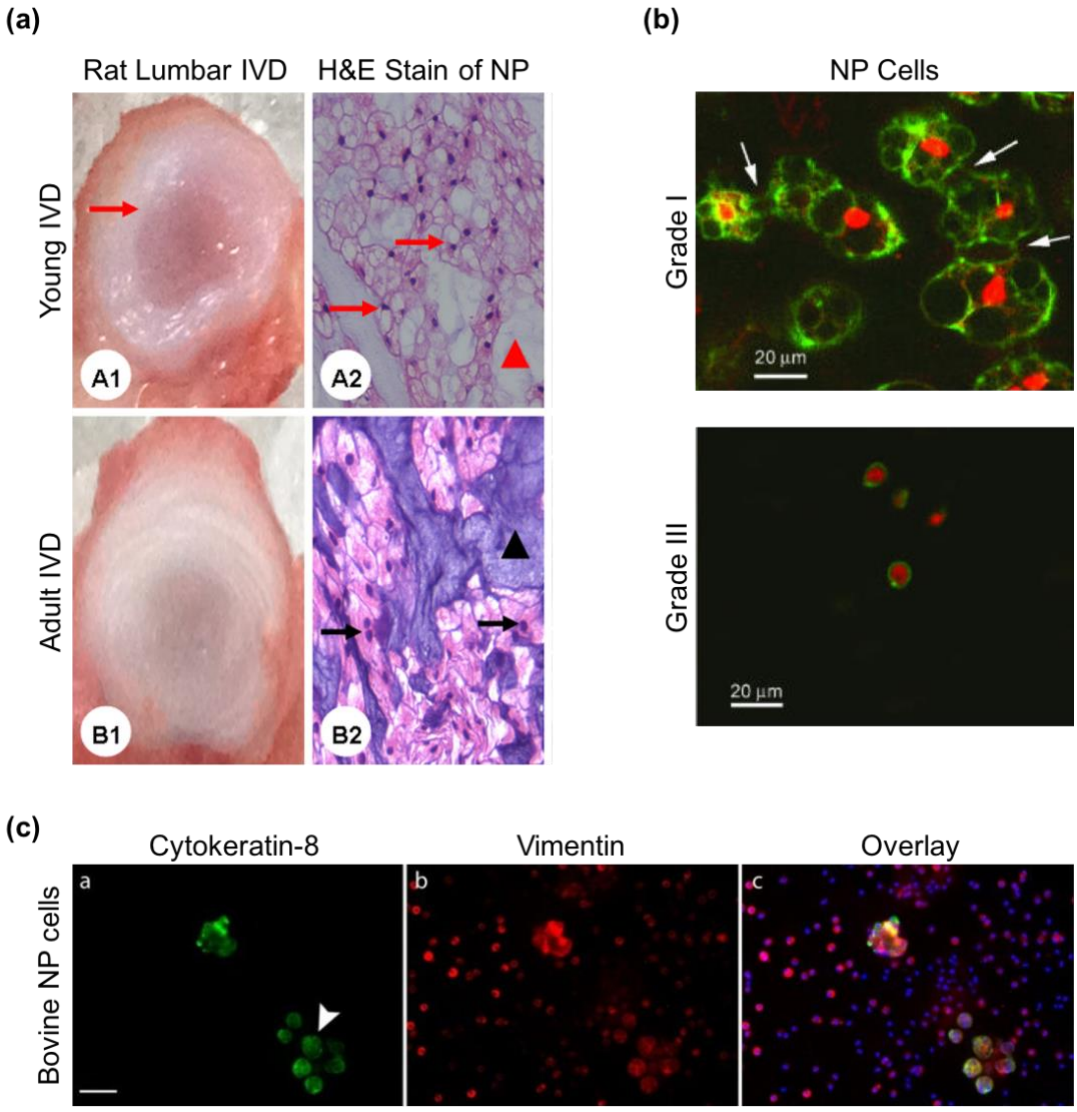

Figure 2.2: Age-associated changes of the NP. (a) Middle transverse sections of rat lumber IVDs at 6 (A1) and 20 (B1) weeks old. In the young IVD (A1), there is a distinct separation between the NP and the annulus fibrosis (AF) (red arrow). Hematoxylin-Eosin staining shows that the young NP contains predominantly vacuolated NCs (A2, red arrows) in an ECM rich in hyaluronic acids and proteoglycans (A2, red triangle); whereas the adult NP has a more cartilaginous matrix (B2, black triangle) and is sparsely populated with smaller, chondrocyte-like NP cells (B2, black arrows). (Adapted from Wang, F, 2016 [51]); (b) NP cells from grade I and III IVDs. Discs were graded based on the Thompson scale, where grade I NP were gelatinous with a clear annular-nuclear demarcation and grade III NP were more fibrous with unclear annular-nuclear demarcation. NP tissue was harvested from skeletally mature non-chondrodystrophoid dogs, embedded in alginate, and stained for actin (green) and nuclei (red).

Cells in grade I NP have large vacuoles, which were surrounded by F-actin. In contrast, cells in mature, grade III NP were small, dispersed, and non-vacuolated. (Adapted from Hunter, CJ, 2003 [40]); (c) Bovine (18– to 24-month-old) NP cells stained for cytokeratin-8 (green), vimentin (red), and nuclei (blue). Characteristic of NCs, some NP cells organized in clusters, as indicated by an arrowhead, and were also cytokeratin-8 positive. Scale bar: 60 μm. (Adapted from Gilson, A, 2010 [41]).

2.3 Chordoma

Chordomas are malignant bone tumors that occur along the spine and are most commonly found in the sacrococcygeal (pelvic) region and at the base of the skull [52], [53]. While rare, chordomas are often recurring and difficult to treat due to their growth near vital structures such as the spinal cord and brainstem [1], [54]. Chordomas are presumed to originate from remnants of the embryonic notochord due to their vacuolated cellular morphology and expression of genes specific to NCs [[52], [55], [56]]. For instance, the transcription factor T brachyury (T), a key regulator of notochord formation, is highly expressed in nearly every chordoma tumor [52], [55] and is critical for chordoma cell proliferation [57]. Additional notochordal markers expressed in the majority of chordomas include cytokeratin-8 (KRT8), cytokeratin-18 (KRT18), cytokeratin-19 (KRT19), vimentin (VIM), CD24 molecule (CD24), and sonic hedgehog (SHH) [52], [55], [58]–[61]. What causes notochordal remnants, which generally disappear in humans with age, to become malignant is unknown and is actively being researched.

Currently, only five chordoma cell lines have been approved by the Chordoma Foundation: U-CH1, U-CH2, MUG-Chor1, JHC7, and UM-Chor1 [55]. Similar to primary chordomas, these cell lines have been shown to express characteristic

notochordal genes [58], [62]–[64]. MUG-Chor1, the cell line we use in our studies, was derived from a sacral chordoma in a 57-year old female. MUG-Chor1 cells resemble NCs both morphologically and phenotypically, having a vacuolated cytoplasm and expressing T brachyury, cytokeratin, and vimentin proteins (Figure 2.3) [63]. Their notochordal phenotype and ability to be maintained in long-term cultures makes them an ideal NC source for *in vitro* assays.

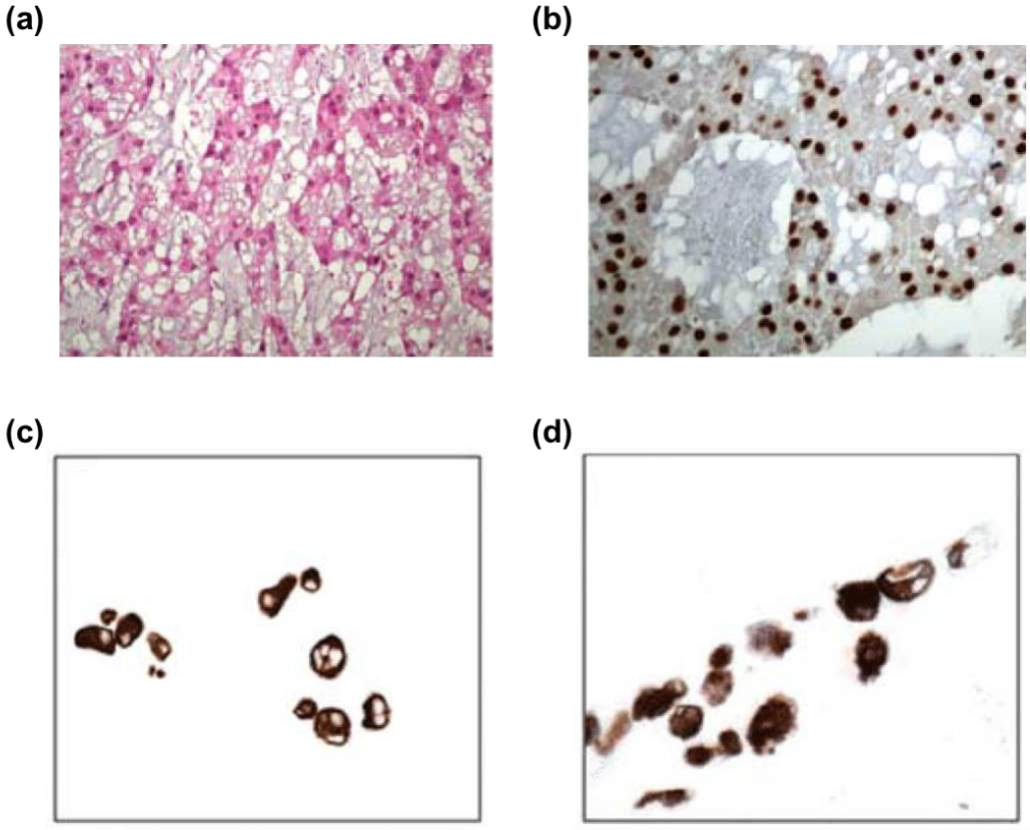

Figure 2.3: Characterization of the MUG-Chor1 cell line. (a) Histology of the primary tumor used to establish the MUG-Chor1 chordoma cell line reveals vacuolated tumor cells; (b) Immunohistochemistry (IHC) of the primary MUG-Chor1 tumor shows positive brachyury expression; IHC of MUG-Chor1 cells in culture shows positive (c) cytokeratin and (d) vimentin expression. (Adapted from Rinner, B, 2012 [63]).

2.4 Treatment of Chordoma

The primary treatment option for patients living with chordoma is surgery. The goal of surgery is to obtain wide margins with a complete en bloc tumor resection, as intralesional resection is associated with an increased rate of recurrence [65]. However, achieving wide margins is not always possible due to chordomas proximity to vital structures and often times can lead to nerve sacrifice and motor dysfunction. If patients are not a candidate for surgery or if a complete resection was not achieved, radiation therapy is often administered. Because chordomas are resistant to radiation, large doses are required for treatment. To prevent damage to the surrounding tissue, conformal radiotherapy, such as proton beam therapy or radiosurgery, must be utilized. Radiation, especially near the skull and spine, is associated with numerous side effects and risks such as paralysis. Chordomas are also resistant to standard cytotoxic chemotherapy drugs such as cisplatin, doxorubicin, and paclitaxel [66]–[68]. While these cytotoxic drugs may be used to slow chordoma growth, they are ultimately an ineffective form of treatment. Due to the complications presented with treating chordoma, targeted therapies and immunotherapies are actively being researched. No drugs are currently approved by the FDA to treat chordoma; however, multiple clinical trials are open for various systemic therapies, including an anti-brachyury vaccine [69].

2.5 Vacuoles of Notochordal and Chordoma Cells

While cytosolic vacuoles are a defining feature of NCs and chordoma cells, their contents and function have not been conclusively determined. In developing Xenopus and zebrafish embryos, notochord vacuoles have been found to play an

essential role in embryonic axis elongation and spine morphogenesis [24], [27], [70]. The mechanical contribution of vacuoles to embryonic development is presumed to occur through the generation of turgor pressure, resulting in stiffening of the notochord. Recently, notochordal vacuoles have been suggested to be lysosome-related organelles, following the discovery of lysosomal-associated membrane protein 1 (LAMP1) on the vacuolar membrane of zebrafish NCs [24]. Although vacuoles of NCs are essential for embryonic development, the significance of cells maintaining vacuoles in the developed IVDs and in chordomas is unclear. Only one study was found to explore vacuolar function in mature NCs, which proposes vacuoles function as osmoresponsive organelles containing a low osmolality solution that can be used to regulate cell volume under hypotonic stress [71].

2.6 Vimentin and Cytokeratin Intermediate Filaments

IFs are an essential component of the cytoskeleton. The molecular building blocks of IFs are alpha-helical proteins, which form coiled-coil dimers. Dimers then stagger together to form tetramers, and groups of tetramers form unit-length filaments that join to form mature, ~10 nm wide IFs (Figure 2.4). In contrast to the consistent composition and expression of the other principal elements of the cytoskeleton, microtubules and actin microfilaments, many different types of IF proteins have been identified and their expression is typically cell-type specific. The different types of IF proteins have been categorized into six groups based off of their amino acid sequences. Types I and II are acidic and basic/ neutral cytokeratins, respectively. Acidic (cytokeratins 9-20) and basic (cytokeratins 1-8) cytokeratin proteins bind to form

heterodimers, the basic building blocks of cytokeratin IFs, which are characteristically expressed in epithelial cells. Type III IF proteins include vimentin, and unlike cytokeratin IFs, vimentin IFs are composed of vimentin monomers. Vimentin IFs are characteristically expressed in mesenchymal cells. Types IV, V, and VI include neurofilament proteins, nuclear lamins, and nestin. This study focuses specifically on cytokeratin and vimentin IFs, which are co-expressed in NCs and chordoma cells. The most commonly expressed cytokeratin proteins in NCs and chordoma cells are those of the simple epithelium: cytokeratins 8, 18, and 19 [48], [72], [73]. Cytokeratins 8 and 18 typically dimerize together, while cytokeratin-19 is unique in that it generally is not paired with a basic cytokeratin.

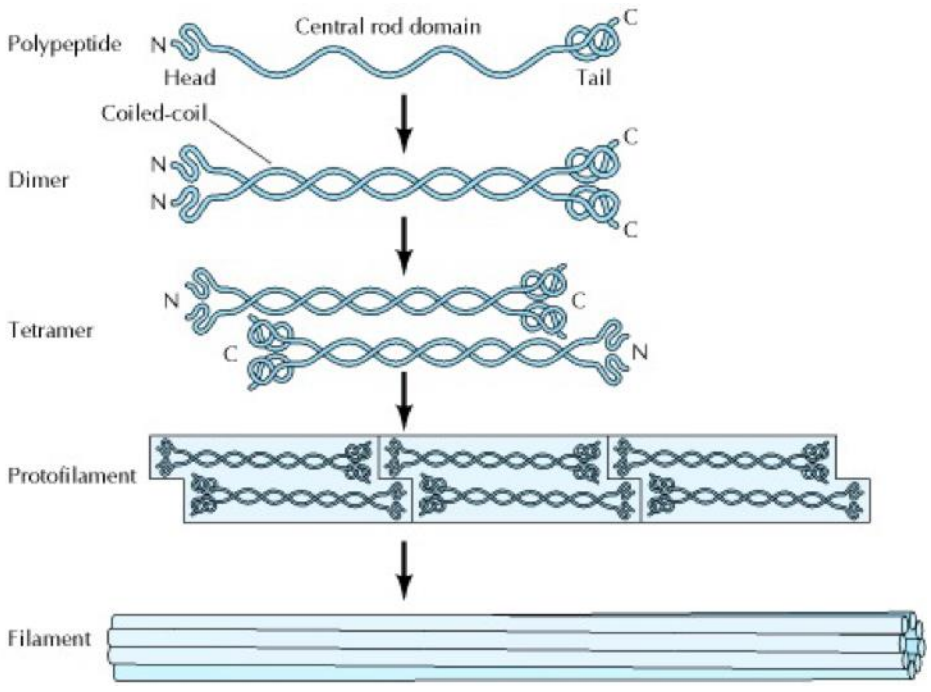

Figure 2.4: Assembly of intermediate filaments. (Figure 11.32 from Cooper, GM, 2000 [74]).

Until recently, the mechanical function of IFs has received little attention compared to actin microfilaments and microtubules, which have established roles in processes such as cell adhesion, migration, mechanotransduction, division, and (mediated by their specific motor proteins) intracellular organelle and protein transport [75]. The majority of functions associated with vimentin and cytokeratin IFs have been elucidated via genetic mutations of genes encoding cytokeratin and/or vimentin proteins, ultimately disrupting the IF network. Both cytokeratin and vimentin IFs have been found to contribute to cell stiffness, maintenance of cell structural integrity, and resistance to mechanical stress [3], [4], [8], [76]–[80]. For example, vimentin deficient fibroblasts were found to be significantly less stiff compared to wild-type cells and mutations in cytokeratins of keratinocytes resulted in reduced cell stiffness and increased (60%) cell deformability [3], [4], [78].

Vimentin and cytokeratin IFs have also been found to be involved in cell mechanotransduction [7], [8], [81], [82] and migration [10], [12], [83], [84]. In support of mechanosensing roles, decreasing vimentin and cytokeratin expression have both been observed to cause substrate stiffness dependent changes in cell spreading [7, p. 18], [8]. Additionally, the decoupling of vimentin and focal adhesions in fibroblasts resulted in decreased activation of the major mechanosensor molecule FAK [81]. For cell migration, a more established role has been identified for vimentin, rather than cytokeratin, IFs. The expression of vimentin IFs is often associated with increased cell migration and invasion [10], [12], [85], while the involvement of cytokeratin IFs in cell motility is controversial [11], [84].

2.7 Methods for Studying Cellular Functions of Intermediate Filaments

Following their discovery, IF networks were initially presumed to be static and to primarily play a structural role [86]. However, IFs have since been identified as highly dynamic structures involved in cell migration and signaling pathways and mutations in IF proteins have been associated with various diseases [86]. Consequently, various methods have been established and optimized for further investigating the functional roles of IFs. Techniques typically rely on disruption of the IF network or silencing of genes encoding IF proteins. Microinjection of mimetic peptides, transfection of dominant-negative mutants, and treatment of cells with agents such as withaferin-A and acrylamide have all been used for dissembling and disrupting the organization of IF networks [87]–[89]. To eliminate off-target effects and more specifically analyze IF functions, strategies that knockdown or knockout IF protein expression are often employed. For instance, RNAi using small-interfering RNA (siRNA) or short hairpin RNA (shRNA) has shown success in decreasing both vimentin and cytokeratin protein expression in mammalian cells [11], [90]. Through RNAi, the roles of vimentin and cytokeratin IFs in process associated with cancer progression such as integrin signaling, cell migration, and cell invasion have been examined [9], [12]. Primary cells isolated from knockout mice, which do not express the IF protein of interest, are also commonly used for the analysis of IFs [78], [91].

2.8 RNA Interference with siRNA

RNAi is a commonly used technique for inhibiting gene expression. Endogenously, RNAi is used to protect against viral infections and the insertion of

foreign nucleic acids into the genome. The mechanism is initiated when long double stranded RNA (dsRNA) is detected within the cell and cleaved by a ribonuclease (RNase) III enzyme called Dicer [92]. This produces siRNAs that are generally 21-23-nucleotide (nt) duplexes with symmetric 2-3-nt 3' overhangs [93] (Figure 2.5a). The siRNAs are incorporated into a multiprotein RNA-inducing silencing complex (RISC) and subsequently unwound. The now revealed anti-sense strand of the siRNA guides the RISC to the complementary mRNA sequence resulting in endonucleolytic cleavage of the mRNA (Figure 2.5b). Following the discovery of RNAi in mammalian cells, this technique has been adopted and well established for regulating gene expression *in vitro* and RNAi-based therapeutics are actively being studied in clinical trials [94], [95]. In fact, the first ever siRNA-based drug (Onpattro) was just recently approved by the FDA for the treatment of peripheral nerve disease (polyneuropathy) caused by hereditary transthyretin-mediated amyloidosis (hATTR) in adult patients. Because the introduction of long dsRNA into mammalian cells induces an adverse anti-viral response, RNAi is commonly initiated by directly introducing chemically synthesized siRNA.

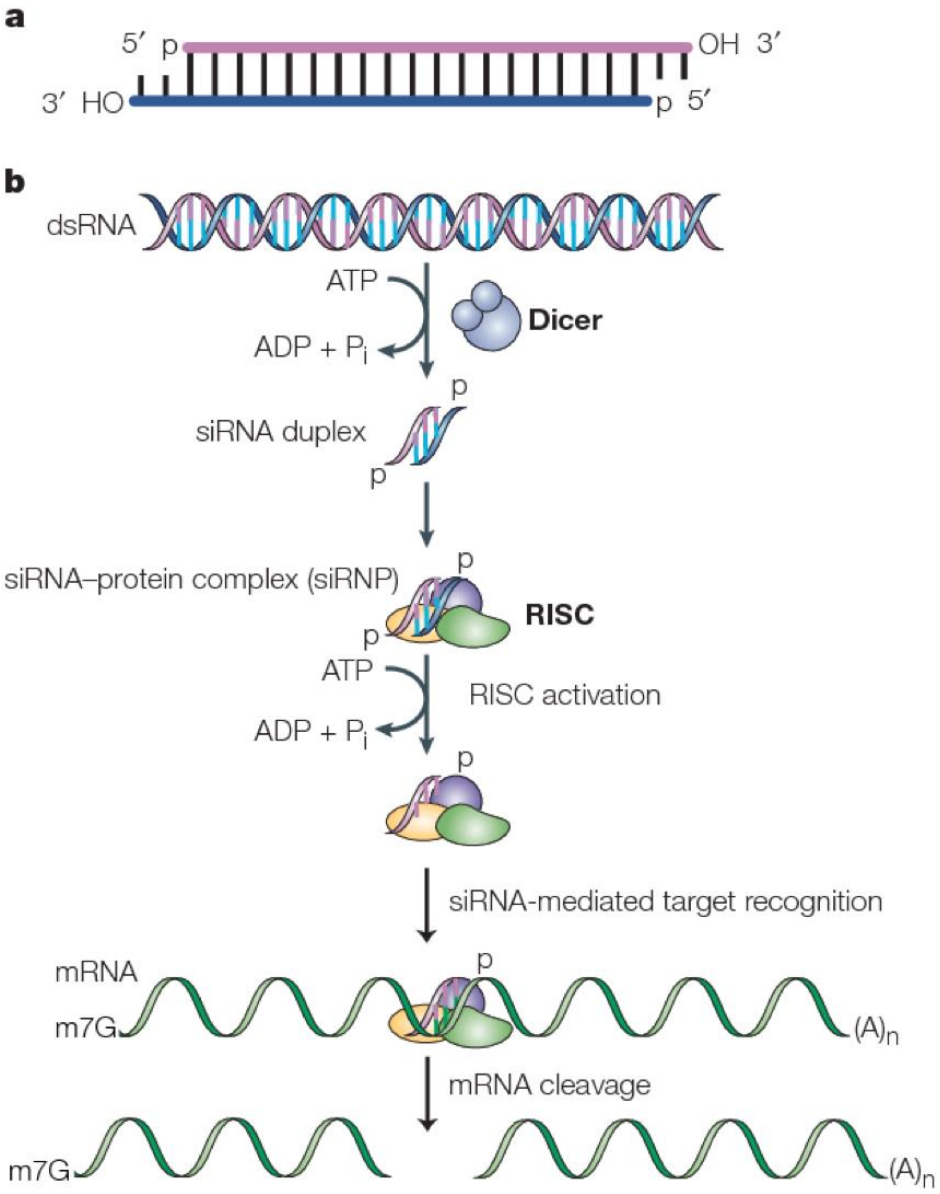

Figure 2.5: Short interfering (si)RNA structure and the RNAi pathway. (a) siRNAs are 21-23-nt duplexes with 5' phosphorylated ends and 2-3-nt 3' overhangs; (b) Schematic of the RNAi pathway. siRNAs are produced through cleavage of long dsRNA and incorporated into a RISC. Once unwound, the anti-sense strand of the siRNA guides RISC to complementary mRNA for subsequent cleavage. (Adapted from Dykxhoorn, DM, 2003 [93]).

2.9 Co-expression of Vimentin and Cytokeratin

Vimentin and cytokeratin co-expression is commonly found in cells with an epithelial origin and a mesenchymal differentiation or vice versa, cancer cells, and cells of developing tissues [17], [48], [96]–[98]. Both NCs of the developing notochord and chordoma cells are consistent with these classifications. The co-expression of vimentin and cytokeratin is also common in cells that are exposed to a fluid/semi-fluid environment with low protein content [48], [99]. These conditions are true of the immature NP, where healthy tissue has a high (~80%) water content [100], [101]. While common environmental and cellular conditions have been identified, the functional significance for cells to co-express vimentin and cytokeratin IFs is not understood. In certain cancers, the co-expression of vimentin and cytokeratin IFs may encourage a more invasive and metastatic cell phenotype [9], [16], [17]. However, the contribution of cytokeratin IFs to the migration of cells co-expressing cytokeratin and vimentin appears to be cell-type specific, as conflicting findings have been reported following the manipulation of cytokeratin expression [9], [11], [84], [102].

2.10 Intermediate Filaments and Cancer

Cancer cells commonly co-express vimentin and cytokeratin IFs, suggesting a dedifferentiated phenotype, which is thought to promote cell invasion and cancer metastasis [17]. The epithelial-mesenchymal transition, characterized by increased vimentin expression, is typically associated with increased metastasis and a poor prognosis. In both cancerous and non-cancerous cells, knockdown of vimentin expression has been shown to reduce cell migration and invasion [10], [12], [85], [103].

Similarly, the overexpression of vimentin has been linked to tumor metastasis in a variety of cancers including melanoma [15], breast cancer [17], prostate carcinoma [19], and hepatocellular carcinoma [18]. Because of the positive correlation between vimentin expression and metastasis, it is unsurprising that vimentin is associated with a poor prognosis. For instance, vimentin-positive basal-like breast cancer samples were significantly associated with poorer recurrence-free survival or overall survival [104].

In contrast to the consistent evidence supporting the role of vimentin in cancer cell migration and its association with a poor cancer prognosis, contradicting results have been reported for the role of cytokeratin IFs in cancer. In non-small cell lung cancer and oral squamous cell carcinoma, knockdown of cytokeratins 8 and 18 decreased cell migration and invasion [9], [84]. The overexpression of cytokeratins 8 and 18 has also been associated with increased migration in melanoma cells [16]. On the other hand, increased expression of cytokeratin 18 reduced cell invasion in breast cancer cells [102] and decreased expression of cytokeratins 8 and 18 increased cell migration and invasion in liver hepatocellular carcinoma cells [83]. The effects of altering cytokeratin expression on cell migration may be attributed to resulting changes in vimentin expression [102]. It is also possible that cytokeratin IFs play a direct role in cell migration, as vimentin expression was unaffected in non-small cell lung cancer cells shown to have decreased cell migration following cytokeratin 18 knockdown [84].

The relationship between cytokeratin expression and cancer prognosis also appears to be cancer-type specific. High cytokeratin 18 expression has been correlated with advanced stages of cancer and poor prognosis in non-small cell lung cancer, oesophageal squamous cell carcinoma, renal cell carcinoma, and oral cavity carcinoma

[84], [105]–[107]. The opposite trend was observed in breast and colorectal cancers, where low cytokeratin 8 and 18 expression has been associated with a poor prognosis [108], [109].

Interestingly, IFs have also been suggested to be involved in cell sensitivity to cytotoxic chemotherapy agents. EMT suppression, associated with decreased vimentin expression, has been found to increase the sensitivity of non-small cell lung cancer and gastric cancer cells to cisplatin [20, p. 30], [22], a cytotoxic agent that initiates apoptosis through its binding with DNA. Knockdown of cytokeratins 8 and 18 has produced similar results, increasing the sensitivity of epithelial cancer and nasopharyngeal carcinoma cells to cisplatin [21], [83] and non-small cell lung cancer cells to paclitaxel [84], a cytotoxic drug that stabilizes microtubules, thereby inhibiting cell division. The mechanism in which disrupting IFs sensitizes cells to cytotoxic chemotherapeutics is currently unknown.

2.11 Biomechanics of Cancer

Abnormal changes in the mechanical properties of tissues are associated with diseases such as cancer. For example, tumors tend to be stiffer than healthy tissue and tissue stiffness is often exploited for cancer screening. For breast cancer, the tumor tissue can be ten times stiffer than normal tissue [110]. Increased tissue stiffness can partly be attributed to lysyl oxidase (LOX) overexpression, which promotes cross linking of ECM components such as collagen [111]. Further, data suggests that overexpression of LOX and subsequent ECM stiffening regulates angiogenesis, a key process in cancer progression [112]. Through integrin-mediated cell adhesions and the

exertion of traction forces, cells are able to sense the mechanical properties of the ECM. As a result, cell behaviors, such as proliferation and migration, are affected by changes to the ECM. For instance, increased ECM stiffness can stimulate integrin signaling and as a result promote cell survival and proliferation [14], [113]. The relationship between ECM rigidity and cancer behavior at the molecular level is unclear; however, studies have shown that increased ECM stiffness is capable of promoting a malignant cell phenotype with increased chemoresistance [13], [14]. Mechanical cues have also shown promise as cancer biomarkers, as cell deformability and traction forces are found to increase in cancer cells [114]–[118].

Chapter 3*: The Roles of Vimentin and Cytokeratin-8 Intermediate Filaments in Maintaining the Chordoma Cell Phenotype

3.1 Introduction

The embryonic notochord consists of highly vacuolated cells surrounded by a basement membrane sheath [24]–[27]. Radial constriction provided by the outer membrane sheath on osmotically swelling vacuoles of the inner cells is essential for driving elongation of the embryo [24], [26], [27]. With development of the vertebral column, notochordal remnants become segmented between vertebral bodies forming the immature NP [32], [33]. In some vertebrates such as pigs, rabbits, rats, and mice cells of presumed notochordal origin (NCs) remain in the NP throughout life [33], [34]. However, as humans age the majority of NCs give way to smaller, more chondrocyte-like, mature NP cells [35]–[37]. This cellular transition coincides with changes in the ECM such as decreases in water and proteoglycan content [44], [119], [100], [120], impairing NP function and increasing the risk of disc degeneration [121], [122].

In certain cases, notochordal remnants may develop into a tumor called chordoma. Because of their proximity to the brain stem and spinal cord, chordomas are difficult to remove surgically and treatment with high doses of radiation therapy is not always possible. Additionally, chordomas are resistant to conventional cytotoxic chemotherapy drugs. Consequently, chordomas are often associated with high

* This chapter was adapted from Resutek, L and Hsieh AH. The vacuolated morphology of chordoma cells is dependent on cytokeratin intermediate filaments. *J Cell Physiol*. 2018;1-11.

recurrence rates and a poor prognosis. An improved understanding of the NC cell phenotype is essential for the development of treatments for both disc degeneration and chordoma.

NCs and chordoma cells are characterized by their large size, expression of phenotypic genes, organization in dense cell clusters, and unique cytosolic vacuoles. In Xenopus and zebrafish embryos, notochord vacuoles have been found to be essential for elongation and morphogenesis of the developing spine [24], [27], [70]. Although vacuoles of embryonic NCs are essential for development, the significance of cells maintaining vacuoles in the developed IVD and in chordomas is unclear, but has remained an area of particular interest [123]. Genes often used to identify NCs and chordoma cells include brachyury (T), SHH, N-cadherin, and cytokeratin-8, -18, and -19 [42], [40], [43]–[47]. Brachyury and SHH play key roles in embryonic development, but in developed tissues their overexpression has been associated with tumor formation and progression [124], [125]. Increased expression of brachyury, SHH, and N-cadherin have all been connected to EMT, characterized by increased vimentin expression [125]–[130]. Therefore, the expression of these phenotypic genes may be dependent on IF protein expression.

Similar to other cells of developing tissues and cancer cells, NCs and chordoma cells co-express cytokeratin and vimentin IFs [44], [48]. In contrast, mature NP cells tend to express only vimentin IFs [44]. Vimentin IFs are composed of vimentin monomers and cytokeratin IFs are composed of acidic, type I cytokeratins (9-20) and basic type II cytokeratins (1-8) heterodimers. Focusing on cytokeratins specific to NCs, cytokeratins-8 and -18 typically dimerize together, while cytokeratin-19 has been

suggested to be capable of substituting for cytokeratin-18 [131]. Individually, vimentin and cytokeratin IFs have been shown to be involved in cell stiffness [3], [4], [8], [78], adhesions [103], [132], [133], and response to mechanical stimuli [7], [81]. They have also been associated with the stabilization and transport of vacuoles, vesicles, and granules [134]–[137]. In NCs, IFs were observed to surround vacuoles, suggesting a structurally supportive role [25]. However, the involvement of vimentin and cytokeratin IFs in NC vacuolation, either individually or in tandem, is unknown.

Due to the concomitant loss of cytokeratin expression and vacuoles in mature NP cells, we sought to investigate the potential relationship between cytokeratin IFs, specifically those containing cytokeratin-8 proteins, and the vacuoles of NCs. Using a human chordoma cell line (MUG-Chor1), we examined the organization of the cytoskeleton in relation to vacuoles and the effect of chemically disrupting IFs, F-actin, and microtubules on the cytosolic vacuoles. We then focused on cytokeratin-8 and vimentin IFs and their individual roles in the existence of vacuoles, utilizing siRNA-mediated RNAi for the knockdown of cytokeratin-8 and vimentin expression. We found that both chemical disruption of IF networks and knockdown of cytokeratin-8 expression were associated with dramatic reduction of cellular vacuolation. Decreased cytokeratin-8 and vimentin expression, in addition to subsequent changes in vacuolation, did not affect gene expression or cell clustering.

3.2 Materials and Methods

3.2.1 Cell Culture

MUG-Chor1 chordoma cells were obtained from ATCC® (ATCC Cat# CRL-3219, RRID:CVCL_9277) and cultured in Iscove's Modified Dulbecco's Medium: Roswell Park Memorial Institute 1640 Medium (4:1) (Gibco/Thermo Fisher Scientific, Waltham, MA, USA) supplemented with 10% fetal bovine serum (FBS) (Gibco/Thermo Fisher) and 1% Penicillin-Streptomycin (Gibco/Thermo Fisher). Cells were expanded on tissue culture-treated polystyrene (TCTP) and plated on adsorbed (50 μg/ml) rat tail type I collagen (Advanced BioMatrix, Carlsbad, CA, USA), as recommended by ATCC®, for all subsequent experiments. Complete media exchange was completed every 2-3 days and cells were cultured at 37°C, 5% CO_2.

3.2.2 Cytoskeletal Disruption

Cells cultured on collagen-coated glass were treated with chordoma media containing 1 μM cytochalasin-D [138] (Sigma-Aldrich, St. Louis, MO, USA), 5 μM nocodazole [139] (Sigma-Aldrich), or 40 mM acrylamide [140], [141] (Thermo Fisher) to disrupt F-actin, microtubules, or IFs, respectively. Cells were incubated with cytochalasin-D and nocodazole for 1h and acrylamide for 3.5h at 37°C, 5% CO_2. Disruption of targeted cytoskeletal elements was visualized with immunostaining and confocal microscopy. Cells were stained with calcein AM (Invitrogen/Thermo Fisher) and ethidium homodimer-1 (Invitrogen/Thermo Fisher) for live/dead cell imaging.

3.2.3 Transfection of siRNA

For all transfections, chordoma cells were plated on adsorbed type I collagen in 6-well plates at a density of 10,000 cells/ cm^2. Twenty-four hours after plating, cells were transfected with Silencer Select Pre-designed siRNA (Ambion/Thermo Fisher) targeting either KRT8 (s7970), VIM (s14798), or Silencer Select Negative Control No. 1 siRNA (Ambion/Thermo Fisher) using Lipofectamine 2000 (Invitrogen/Thermo Fisher). Cells were incubated with siRNA-lipofectamine complexes (300pmol siRNA: 12.5ul Lipofectamine per well) for 24h. Six days after transfection, cells were processed for analysis of vacuoles, cell clustering, cytoskeletal organization, gene expression, or protein content. Due to changes in cell behavior as a result of transfection, non-transfected chordoma cells were excluded from analyses.

3.2.4 Immunostaining and Fluorescence Microscopy

To observe cytoskeletal proteins, cells were fixed with 4% paraformaldehyde (PFA) and permeabilized using 0.1% Triton X-100. Cells were labelled with rabbit IgG anti-β-tubulin polyclonal (Abcam, Cat# ab15568, RRID:AB_2210952), rabbit IgG anti-vimentin [SP20] (Thermo Fisher Scientific, Cat# MA5-16409 , AB_2537928), or mouse IgG1 anti-cytokeratin-8 [M20] (Abcam, Cat# ab9023 RRID:AB_306948) antibodies. A biotinylated (anti-rabbit IgG) secondary antibody (Vector Laboratories, Cat# BA-1000, RRID:AB_2313606) was used in combination with Fluorescein- or Texas Red-labelled streptavidin (Vector Laboratories) to visualize β-tubulin and vimentin. An Alexa Fluor 594-conjugated (anti-mouse IgG) secondary antibody (Thermo Fisher Scientific, Cat# A-11032, RRID:AB_2534091) was used to visualize

cytokeratin-8. Cells were stained with Alexa Fluor 594 Phalloidin (Invitrogen/Thermo Fisher Scientific) to visualize F-actin, and DAPI (Invitrogen/Thermo Fisher Scientific) was used as a nuclear counterstain. All images were captured with a Nipkow (spinning) disk-equipped Olympus IX81 microscope. Confocal fluorescence Z-stacks (1 μm slices) were taken with the spinning disk and projected into single images.

3.2.5 Gene Expression

RNA isolation was performed using phenol-chloroform extraction. Cell monolayers were lysed with TRIzol (Ambion/Thermo Fisher Scientific) and RNA was separated and precipitated from the resulting lysate using chloroform and isopropanol. RNA samples were reverse transcribed, and underwent qRT-PCR (MyiQ System, BioRad) using SsoFast EvaGreen Supermix (BioRad, Hercules, CA, USA) to quantify expression of VIM, KRT8, T, SHH, CDH2, and 18S (Table 3.1). Relative quantitation of qRT-PCR data was performed using the $\Delta\Delta C_t$ method with 18S as a housekeeping gene. Briefly, ΔC_t values were computed by subtracting C_t values of the 18S control gene from those of each gene of interest (i.e., $\Delta C_{t\,SHH} = C_{t\,SHH} - C_{t\,18S}$). For each gene of interest, $\Delta\Delta C_t$ values were computed by subtracting ΔC_t values of the reference sample (e.g. cells transfected with negative control siRNA), from ΔC_t values of cells transfected with siRNA targeting either VIM or KRT8 ($\Delta\Delta C_{t\,SHH;VIM\,siRNA} = \Delta C_{t\,SHH;VIM\,siRNA} - \Delta C_{t\,SHH;NC\,siRNA}$). Using $\Delta\Delta C_t$ values, relative changes in mRNA levels (fold difference) were expressed through the exponential relation: $2^{-\Delta\Delta Ct}$. Technical replicates for each sample, along with appropriate no RT and no template controls, were performed in triplicate. Data collected over three independent cell transfections (n=3) for each of the siRNA groups are reported as the average of the

range of the fold difference, which incorporates the standard deviation of the $\Delta\Delta C_t$ value [142], [143].

Gene	**Forward and reverse sequence**	**GenBank accession no.**
Human RNA18S5	5'-AAACGGCTACCACATCCAAG-3' 5'-CCTCCAATGGATCCTCGTTA-3'	NR_146119
Human VIM	5'-CACGAAGAGGAAATCCGGAGC-3' 5'-CAGGGCGTCATTGTTCCG-3'	NM_003380
Human KRT8	5'-ACCCAGGAGAAGGAGCAGAT-3' 5'-CCGCCTAAGGTTGTTGATGT-3	NM_001256282
Human T (brachyury)	5'-TATGAGCCTCGAATCCACATAGT-3' 5'-CCTCGTTCTGATAAGCAGTCAC-3'	NM_001270484
Human SHH	5'-CTCGCTGCTGGTATGCTCG-3' 5'-ATCGCTCGGAGTTTCTGGAGA-3'	NM_000193
Human CDH2	5'-TCAGGCGTCTGTAGAGGCTT-3' 5'-ATGCACATCCTTCGATAAGACTG-3'	NM_001792

Table 3.1: Sequences of primers used for qRT-PCR

3.2.6 Western Blotting

For protein extraction, cells were detached from culture surfaces using 0.25% trypsin-EDTA (Gibco/Thermo Fisher) and re-suspended in a lysis buffer (50 mM HEPES, 150 mM sodium chloride, 1% Triton X-100, 1 mM EDTA, 10 mM Na-

pyrophosphate, 10% glycerin) supplemented with a 1:100 concentration of protease inhibitor cocktail (Thermo Fisher). Protein concentrations were determined using a sample of the protein extract in a modified Lowry assay with a Folin-Phenol color reaction detected by a ND-1000 Spectrophotometer. Remaining extracts were mixed (1:1) with a loading buffer (13% (v/v) Tris-HCl, 20% (v/v) glycerol, 4.6% (w/v) SDS, 0.02% (w/v) bromophenol blue, 200 mM dithiothreitol) for subsequent SDS-PAGE. For SDS-PAGE, 8µg of protein per sample was loaded into pre-cast Criterion Tris-HCl gels (BioRad). Proteins were then electrophoretically transferred to a polyvinylidene fluoride membrane and detected using rabbit IgG anti-vimentin polyclonal (Abcam, Cat# ab45939, RRID:AB_2257290) and mouse IgG1 anti-cytokeratin-8 [M20] (Abcam) antibodies in combination with Vectastain ABC-AmP for chromogenic detection. Detection of GAPDH using a rabbit IgG anti-GAPDH [EPR16884] (Abcam, Cat# ab181603, RRID:AB_2687666) antibody was used as a loading control. Semi-quantitative analysis was performed using ImageJ (https://imagej.nih.gov/ij/, RRID:SCR_003070) to determine vimentin and cytokeratin-8 band intensities normalized to GAPDH. Protein expression levels are reported as experimental relative to cells transfected with negative control siRNA ± SEM.

3.2.7 Vacuole Analysis

To determine the effect of cytoskeletal disruption on the vacuolar morphology of chordoma cells, phase-contrast images of the same cells before and after cytoskeletal disruption were captured. Cells were stained immediately after cytoskeletal disruption for live/dead imaging, allowing cells to recover for 30min prior to capturing "after"

images. Control cells were imaged before and 3.5h after the addition of untreated medium. For each treatment group, phase-contrast images were used to count the number of vacuoles in the same cells before and after treatment. For each treatment, three independent experiments were performed and between 53-72 cells/cell clusters were observed. Data are reported as the average number of vacuoles per sample (cell or cell cluster) ± SEM. Using these data, the average percent vacuole loss per sample was calculated and reported as the average ± SEM.

To further examine the relationship between vimentin and cytokeratin-8 IFs and cytosolic vacuoles, the number of vacuoles within siRNA-mediated vimentin and cytokeratin-8 knockdown cells was compared to that of cells transfected with negative control siRNA. Six days after transfection, cells were stained with calcein AM (Invitrogen/Thermo Fisher Scientific), a live-cell dye that does not permeate into the vacuole lumen (Figure 3.1a), to visualize vacuoles and the nuclear counterstain Hoechst 33342 (Invitrogen/Thermo Fisher Scientific). For each treatment, three independent cell transfection experiments (n=3) were performed. Each sample was imaged under fluorescence microscopy (100x magnification), five fields of view captured, and the number of vacuoles and cells counted across these five fields of view to obtain the average vacuoles per cell in each experiment. Data are reported as the average ± SEM across the three experimental samples. Additionally, we sought to characterize the distribution of vacuoles per cell for each of the treatments. To do this, we utilized the same images to identify single cells transfected with negative control siRNA (n= 276), siRNA targeting VIM (n=236), and siRNA targeting KRT8 (n=315). For each

transfection group, frequency distributions were obtained by normalizing these data to the number of cells analyzed in each group.

3.2.8 Cell Clustering

To determine the necessity of vimentin and cytokeratin IFs in cell clustering, knockdown cells were cultured on basement membrane extract (BME) gel substrates, which have previously been shown to promote clustering of NCs [144]. BME is extracted from the Engelbreth-Holm-Swarm (EHS) mouse sarcoma tumor, which contains high concentrations of laminin-111 (~60%) and type IV collagen (~30%) [145]. Thin BME gels were created by dispensing 122.5 µl of unpolymerized BME (Trevigen, Gaithersburg, MD, USA) into 14 mm diameter glass-bottom wells and incubating for 30 minutes at 37C. Knockdown cells were seeded onto BME gels at a density of ~32,500 cells/cm^2 (50,000 cells/gel) and cultured for 48 hours. Cells were stained with calcein AM (Invitrogen/Thermo Fisher Scientific) and the nuclear counterstain Hoechst 33342 (Invitrogen/Thermo Fisher Scientific) to observe cell organization. Samples were imaged under phase-contrast and fluorescence microscopy (100x magnification).

3.2.9 Statistical Analysis

Statistical analyses were completed using Microsoft Excel or SPSS (http://www-03.ibm.com/software/products/en/spss-statistics/, RRID:SCR_002865) . The non-parametric Wilcoxon test for matched samples was used to compare the number of vacuoles before and after incubation with media with or without acrylamide,

nocodazole, or cytochalasin-D ($\alpha = 0.001$). Kruskal-Wallis followed by Mann-Whitney U tests for independent samples were utilized to compare percent vacuoles lost among groups subjected to chemical disruption ($\alpha = 0.001$). A one-sample t-test was used to compare the relative expression of cytokeratin-8 and vimentin, as measured by Western blot, in siVIM- and siKRT8-cells to that of siNEG-cells ($\alpha = 0.05$). Mann-Whitney U tests were used to compare gene expression of siVIM- and siKRT8-cells to siNEG-cells ($\alpha = 0.05$). For siRNA treated cells, after confirming normality of residuals for the data, one-way analysis of variance (ANOVA) followed by Tukey's HSD post hoc tests were used to compare average number of vacuoles per cell between transfection groups ($\alpha = 0.05$). The Kolmogorov-Smirnov Test was used to compare the distributions of the number of vacuoles per cell for siRNA transfection groups ($\alpha = 0.001$).

3.3 Results

3.3.1 Cytokeratin-8 Intermediate Filaments Organize around Cytosolic Vacuoles in Chordoma Cells

To gain a better understanding of the structural relationship between the cytoskeleton and cytosolic vacuoles of chordoma cells, localization of F-actin, microtubules, vimentin, and cytokeratin-8 IFs was examined relative to vacuole positions. Similar to NCs derived from non-chondrodystrophoid dogs [71], we confirmed that calcein AM fluorescence was consistently excluded from chordoma cell vacuoles as clearly evident from comparing bright field and fluorescence images of cells (Figure 3.1a). Therefore, we used calcein AM exclusion as a means to identify

vacuoles in all subsequent fluorescence labeling procedures. Fluorescence visualization of calcein AM and labelled cytoskeletal proteins of the same cells revealed that only cytokeratin-8 IFs organize immediately around vacuoles (Figure 3.1b). This peri-vacuolar relationship was not observed for vimentin IFs, F-actin, or microtubules (Figure 3.1b).

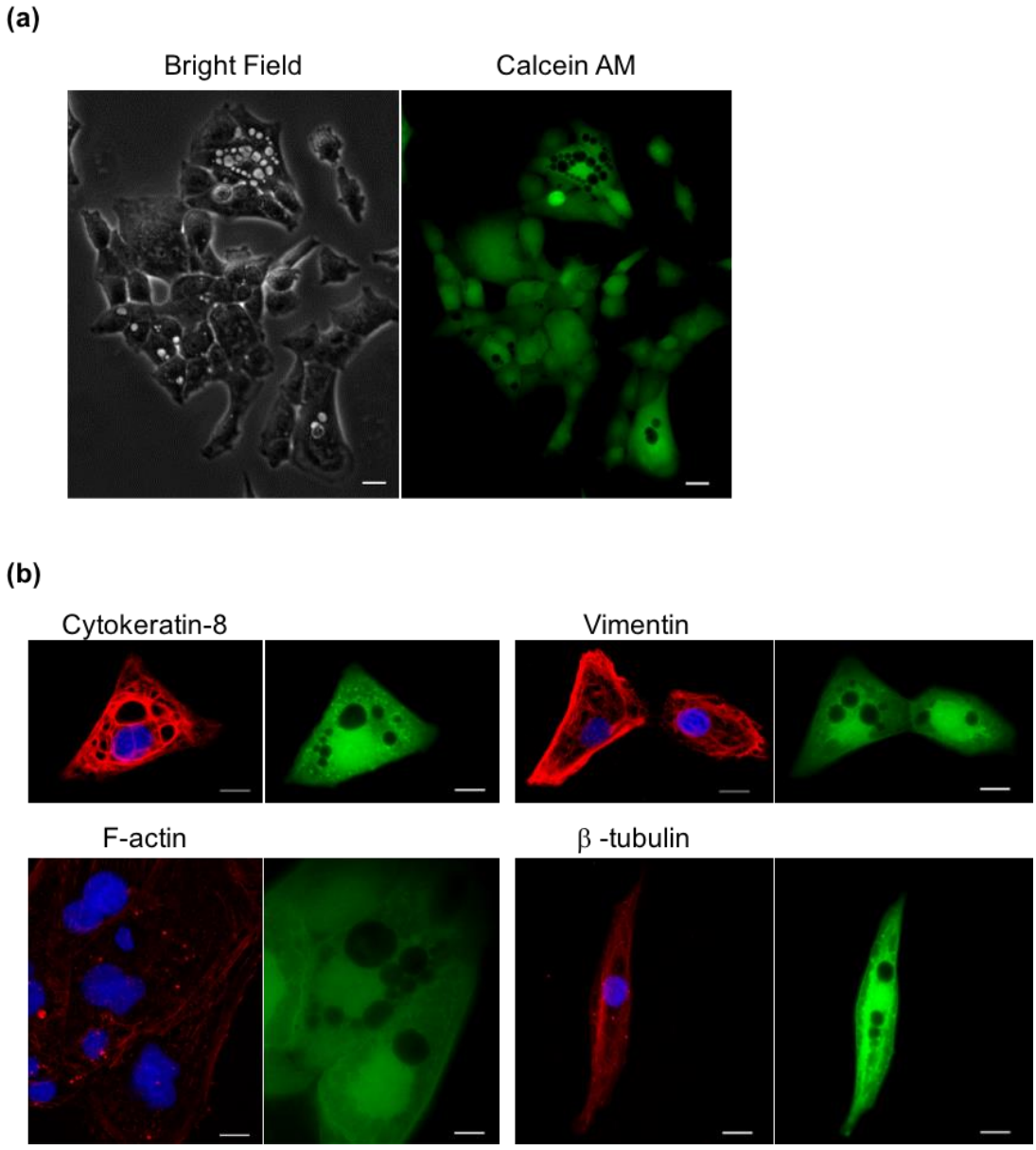

Figure 3.1: Organization of vacuoles and the cytoskeleton in chordoma cells cultured in monolayer. (a) Bright field and fluorescence images of cells stained with calcein AM (green) for the identification of vacuoles. Scale bars: 20 μm; (b) Representative confocal images of chordoma cells stained with calcein AM (green) and labeled for cytoskeletal proteins (red). Scale bars: 10 μm.

3.3.2 Disruption of the Cytoskeleton, Primarily Intermediate Filaments, Decreases the Number of Cytosolic Vacuoles in Chordoma Cells

To elucidate any potential structural relationship between the cytoskeleton and cytosolic vacuoles of chordoma cells, we quantified vacuole number before and after chemical disruption of IFs, F-actin, and microtubules. For these cells, vimentin and cytokeratin-8 IFs were successfully disrupted with 40 mM acrylamide, F-actin with 1 μM cytochalasin-D, and microtubules with 5 μM nocodazole (Figure 3.2b). Treatment of cells with acrylamide, cytochalasin-D, and nocodazole all resulted in a significant ($p< 0.001$) loss of vacuoles compared with images of the same cells prior to treatment, whereas control cells were not markedly affected (Figure 3.3a, b). However, vacuole loss was the greatest in cells treated with acrylamide (Figure 3.3c). The percent vacuole loss caused by acrylamide was significantly ($p< 0.001$) larger than that caused by cytochalasin-D or nocodazole. Both acrylamide and cytochalasin-D treated cells exhibited significantly ($p< 0.001$) higher percent vacuole loss than control cells. In addition to a significant reduction in the number of vacuoles, disruption of IFs with acrylamide appeared to affect vacuole morphology, where remaining vacuoles were observed to be less circular than those of control cells (Figure 3.3a). This qualitative effect on vacuole morphology was not observed in cytochalasin-D or nocodazole treated cells.

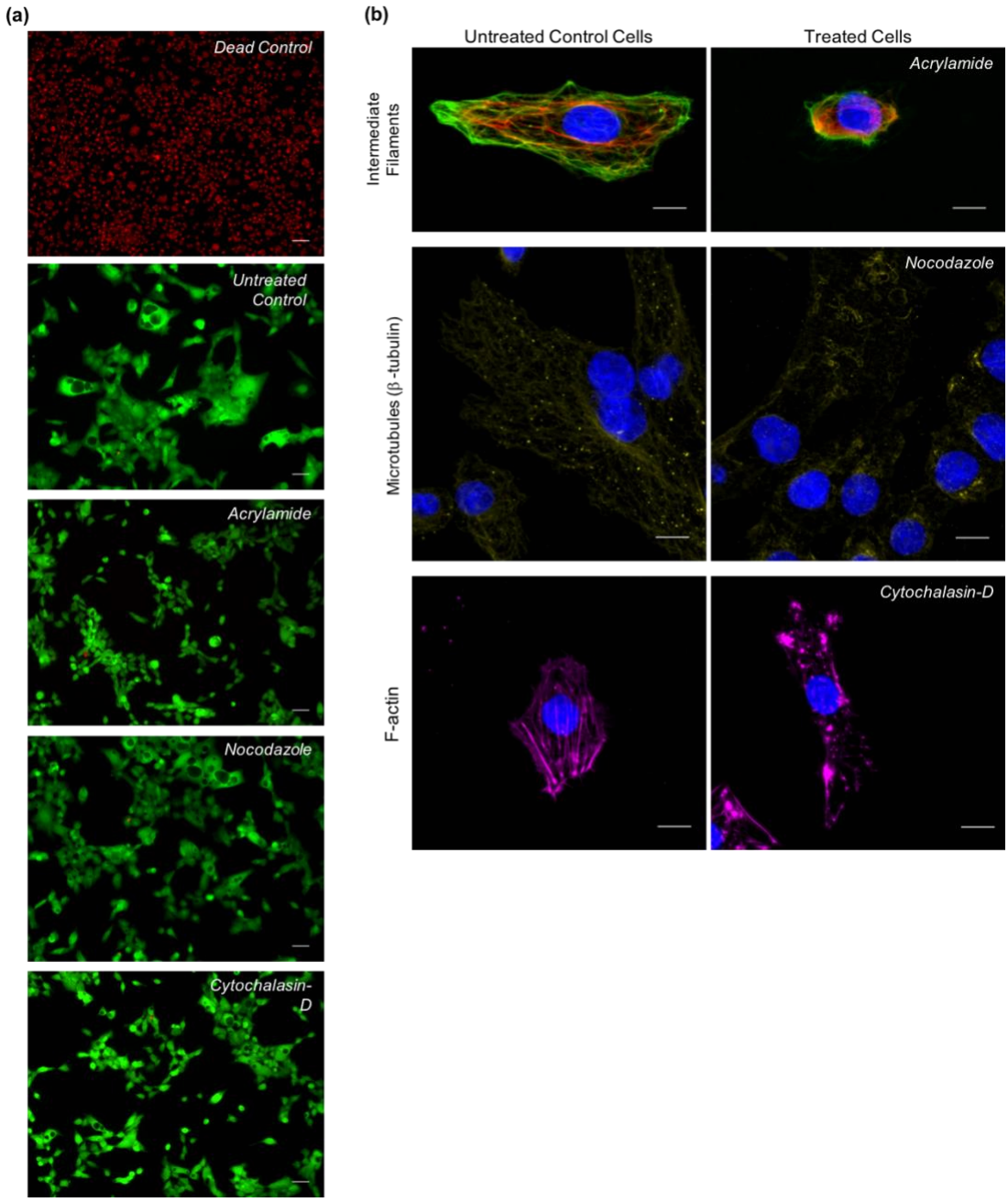

Figure 3.2: Chemical disruption of the cytoskeleton in chordoma cells. (a) Live-dead stain of chordoma cells after cytoskeletal disruption with 40 mM acrylamide for 3.5h, 5 µM nocodazole for 1h, or 1 µM cytochalasin-D for 1h. 'Untreated Control' cells were not incubated with cytoskeleton disrupting agents and 'Dead Control' cells were killed with 70% ethanol. Calcein-AM (green) and ethidium homodimer-1 (red). Scale bars: 50 µm; (b) Representative confocal images of untreated chordoma cells and cells treated with 40 mM acrylamide for 3.5h, 5 µM

nocodazole for 1h, or 1 µM cytochalasin-D for 1h. Intermediate filaments: vimentin (green) and cytokeratin-8 (red). Scale bars: 10 µm.

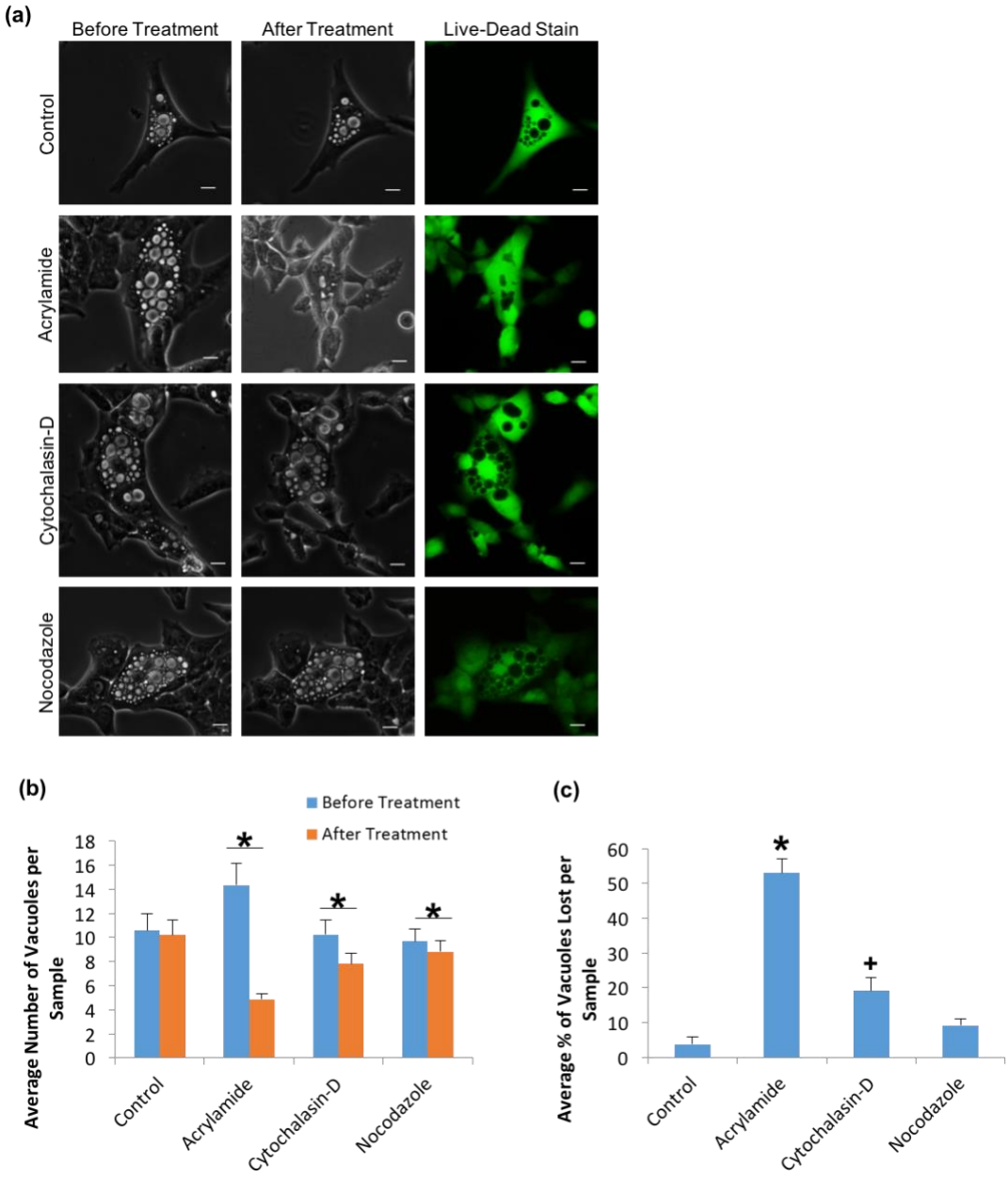

Figure 3.3: The effect of chemical disruption of the cytoskeleton in chordoma cells on cytosolic vacuoles. (a) Representative bright field images of chordoma cells before and after cytoskeletal disruption. Live-dead stain of cells after cytoskeletal disruption, calcein-AM (green) and ethidium homodimer-1 (red). Scale bars: 16 µm; (b) The average number of vacuoles per sample before and after treatment with 40 mM acrylamide for 3.5h (n=53), 1 µM

cytochalasin-D (n=59) for 1h, 5 μM nocodazole (n=72) for 1h, or control medium (n=57) for 3.5h reported as average ± SEM. *p< 0.001, comparing before and after treatment; (c) The average percent of vacuoles lost per sample following treatment with 40 mM acrylamide (n=53) for 3.5h, 1 μM cytochalasin-D (n=59) for 1h, 5 μM nocodazole (n=72) for 1h, or control medium (n=57) for 3.5h reported as average ± SEM. *p< 0.001, relative to control, cytochalasin-D, and nocodazole; +p< 0.001, relative to control.

3.3.3 siRNA Mediated Knockdown of Vimentin and Cytokeratin-8 Expression in Chordoma Cells

When cells were examined six days after transfection, chordoma cells transfected with siRNA targeting VIM (siVIM) and KRT8 (siKRT8) exhibited significant decreases in their respective expression of vimentin and cytokeratin-8. Compared to cells transfected with negative control siRNA (siNEG), siVIM-transfected cells exhibited a 41% decrease in vimentin and siKRT8-transfected cells exhibited a 26% decrease in cytokeratin-8, as observed by Western blotting (Figure 3.4a). In addition to decreased expression of cytokeratin-8, siKRT8-transfected cells exhibited an almost equivalent decrease in vimentin. The reciprocal off target effect was less dramatic for siVIM-transfected cells, which only exhibited a slight decrease in cytokeratin-8 (~2%). Observed decreases in vimentin and cytokeratin-8 proteins in siVIM- and siKRT8-transfected cells were corroborated by immunofluorescence (Figure 3.4b). Assessment by qRT-PCR showed that siVIM- and siKRT8-transfected cells possessed significant decreases in respective VIM and KRT8 expression (Figure 3.6a). Curiously, we found that in contrast to Western blot analysis data, qRT-PCR indicated increased gene expression of the non-targeted IF in siVIM- and siKRT8-transfected cells.

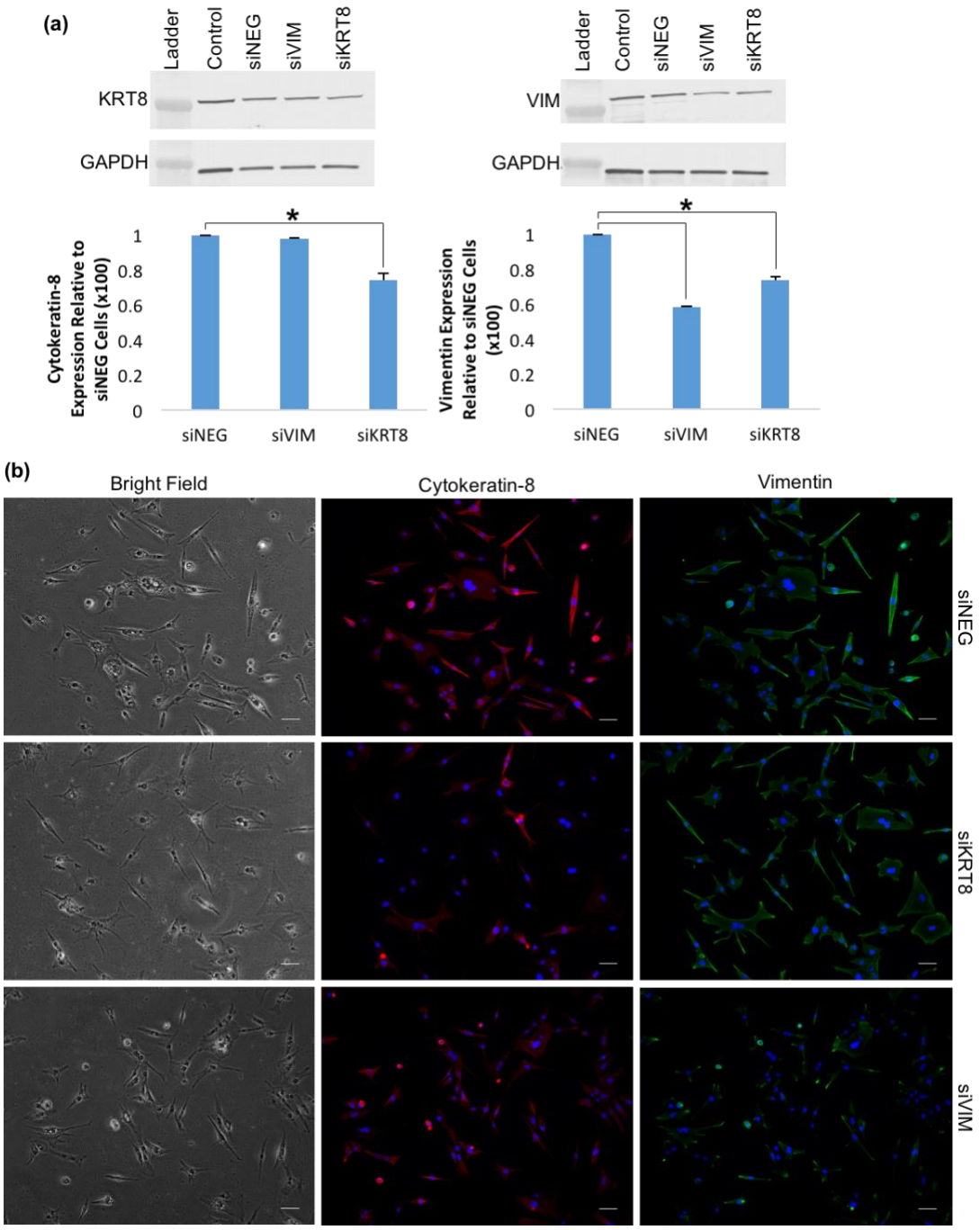

Figure 3.4: Characterization of cytokeratin-8 and vimentin knockdown in chordoma cells six days after transfection with siRNA. (a) Western blot of siKRT8- and siVIM-transfected cells analyzed relative to siNEG-transfected cells. Data is reported as the average ± SEM. *p< 0.05, relative to siNEG-cells. KRT8 and VIM band intensities normalized to GAPDH. 'Control' is a chordoma cell lysate for KRT8 and VIM positive controls; (b) Representative bright field and

fluorescence images of siNEG-, siKRT8- and siVIM-transfected cells. Cytokeratin-8 (red) and vimentin (green). Scale bars: 50 μm.

3.3.4 Cytokeratin-8 Knockdown, but not Vimentin Knockdown, Leads to Reduction in Cytosolic Vacuoles in Chordoma Cells

To determine whether or not vimentin and cytokeratin-8 IFs each play a functional role in supporting vacuole presence in chordoma cells, we compared the number of vacuoles in cultures treated with siVIM, siKRT8, and siNEG (Figure 3.5a). Analyses of calcein AM fluorescence images revealed that siKRT8-cells possessed significantly ($p < 0.001$) fewer vacuoles per cell compared to siVIM- and siNEG-cells (Figure 3.5b). There was no significant difference between siVIM- and siNEG-cells ($p=0.081$). The distributions of vacuole number per cell was also significantly ($p < 0.001$) different for siKRT8-cells compared to siVIM- and siNEG-cells (Figure 3.5c). In contrast to siKRT8-cells, which more frequently had 0-1 vacuoles per cell, siVIM- and siNEG-cells more frequently had greater than 3 vacuoles per cell.

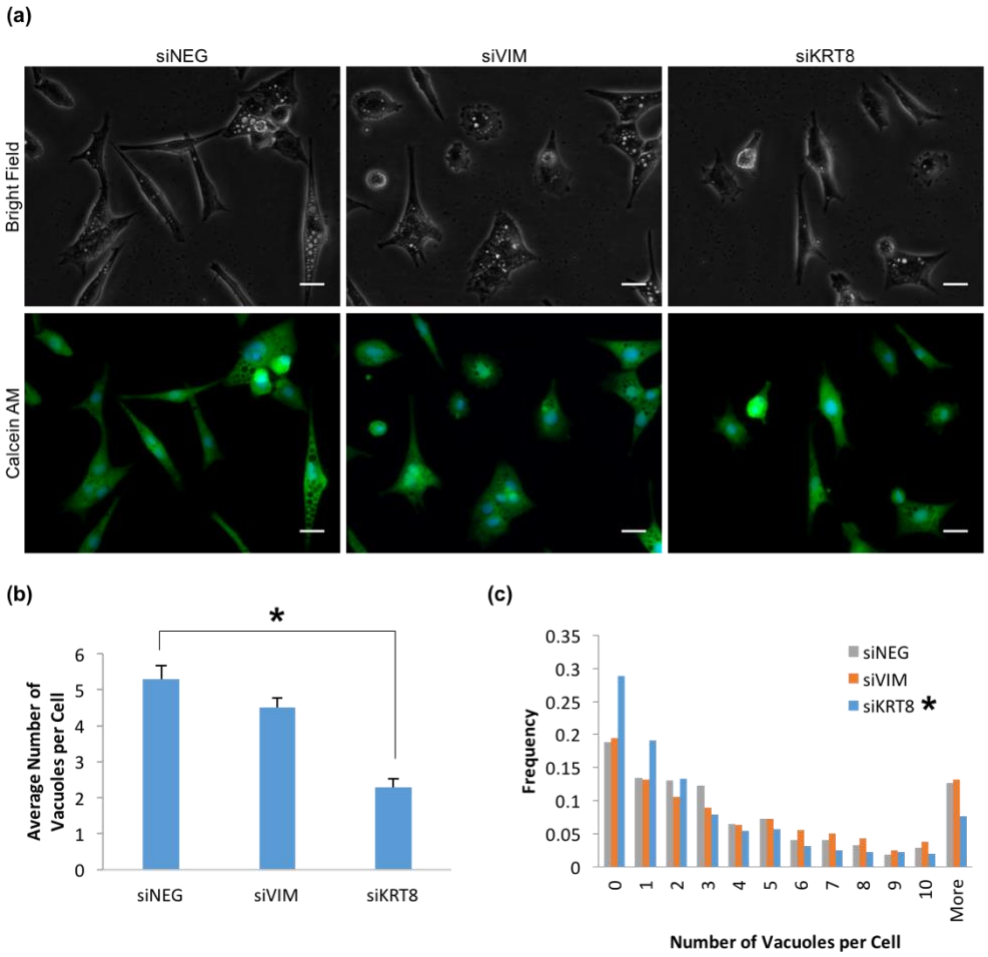

Figure 3.5: The effect of vimentin and cytokeratin-8 knockdown on the number of cytosolic vacuoles in chordoma cells. (a) Representative bright field and fluorescence images of siNEG-, siVIM-, and siKRT8-cells stained with calcein AM (green) and Hoechst 33342 (blue). Scale bars: 25 µm; (b) The average number of vacuoles per cell in siNEG-, siVIM-, and siKRT8-cells reported as average ± SEM. *p< 0.001, relative to siNEG- and siVIM-cells; (c) The distribution of the number of vacuoles per cell in siNEG- (n=276), siVIM- (n=236), and siKRT8-cells (n=315) normalized to the number of cells analyzed. *p< 0.001, relative to siNEG- and siVIM-cells.

3.3.5 Knockdown of Cytokeratin-8 and Vimentin in Chordoma Cells does not Immediately Affect Gene Expression or Cell Clustering

The effects of cytokeratin-8 and vimentin knockdown on the NC and chordoma cell phenotype were further investigated through gene expression and cell clustering analysis. Despite the reduction of cytosolic vacuoles in siKRT8-cells, cytokeratin-8 knockdown did not significantly alter gene expression of the phenotypic cell markers T, SHH, and CDH2 (Figure 3.6a). Expression of these characteristic genes were also not altered in siVIM-cells (Figure 3.6a). Additionally, characteristic cell clustering on soft, laminin-rich BME gels was not inhibited in siVIM- and siKRT8-cells (Figure 3.6b).

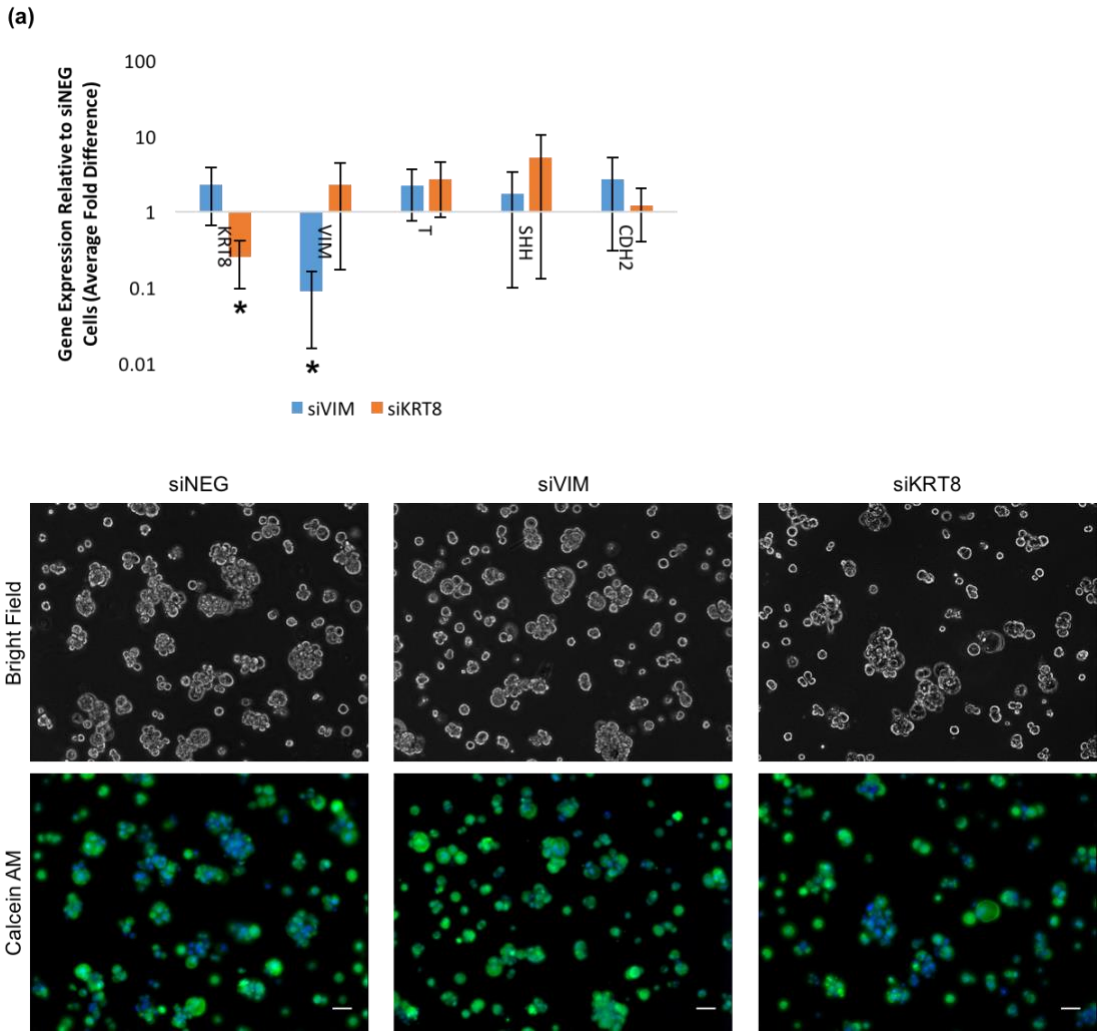

Figure 3.6: The effect of vimentin and cytokeratin-8 knockdown in chordoma cells on gene expression of phenotypic markers and cell clustering. (a) Gene expression of siKRT8- and siVIM-transfected cells analyzed relative to siNEG-transfected cells. *$p<0.05$, relative to siNEG-cells; (b) Representative bright field and fluorescence images of cells stained with calcein AM (green) and Hoechst 33342 (blue). Scale bars: 50 µm.

3.4 Discussion

Results of this study show that IFs play a significantly greater role in supporting cytosolic vacuoles in chordoma cells than microfilaments and microtubules. Further parsing the specific involvement of different types of IFs indicated that cytokeratin-8 plays a functional role in vacuolation, while vimentin does not. Our current findings

are consistent with prior observations of age-associated morphologic and coincident phenotypic cytoskeletal changes observed in cells populating the NP. NCs, of the immature NP and chordoma, are characterized by their vacuolated cytoplasm and co-expression of cytokeratin and vimentin IFs [32], [33], [40], [44], [47], [48], while smaller, more chondrocyte-like cells populating the adult NP are not vacuolated and typically only express vimentin IFs [35]–[37], [44].

While the formation of cytosolic vacuoles is a defining feature of NC differentiation, the contents and function of these vacuoles in mature, mammalian NCs have not been conclusively established. In developing Xenopus and zebrafish embryos, notochord vacuoles have been found to be required for elongation of the embryonic body axis and play an active role in spine morphogenesis, presumably serving to generate turgor for stiffening the notochord [24], [27], [70]. Cell-matrix interactions and cell motility patterns have been shown to be centrally important to the notochordal vacuolation process [146], [147]. Recently, it has been shown that LAMP1 can be found on the vacuolar membrane of zebrafish NCs and that H^+-ATPase is required for vacuole integrity; yet, the vacuole lumen itself is not acidic [24]. Taken together, these observations suggest that notochordal vacuoles are unique lysosome-related organelles unlike others that have been characterized [148]. Interestingly, the only other known vacuolar organelle that utilizes H^+-ATPase for anything besides acidification are contractile vacuoles, which are used for osmoregulation and fluid segregation, in protists [149]–[151]. Although vacuoles of embryonic NCs are essential for development, the significance of cells maintaining vacuoles in the developed IVDs and in chordomas is unclear, but has remained an area of particular interest [123]. The only

study that explores vacuolar function in mature NCs proposes vacuoles to be osmoresponsive organelles containing low osmolality solution that can be used to regulate cell volume under hypotonic stress [71]. Similar to their role in embryonic NCs, vacuoles within chordoma and the developed NP may serve some sort of mechanobiological function.

Previous studies have implicated the cytoskeleton in the formation, localization, transport, and structural stabilization of vacuoles and vacuole-like structures such as vesicles and granules [134]–[137], [152]. However, the role of IFs in supporting vacuoles of NCs and chordoma cells has not been thoroughly examined. To investigate this relationship, we used a human chordoma cell line (MUG-Chor1), which has previously been shown to possess a vacuolated morphology and co-express vimentin and cytokeratin IFs [63]. The peri-vacuolar network of cytokeratin-8 IFs we observed in chordoma cells suggest that they are structurally involved in maintaining the vacuoles. This finding is consistent with previous studies of the hagfish notochord, where IFs were observed to organize around vacuoles [25]. Contrary to previous studies of canine NCs, we did not observe F-actin networks around vacuoles [40]. We also did not observe networks of microtubules or vimentin IFs to surround vacuoles.

To elucidate the relationship between the cytoskeleton and cytosolic vacuoles further, cells were treated with cytoskeleton disrupting agents targeting IFs, F-actin, and microtubules. The significant decrease in the number of vacuoles per cell as a result of disrupting IFs with acrylamide, F-actin with cytochalasin-D, and microtubules with nocodazole confirmed the involvement of the cytoskeleton. Because cells with disrupted IFs experienced the greatest decrease in vacuole number, IFs may have a

more prominent role in supporting vacuoles than F-actin and microtubules. In addition to the significant decrease in the number of vacuoles in cells with disrupted IFs, remaining vacuoles appeared collapsed and tended be less circular than controls. Although the number of vacuoles significantly decreased in cells with disrupted F-actin and microtubules, the reduction was far less pronounced, and remaining vacuoles appeared to maintain their circular shape. Thus, it may be that the decrease in the number of vacuoles in cells with disrupted F-actin and microtubules is an indirect effect of chemical disruption of these targeted elements caused by accompanying changes such as cell shape and size. Since we have not analyzed the off-target effects of acrylamide, cytochalasin-D, and nocodazole, it is also possible that the application of these agents affects non-targeted cytoskeletal elements [140], [153]–[156].

Based on the significant effect of IF disruption on vacuoles, we sought to target IFs containing vimentin and cytokeratin-8 more specifically using siRNA-mediated RNAi. In agreement with our observations of cytokeratin-8 IFs surrounding vacuoles, chordoma cells with reduced cytokeratin-8 expression (siKRT8-cells) exhibited fewer vacuoles per cell compared to controls (siNEG-cells) and cells with reduced vimentin expression (siVIM-cells). Because siKRT8-cells exhibited decreases in both cytokeratin-8 and vimentin expression, it is possible that co-expression of cytokeratin and vimentin IFs is involved in the vacuolated cytoplasm characteristic of chordoma cells. However, the fact that siKRT8-cells possessed significantly fewer vacuoles than siVIM-cells, which exhibited only decreased vimentin expression, suggests that cytokeratin-8 IFs plays a dominant role in the vacuolation of chordoma cells. As both cytokeratin expression and vacuoles are known to disappear contemporaneously in

mature NP cells [33], [40], [42], [44], [45], the decrease in cytokeratin expression observed with NP maturation may potentially be a factor responsible for the loss of a vacuolated cytoplasm.

Another possible interpretation of our data is that cytokeratin-8 IFs are necessary for vacuole formation. Cells transfected with our negative control siNEG using Lipofectamine2000 appeared to contain more vacuoles following a week of subconfluent culture compared to untreated control cells. In untreated chordoma cells, we have observed similar increases in vacuole number after cultures reach confluence. If vacuolation is enhanced by transfection, the reduced number of vacuoles observed in siKRT8-cells compared to siVIM- and siNEG-cells may be the result of inhibited vacuole formation. Because knockdown of IFs with RNAi (in contrast to chemical disruption) is a gradual process, we could not examine the same cells before and after IF protein knockdown and therefore were unable determine the change in the number of vacuoles for a particular cell/ cell cluster. Consequently, it is not clear whether greater numbers of vacuoles were lost or fewer vacuoles were formed in cells with decreased cytokeratin-8 expression. Future studies of cytokeratin-8's involvement during embryonic NC fate determination and notochord morphogenesis would provide a clearer picture of how cytokeratin-8 might participate in vacuologenesis.

To explore how the co-expression of cytokeratin-8 and vimentin IFs, in addition to cytosolic vacuoles, are associated with the NC and chordoma cell phenotype, cell clustering and gene expression were examined in siKRT8- and siVIM-cells relative to siNEG-cells. In the developing notochord and chordomas, cells tend to aggregate in dense cell clusters. Based on previous studies, it is suggested that vimentin IFs play a

more significant role in cell-substrate adhesions compared to cytokeratin IFs, which have been more strongly associated with cell-cell adhesions [91], [98], [132, p.]. This is consistent with developmental changes in the notochord, as cytokeratin expression and the presence of cell clusters are both reduced with maturation. In addition to decreased cytokeratin expression, vimentin expression tends to increase with notochord development, which has been associated with a decrease in the desmosomal protein desmoplakin [157]. In contrast, cytokeratin IFs form direct attachments to desmosomes for the formation of cell-cell adhesions. Based on these findings, we decided to examine the effect of decreased vimentin and cytokeratin-8 expression on the ability of chordoma cells to form cell clusters on soft, BME gels, which have previously been shown to promote NC clustering [144]. Knockdown of vimentin and, to our surprise, cytokeratin-8 did not appear to affect chordoma cell clustering, suggesting IFs are not essential for the formation of chordoma cell-cell adhesions.

For gene expression analysis, the expression of T brachyury (T), Sonic Hedghog (SHH), and N-cadherin (CDH2) were examined, as these genes are highly expressed in NCs and chordoma [42], [40], [43]–[47]. When cells were examined six days after transfection with siRNA, we did not find any differences in the expression of T, SHH, and CDH2 in siKRT8- and siVIM-cells relative to siNEG-cells. Similar to cell clustering results, this suggests the expression of phenotypic genes is not dependent on IF protein expression in NCs and chordoma cells. Because siKRT8-cells were found to have reduced cytosolic vacuoles, this also suggests the expression of phenotypic genes is not dependent on the presence of cytosolic vacuoles. This is in agreement with previous studies that show Xenopus notochord vacuolation and NC fate specification

are essentially decoupled [70]. While immediate effects of cytokeratin-8 and vimentin knockdown on gene expression and cell clustering were not observed, long-term stable knockdown or gene deletion may be necessary to detect changes in the chordoma cell phenotype.

3.5 Conclusion

To our knowledge, this is the first study to reveal the involvement of cytokeratin IFs in the vacuolated cytoplasm of chordoma cells. Although additional studies are required to elucidate the mechanism, our results suggest cytokeratin-8 IFs are critical for the vacuolation of NCs and chordoma cells, and are consistent with the previously observed concomitant loss of cytokeratin expression and vacuoles in mature NP cells. Insight into factors that function to maintain the NC phenotype is critical for assisting in the development of regenerative therapies for disc degeneration and targeted therapies for chordoma.

Chapter 4: The Roles of Vimentin and Cytokeratin-8 Intermediate Filaments in Chordoma Cell Mechanobiology

4.1 Introduction

Abnormal changes in the mechanical properties of the ECM affect normal cell function and are associated with various diseases. For instance, degenerated IVDs have been reported to be stiffer than normal discs [158]. Additionally, tumors tend to be stiffer than healthy tissue and increased ECM stiffness has been linked to a malignant cell phenotype [13], [14]. Cells are able to probe the mechanical properties of their surrounding ECM through traction forces and respond by adjusting their focal adhesions, cytoskeleton, and mechanical properties. Ultimately, these adjustments can affect cell behaviors such as proliferation and migration. Mechanical cues are important determinants of cell function and have shown promise as cancer biomarkers, as cell deformability and traction forces are found to increase in cancer cells [114]–[118].

Cell stiffness, traction force generation, and mechanosensitivity have primarily been attributed to F-actin. However, increasing evidence supports roles for microtubules and IFs in these processes. NCs, observed in the immature NP and chordoma, co-express cytokeratin and vimentin IFs, a unique cellular characteristic that is not uncommon in cells of developing tissues and cancer cells [96], [98]. In contrast, mature NP cells typically only express vimentin IFs [44]. Cytokeratin IFs are composed of heterodimers formed between acidic, type I cytokeratins (9-20) and basic, type II cytokeratins (1-8) and are characteristically expressed in epithelial cells. The expression of different cytokeratin proteins is tissue specific, and NCs primarily

express cytokeratins 8, 18, and 19. For filament formation, cytokertin-8 and -18 typically dimerize together, while cytokeratin-19 has been suggested to be capable of substituting for cytokeratin-18 [131]. Vimentin IFs are composed of vimentin monomers and are normally expressed in mesenchymal cells.

Individually, vimentin and cytokeratin IFs have been found to be involved in various cell mechanical properties and behaviors. Both vimentin and cytokeratin IFs interact with actin filaments, and changes in their expression and organization have been shown to affect actin stress fibers and cell traction forces [5], [6]. Additionally, vimentin and cytokeratin IFs have been found to contribute to cell stiffness. For example, vimentin deficient fibroblasts and cytokeratin deficient keratinocytes were found to be less stiff than wild type cells [3], [4]. Decreased vimentin and cytokeratin expression has also been observed to cause substrate stiffness dependent changes in cell spreading [7, p. 18], [8]. In certain cancers, it is suggested that the co-expression of vimentin and cytokeratin IFs encourages cell invasion and a metastatic cell phenotype [9], [16], [17]. However, the functional roles of vimentin and cytokeratin IFs in chordoma cells are unknown.

In this study, we investigated the involvement of vimentin and cytokeratin IFs in NC mechanical properties and functions. We used RNAi to knock down vimentin and cytokeratin-8 expression in a human chordoma cell line (MUG-Chor1) and subsequently examined cell stiffness, traction forces, and sensitivity to substrate stiffness. Our findings indicate that vimentin IFs are involved in chordoma cell mechanics, while cytokeratin IFs are not. Specifically, knockdown of vimentin

expression resulted in decreased cell longitudinal modulus, increased cell traction forces, and disrupted cell sensitivity to substrate stiffness.

4.2 Materials and Methods

4.2.1 Cell Culture

MUG-Chor1 chordoma cells (ATCC Cat# CRL-3219, RRID:CVCL_9277) were cultured in Iscove's Modified Dulbecco's Medium: Roswell Park Memorial Institute 1640 Medium (4:1) (Gibco/Thermo Fisher Scientific) supplemented with 10% FBS (Gibco/Thermo Fisher) and 1% Penicillin-Streptomycin (Gibco/Thermo Fisher). Complete media exchange was completed every 2-3 days and cells were cultured at 37°C, 5% CO_2.

4.2.2 Transfection of siRNA

To knockdown vimentin and cytokeratin-8 expression, chordoma cells were transfected with siRNA, as previously described. Cells were plated at a density of 10,000 cells/cm^2 on rat tail type I collagen (Advanced BioMatrix) absorbed (50 μg/ml) on TCTP. Twenty-four hours after plating, cells were transfected with Silencer Select Pre-designed siRNA (Ambion/Thermo Fisher) targeting either KRT8 (s7970), VIM (s14798), or Silencer Select Negative Control No. 1 siRNA (Ambion/Thermo Fisher) using Lipofectamine 2000 (Invitrogen/Thermo Fisher) diluted in reduced serum opti-MEM (Thermo Fisher). Cells were incubated with transfection reagents for 24h. Six days after transfection, cells were detached using 0.25% trypsin-EDTA (1x) and

processed for the analysis of cell spreading, traction forces, contraction of collagen, and stiffness.

4.2.3 Polyacrylamide Gel Preparation

Polyacrylamide (PA) gels corresponding to stiffnesses of 0.42 kPa (3% acrylamide + 0.06% bis acrylamide), 5 kPa (8% acrylamide + 0.07% bis acrylamide), and 13 kPa (8% acrylamide + 0.2% bis acrylamide) were prepared on glass coverslips. Gel stiffness for these acrylamide to bis-acrylamide ratios have previously been confirmed using dynamic mechanical analysis (DMA) and atomic force microscopy (AFM) [159], [160]. To enable gel attachment, glass coverslips (25 mm) were first coated with 0.1M NaOH, air dried, coated with 3-amino-propyltrimethoxysilane, and fixed with 0.5% glutaraldehyde in phosphate buffered saline (PBS). Gel polymerization was initiated with 10% ammonium persulfate and catalyzed with N,N,N',N'-Tetramethylethylenediamine (TEMED). For traction force microscopy, fluorescence beads (1 μm) were added to the gel solution prior to initiating polymerization. Gel solutions (30 μl) were added onto activated glass coverslips and distributed evenly across the surface by placing an additional coverslip of equivalent size on top of the solution. Following 30 minutes of polymerization, the top coverslip was removed and gels were treated with sulfo-SANPAH for the chemical crosslinking of either type I collagen (Advanced BioMatrix) or laminin (MilliporeSigma, Burlington, MA, USA) (50-65 μg/ml) to the gel surface.

4.2.4 Immunofluorescence

Immunofluorescence was used to visualize cytoskeletal proteins and examine cell spreading. Cells were fixed with 4% PFA, permeabilized using 0.1% Triton X-100, and labelled with rabbit IgG anti-vimentin [SP20] (Thermo Fisher Scientific, Cat# MA5-16409 , AB_2537928) or mouse IgG1 anti-cytokeratin-8 [M20] (Abcam, Cat# ab9023 RRID:AB_306948) antibodies. A biotinylated (anti-rabbit IgG) secondary antibody (Vector Laboratories, Cat# BA-1000, RRID:AB_2313606) was used in combination with Texas Red-labelled streptavidin (Vector Laboratories) to visualize vimentin. An Alexa Fluor 594-conjugated (anti-mouse IgG) secondary antibody (Thermo Fisher Scientific, Cat# A-11032, RRID:AB_2534091) was used to visualize cytokeratin-8. Cells were stained with Alexa Fluor 488 Phalloidin (Invitrogen/Thermo Fisher Scientific) to visualize F-actin, and DAPI (Invitrogen/Thermo Fisher Scientific) was used as a nuclear counterstain. A Nipkow (spinning) disk-equipped Olympus IX81 microscope was used to capture images at x100 magnification. Confocal fluorescence images were taken at x600 magnification and Z-stacks (1 μm slices) were projected into a single image for analysis. ImageJ was used to quantify the fluorescence intensity of labelled proteins. Cells were manually traced and the corrected total cellular fluorescence (CTCF) was calculated per cell using the following equation: CTCF = [integrated density – (area of selected cell x mean fluorescence of background reading)]. The corrected mean cellular fluorescence (CMCF) per cell was then calculated: CMCF = [CTCF/cell area (pixels)]. Data are shown as average CMCF ± SEM.

4.2.5 Cell Spreading

Control and siRNA-mediated vimentin and cytokeratin-8 knockdown cells were plated at a density of 2,000 cells/cm^2 onto PA gels or glass coated with either type I collagen or laminin (50-65 μg/ml). After 20h of culture, cells were fixed with 4% PFA and immunostained, as described above. Samples were imaged under phase and fluorescence microscopy (100x magnification). Cells stained for F-actin were used to measure cell area and circularity (shape factor) in ImageJ (https://imagej.nih.gov/ij/, RRID:SCR_003070). For each condition, 3 independent experiments were performed and 72-75 cells were analyzed.

4.2.6 Traction Force Microscopy

Control and vimentin and cytokeratin-8 knockdown cells were plated at a low cell density onto 5 kPa PA gels coated with type I collagen (50 μg/ml). To examine the contribution of actomyosin-mediated contractility in traction force generation, cells were treated with 50 μM (-)-blebbistatin (MilliporeSigma). Following approximately 20h of culture, cells were imaged under phase and beads under fluorescence microscopy (400x magnification). Cells were then detached from the gel surface using 0.25% trypsin-EDTA (1x) and beads were re-imaged under fluorescence. Fluorescence bead images of the same (x,y) position before and after cell detachment were aligned using ImageJ to account for shifting of the sample. Bead images were processed with MATLAB software generated by the Danuser Lab to calculate bead displacement and for traction force reconstruction via FTTC [161].

In ImageJ, phase images of cells were used to trace the cell boundary and create a mask of the cell, where the area under the cell was white and the surrounding area black. To extract traction stresses immediately under the cell, an element-by-element product of two matrices was calculated using the cell's mask and the corresponding traction map generated by traction force reconstruction. The resulting matrix of traction stress values was used to determine the total force, maximum stress, and average stress exerted by each cell. The total force exerted by a single cell was calculated as a summation of the traction force magnitudes across the cell area. The total force was normalized by the cell area and reported as the cell's average traction stress. A maximum stress value, corresponding to the stress at a particular point (pixel within captured image), was also determined for each cell.

4.2.7 Collagen Gel Contraction

Collagen gels were prepared by mixing 9 parts of 2.5 mg/ml rat tail type I collagen (Advanced BioMatrix) with 1-part neutralization solution (Advanced Biomatrix). Control and vimentin and cytokeratin-8 knockdown cells suspended in chordoma growth media were mixed into collagen pre-gel solutions for final cell and collagen concentrations of $1x10^6$ cells/ml and 0.75 mg/ml, respectively. Collagen solutions containing cells were added to 48 well plates (250 µl/well) and allowed to incubate for 20 minutes at room temperature. Once gels had formed, a scoopula was used to detach gels from the edges of the well and each gel was transferred to 5 ml of media in a 6 well plate. Gels were cultured at 37C, 5% CO_2 for 8 days and imaged daily using a Canon DS6041 digital camera connected to an Olympus SZX7 stereo

microscope. In ImageJ, captured images were used to measure gel surface areas and the percent of the initial gel surface area was calculated for each time point. Four independent experiments were performed for each group and data are reported as the average ± SEM.

4.2.8 Brillouin Confocal Microscopy

The principle of Brillouin scattering is based on the interaction of incident photons with collections of molecules oscillating within matter (referred to as phonons) resulting in a frequency shift in the gigahertz range. Brillouin frequency shift is related to the longitudinal modulus (constrained ratio of axial stress to axial strain) by the equation $M' = (\rho\lambda^2*\Omega^2)/(4n^2)$, where M' is the real part of the longitudinal modulus, ρ is the sample mass density, Ω is the frequency shift, λ is the wavelength of incident light, n is the index of refraction of the sample. Since the ratio of ρ/n^2 varies insignificantly in cell samples [162], Ω is positively correlated to M'. Prior research in cell samples has established a correlation between the longitudinal modulus, as extracted by Brillouin confocal microscopy, and the Young's modulus, as calculated from AFM, thus confirming Brillouin shift as a proxy for mechanical properties within a material [163].

Brillouin instrumentation used for these experiments was similar to previous reports [163], [164]. A single mode linearly-polarized laser with 532 nm or 660 nm wavelength was focused into the sample using a 40X/0.6 NA objective. Brillouin mapping was performed in the XY plane (parallel to the gel) through the mid-plane of the cell where Brillouin shift was measured to be a maximum value along the z-axis.

siNEG-, siVIM-, and siKRT8-cells were cultured as previously described and plated on 5 kPa PA gels coated with type I collagen. A total of 65 siNEG-, 34 siVIM-, and 34 siKRT8-cells were analyzed in total, measured across 7 experimental days. To extract the average Brillouin frequency shift for a cell, values below 6.25 GHz, corresponding to extracellular medium, were removed and the remaining cell area was averaged. Both circular and attached cells were analyzed, and siVIM and siKRT8 were normalized to the average of their respective circular or attached siNEG control group measured on the same day.

4.2.9 Statistical Analysis

Statistical analyses were completed using SPSS (http://www-03.ibm.com/software/products/en/spss-statistics/, RRID:SCR_002865). For all studies, Kruskal-Wallis followed by Mann-Whitney U tests for independent samples were performed. Statistical significance was set to $(\alpha = 0.05)$.

4.3 Results

4.3.1 Knockdown of Vimentin Disrupts Chordoma Cell Mechanosensitivity to Substrate Stiffness

To examine the involvement of vimentin and cytokeratin-8 IFs in chordoma cell mechanosensing of substrate stiffness, knockdown cells were plated on collagen (Col-PA) or laminin (Lam-PA) coated PA gels of varied stiffness. Cell area and circularity were measured after 20h of culture. On Col-PA gels, vimentin knockdown (siVIM) cells had larger cell areas and were less circular relative to cells transfected

with negative control siRNA (siNEG-cells) and cytokeratin-8 knockdown (siKRT8) cells (Figure 4.1a, b). While these differences were observed on Col-PA gels of all stiffnesses (0.42, 5, 13 kPa), they were not significant on stiffer (13 kPa) substrates. Similarly, on 5 kPa Lam-PA gels, siVIM-cell area was significantly larger relative to siNEG-cells (Figure 4.1a). However, on soft (0.42 kPa) Lam-PA gels, all cell types had a small and circular morphology (Figure 4.1a, b). All cell types had significantly larger cell areas, corresponding to decreased circularity, on stiff (13 kPa) compared to soft (0.42 kPa) gels except for siVIM-cells on Col-PA gels (Figure 4.1a, b).

On soft (0.42 kPa) gels, cells were significantly larger (increased cell area) and less circular on collagen compared to laminin for all cell types (Figure 4.1a, b). With increasing PA gel stiffness, the effect of substrate composition on cell area and circularity was less apparent. On glass surfaces, siVIM- and siKRT8-cells had significantly larger cell areas on laminin than collagen (Figure 4.1c). Although differences were not observed between siKRT8- and siNEG-cell areas on PA gels, siKRT8-cells were significantly smaller on collagen-coated glass (Figure 4.1c).

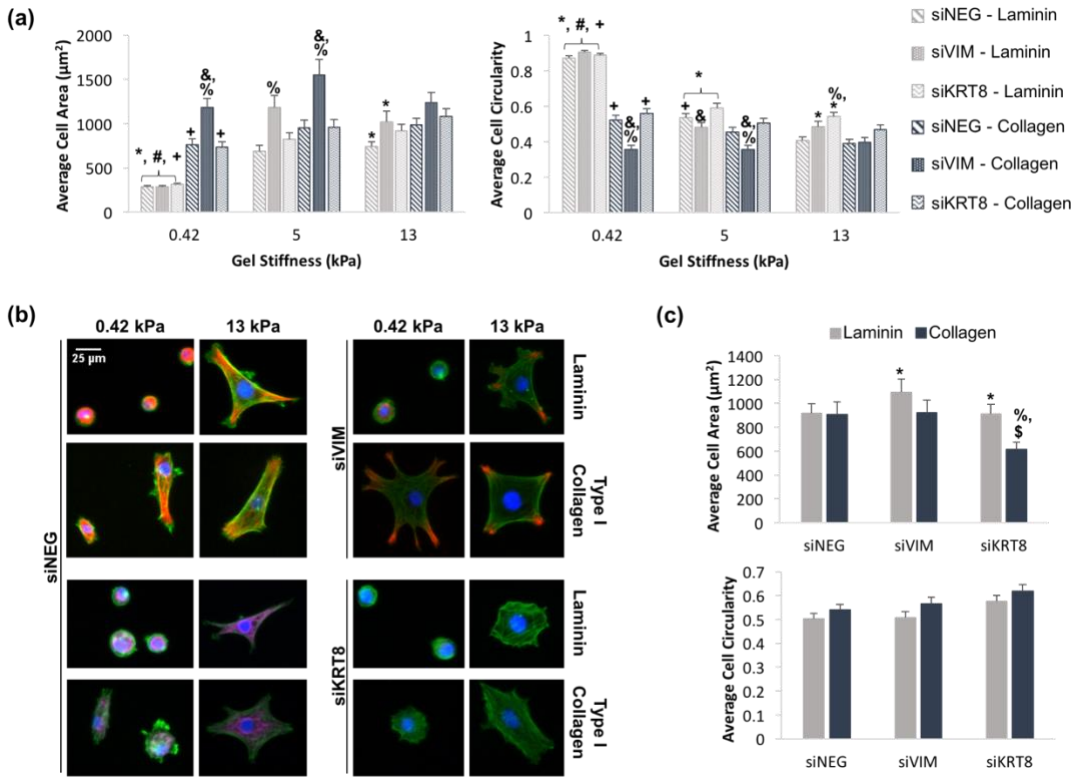

Figure 4.1: The effect of vimentin and cytokeratin-8 knockdown on chordoma cell sensitivity to substrate stiffness. (a) Cell area and circularity of cells on PA gels of varying stiffness and substrate protein reported as average ± SEM. $p < 0.05$: * relative to same stiffness same cell type on collagen; # relative to same protein same cell type on 5kPa; + relative to same protein same cell type on 13kPa; % relative to same stiffness same protein siNEG-cells; & relative to same stiffness same protein siKRT8-cells; (b) Representative fluorescence images of chordoma cells on soft and stiff PA gels coated with either laminin or type I collagen labeled for F-actin (green), and vimentin (red) or cytokeratin-8 (magenta); (c) Cell area and circularity of cells on glass reported as average ± SEM. $p < 0.05$: * relative to same cell type on collagen; % relative to same protein siNEG-cells; $ relative to same protein siVIM-cells.

4.3.2 Cell Traction Forces Increase in Chordoma Cells Lacking a Continuous Vimentin Network

To investigate the role of vimentin and cytokeratin-8 IFs in chordoma cell traction forces, knockdown cells were plated onto 5 kPa Col-PA gels embedded with 1

μm fluorescence beads. To minimize effects due to cell size variation of siVIM-cells relative to siNEG- and siKRT8-cells observed on 5 kPa Col-PA gels, cells of similar size were chosen for analysis (Appendix B; Figure B.2). Additionally, the sum of traction force magnitudes across the cell (total traction force), was normalized by cell area to calculate the average traction stress for each cell. The maximum traction stress exerted by each cell was also calculated to examine localized traction stress. On average, siVIM-cells had significantly larger maximum traction stresses when compared to siKRT8- and siNEG-cells (Figure 4.2c). A similar trend was observed when analyzing the average traction stress, which was increased in siVIM-cells compared to siNEG-cells (Figure 4.2b); however, this differences was not statistically significant.

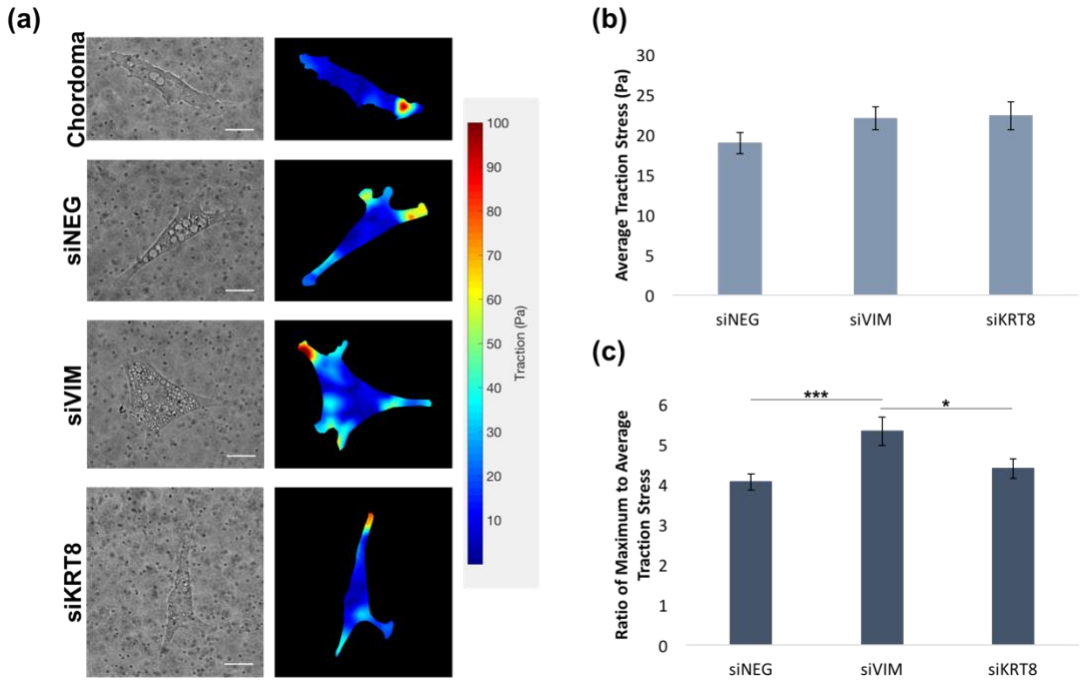

Figure 4.2: Traction force analysis of vimentin and cytokeratin-8 knockdown chordoma cells. (a) Representative phase images and corresponding traction maps of non-transfected

chordoma, siNEG-, siVIM-, and siKRT8-cells on 5 kPa polyacrylamide gels coated with type I collagen. Scale bars: 25 μm; (b) Average traction stress and (c) Normalized maximum traction stress of siNEG- (N=46), siVIM- (N=43), and siKRT8- (N=44) cells reported as average ± SEM. *$p < 0.05$; ***$p < 0.001$.

To examine the involvement of actin in cell traction forces, actin was labelled with Alexa Fluor 488 Phalloidin to visualize stress fibers and actin content was semi-quantitatively determined from fluorescence microscopy. Despite differences in traction forces, cells were not found to have visual differences in actin stress fibers (Figure 4.3a) or statistically significant differences in fluorescence intensities of actin staining (Figure 4.3b). To further investigate the mechanism responsible for increased traction forces of siVIM-cells, cells were treated with 50 μM (-)-blebbistatin to inhibit myosin II and prevent actomyosin-mediated contractility. Traction forces exerted by blebbistatin-treated siVIM-cells were similar to those exerted by siNEG-cells, both of which were significantly reduced compared to DMSO-treated control cells (Figure 4.3c). Following blebbistatin treatment, the average total traction force exerted by siNEG- and siVIM-cells was decreased by approximately 88% and 85%, respectively.

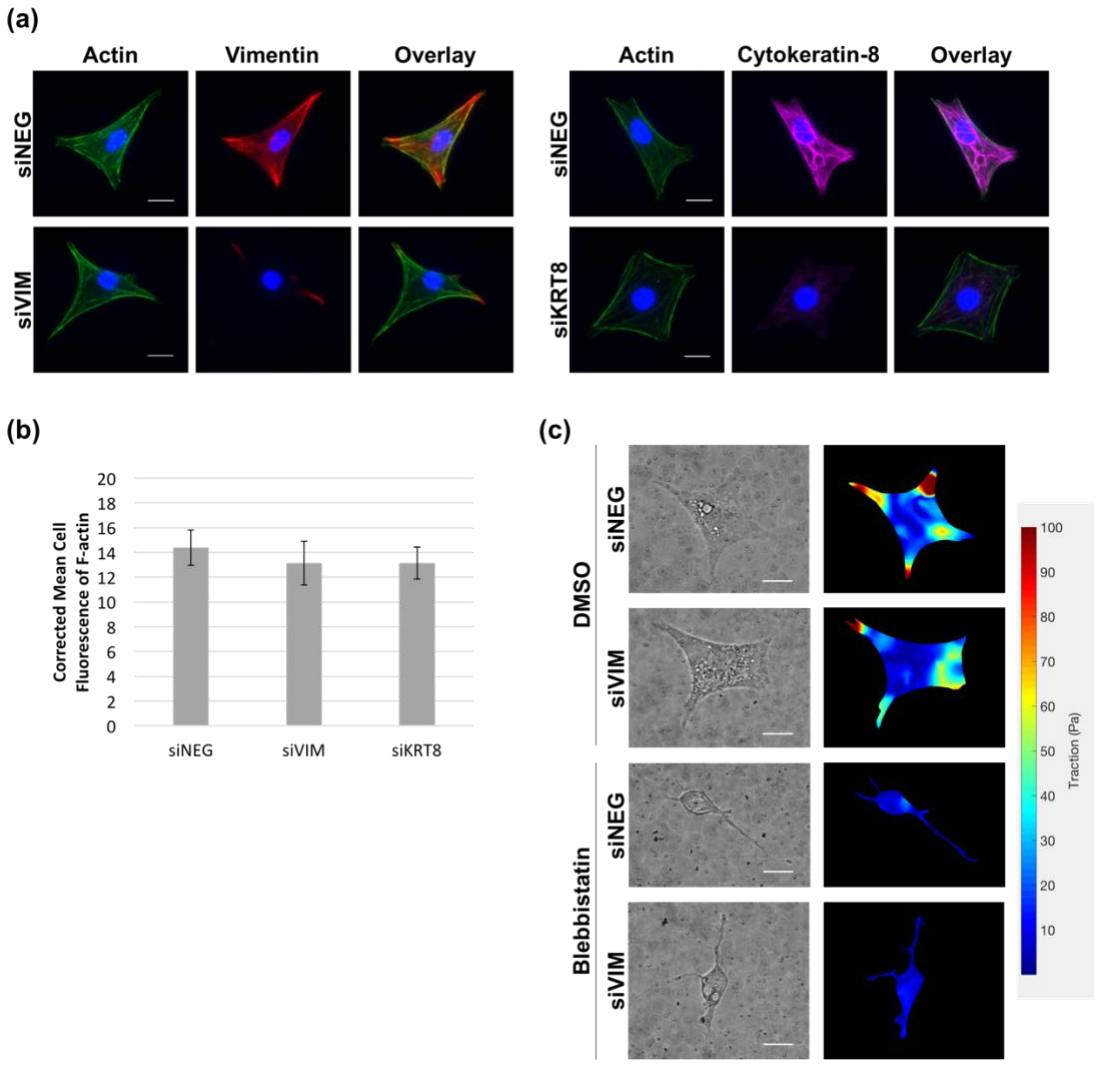

Figure 4.3: F-actin in knockdown cells and its role in cell traction forces. (a) Representative fluorescence images of siNEG-, siVIM, and siKRT8-cells on 5 kPa polyacrylamide gels labeled for vimentin (red) or cytokeratin-8 (magenta), and F-actin (green). Scale bars: 15 µm; (b) Corrected mean cell fluorescence of F-actin in siNEG- (N=38), siVIM- (N=21), and siKRT8- (N=27) cells reported as average ± SEM; (c) Representative phase images and corresponding traction maps of siNEG- and siVIM-cells treated with 50 µM (-)-blebbistatin or DMSO on 5 kPa polyacrylamide gels coated with type I collagen. Scale bars: 25 µm.

4.3.3 Vimentin and Cytokeratin-8 Intermediate Filaments Are Not Essential for Contraction of Collagen Gels

To gain a better understanding of the functional consequences of altered traction force, we examined the effects of decreased vimentin and cytokeratin-8 expression on the ability of chordoma cells to contract collagen gels. Type I collagen gels (0.75 mg/ml) containing siNEG-, siVIM-, and siKRT8-cells all became significantly smaller, as measured by gel surface area, compared with no-cell control gels at all time points (Figure 4.4). While siVIM-cells exhibited increased traction forces relative to siNEG-cells in 2D culture, decreased vimentin expression did not appear to alter contraction of collagen gels (Figure 4.4). Surprisingly, we found that siKRT8-cells consistently contracted collagen gels less than siVIM- and siNEG-cells after 1 day of culture (Figure 4.4), but exhibited faster contraction thereafter, such that there was no difference in gel size by day 8.

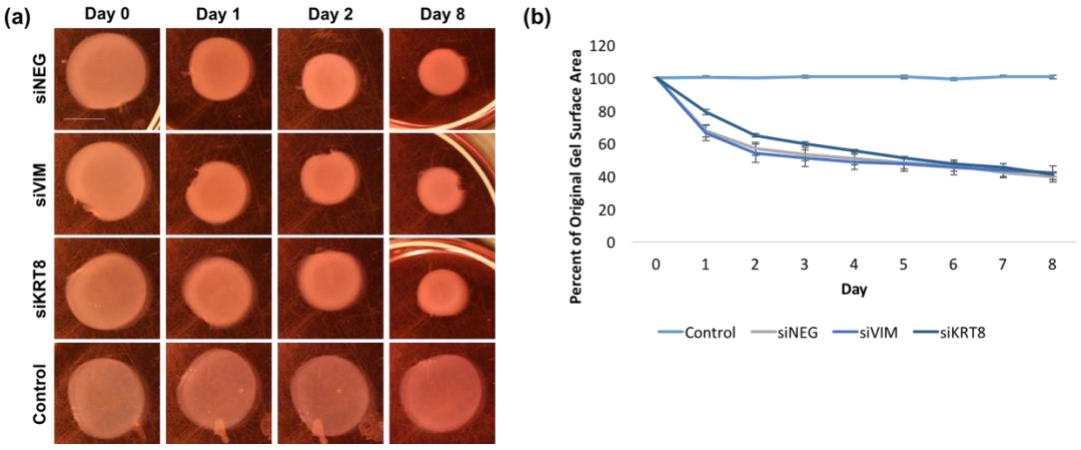

Figure 4.4: The involvement of vimentin and cytokeratin-8 in chordoma cell contraction of collagen in a 3D culture system. (a) Bright field images of collagen gels embedded with siNEG-, siVIM-, and siKRT8-cells on days 0, 1, 2, and 8. No cells were embedded in control gels.

Scale bar: 0.5 mm; (b) Change in gel surface area over 8 days calculated as a percent of the original gel surface area reported as daily averages ± SEM.

4.3.4 Vimentin Intermediate Filaments Contribute to Chordoma Cell Stiffness

The contribution of vimentin and cytokeratin IFs to chordoma cell longitudinal modulus was investigated using vimentin (siVIM) and cytokeratin-8 (siKRT8) knockdown cells. Following overnight culture on 5 kPa Col-PA gels, cell longitudinal modulus was measured using Brillouin confocal microscopy. To control for cell size, cells of similar spread area were selected for analysis. As a result, the average cell area and circularity were not statistically different comparing siNEG, siVIM, and siKRT8 cells measured for cell stiffness analysis (Appendix B; Figure B.1). Cell modulus was significantly decreased in siVIM-cells relative to siNEG- and siKRT8-cells (Figure 4.5b). In contrast, the modulus of siKRT8-cells was not significantly different ($p = 1.0$) than the modulus of siNEG-cells (Figure 4.5b).

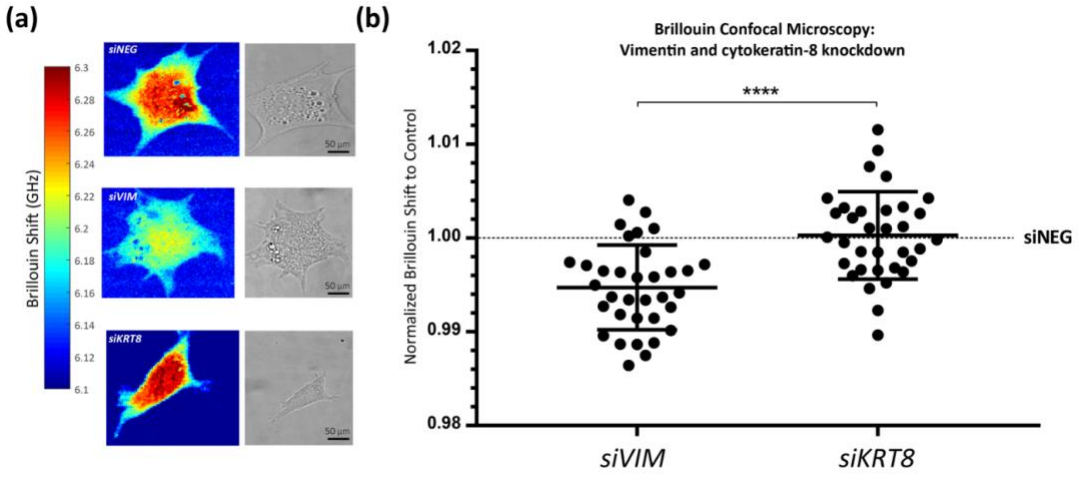

Figure 4.5: The effect of vimentin and cytokeratin-8 knockdown on cell longitudinal modulus. (a) Representative Brillouin maps and bright field images of siNEG-, siVIM-, and siKRT8-

cells. Brillouin shift, represented by the color bar, scales from 6.1 GHz to 6.3 GHz, with increased values referring to increased Brillouin shift (and longitudinal modulus). Scale bars: 50 μm; (b) Brillouin shift of siVIM- and siKRT8-cells normalized to siNEG-cells. Data of each siVIM and siKRT8 cell is reported. *$p < 0.0001$: significance between siVIM- and siNEG-cells, as well as siVIM- and siKRT8-cells.

4.4 Discussion

Because IF protein expression is typically tissue-specific, it is believed that vimentin and cytokeratins have specialized roles. While cell mechanics is primarily attributed to F-actin, both vimentin and cytokeratin IFs have been found to contribute to cell mechanical properties such as cell stiffness and play functional roles in cell mechanosensitivity and contractility [3]–[8]. Additionally, the co-expression of vimentin and cytokeratin IFs has been suggested to enhance cancer cell migration and invasion. However, the roles of vimentin and cytokeratin IFs in chordoma cells have not yet been reported. Results of this study reveal that vimentin IFs are involved in chordoma cell mechanobiology. We found that decreased vimentin expression via RNAi disrupted chordoma cell mechanosensitivity to substrate rigidity, increased cell traction forces, and decreased cell stiffness. Surprisingly, significant differences were not observed in chordoma cells with decreased cytokeratin-8 expression. Together, our findings suggest that chordoma cell mechanobiology is more dependent on vimentin than cytokeratin IFs.

The involvement of vimentin and cytokeratin IFs in chordoma cell mechanosensitivity to substrate stiffness was examined by measuring cell spread area and circularity of vimentin and cytokeratin-8 knockdown chordoma cells cultured on PA gels of varied stiffness. Generally, increased substrate stiffness encourages greater

cell spreading [165]. This behavior was observed for siNEG chordoma cells and did not appear to be affected by decreased cytokeratin-8 expression. In contrast, knockdown of vimentin expression appeared to dysregulate chordoma cell mechanosensing. Interestingly, significant cell spreading was observed in vimentin knockdown cells on 0.42 kPa Col-PA gels, a modulus on the order of brain tissue. This contradicts previously reported studies by others showing vimentin knockdown reduced cell spreading and adhesions [166], [167].

Visualizing the cytoskeleton via immunofluorescence, we have generally observed vimentin IFs to concentrate at the chordoma cell periphery and focal adhesions. Similarly, residual vimentin in our vimentin knockdown cells tended to localize only at the cell periphery and the distal ends of cell protrusions. However, whereas normal chordoma cells also exhibit a vimentin network across the cell body, this was completely absent in vimentin knockdown cells. Previous studies have also reported the association between vimentin IFs and focal adhesions [81], [91], [133]. Additionally, when vimentin was transfected into human breast cancer cells, vimentin quickly (within 12 h) became associated with focal adhesions, when the majority of vimentin was still in the form of particles and short filaments [91]. It is possible that despite decreased vimentin expression, the strong association of residual vimentin with focal adhesions is contributing to cell spreading.

In addition to significant cell spreading, vimentin knockdown cells cultured on 5 kPa PA gels exerted greater traction forces than control and cytokeratin-8 knockdown cells. Specifically, the maximum traction stress was significantly greater in vimentin knockdown cells. As the maximum traction stress corresponds to a particular point

under the cell, measurements were not skewed by cell area. In support of our findings, vimentin depletion in human osteosarcoma cells was found to induce the assembly of actin stress fibers and increase cell traction forces [6]. Blebbistatin-treatment of our vimentin knockdown cells resulted in decreased traction forces similar to those of blebbistatin-treated control cells. Our interpretation of these results is that greater traction forces are most likely due to over compensation of F-actin following the loss of a vimentin IF network. Others have observed in vimentin knockout cells with increased stress fiber assembly, that reintroducing nonfilamentous 'unit length form' vimentin could not rescue the stress fiber phenotype. However, introduction of full-length GFP-vimentin was capable of diminishing stress fiber assembly [6]. Despite vimentin remnants in our vimentin knockdown cells, the lack of a vimentin IF network throughout the cell body may be encouraging the assembly of actin stress fibers, leading to increased cell contractility.

To further examine the functional impact of vimentin and cytokeratin knockdown on cell contractility, we embedded cells within type I collagen gels and measured their ability to contract the 3D collagen matrix. Inconsistent with traction force observations in 2D, knockdown of vimentin expression did not appear to increase cell contractility in 3D culture. However, altered cell traction forces may have a greater impact on cell migration, rather than collagen contraction. Examining collagen gels over an 8-day period, we found both vimentin- and cytokeratin-deficient cells were capable of contracting collagen gels and no significant differences in collagen gel diameter were observed when compared to control cells. In contrast with our findings, vimentin-deficient fibroblasts derived from mouse embryos displayed significantly

impaired contraction of collagen gels [85]. We may not be observing impaired contraction of collagen gels in vimentin knockdown chordoma cells because of their continued expression of cytokeratin IFs, which are not present in fibroblasts. When compared to fibroblasts, keratinocytes, which co-express cytokeratins and vimentin [90], [168], have been found to produce greater collagen gel contraction [169]. The decrease in collagen gel contraction we observed in our cytokeratin-8 knockdown cells suggests cytokeratin, rather than vimentin, IFs may play a greater role in chordoma cell contractility in 3D.

Finally, we utilized Brillouin microscopy to measure cell mechanical properties. We found cell longitudinal modulus was significantly reduced in vimentin-knockdown chordoma cells, but unchanged in cytokeratin-8-knockdown cells. Using the relationship between Brillouin shift and longitudinal modulus previously reported [163], we were able to estimate the percent difference in the Young's moduli between knockdown and control cells. Based on the average Brillouin shift for each sample, we estimate the respective Young's moduli of vimentin- and cytokeratin-8-knockdown cells to be approximately 13% and 1% less than that of control cells. Similarly, vimentin-deficient fibroblasts have been found to have reduced cell stiffness compared to wild-type cells [4], [85], [170], and a comparable decrease (20%) in the Young's modulus of vimentin-null relative to normal fibroblasts has been measured by AFM [8]. We may not have observed as great of a decrease in the Young's modulus as 20% because vimentin is not completely ablated in our system. Additionally, our vimentin-knockdown chordoma cells continue to express cytokeratin IFs, which are not present in fibroblasts. In contrast to our results, cytokeratin-knockout keratinocytes were

previously found to be 60% more deformable than wild-type keratinocytes which also inherently co-express vimentin and cytokeratins [3]. It is unclear whether our observations differ for cytokeratin-8-knockdown cells because of the differences in cell type, degree of knockdown, or method of measuring cell stiffness. Our findings implicate vimentin IFs contribute to chordoma cell stiffness to a greater degree than cytokeratin-8 IFs.

4.5 Conclusion

To our knowledge, this is the first study to investigate the roles of vimentin and cytokeratin IFs in chordoma cell mechanobiology. Our findings suggest vimentin IFs play a critical role in maintaining cell stiffness, sensing substrate rigidity, and generating traction forces in chordoma cells. Because we did not observe significant changes in chordoma cell mechanics following cytokeratin-8 knockdown, it is suggested vimentin IFs have a more prominent role than cytokeratin IFs. Mechanical cues are critical determinants of cell function and abnormal changes in cell and tissue mechanics can lead to disease. Understanding the involvement of vimentin and cytokeratin IFs in chordoma cell mechanobiology may provide insight into chordoma progression, which is necessary for the development of effective treatments.

Chapter 5: The Involvement of Vimentin and Cytokeratin-8 Intermediate Filaments in Chordoma Cell Malignant Behaviors

5.1 Introduction

Chordoma, a malignant tumor that develops from notochordal remnants, is often associated with poor prognosis due to delayed diagnosis (1.5 years on average) [171], with a propensity toward recurrence (68%) [172], [173], and with resistance to radiation [174] and traditional cytotoxic chemotherapeutic agents [1], [66]. Based on the sparse clinical data collected on chordoma, the incidence of chordoma metastases has been reported to be between 3 to 48% [173], [175]. Similar to other cancers, chordoma metastasis increases the risk of tumor-related death [176]. Compared to healthy tissue, tumors tend to be stiffer and the increased tissue stiffness has been found to promote a malignant cell phenotype [13], [14]. Through integrins and the cytoskeleton, cells are capable of probing the mechanical properties of their surrounding ECM and adjusting their mechanical properties and behaviors in response. As a result, cellular processes, such as migration and proliferation, are affected by cell-ECM interactions [177], [178]. Cell mechanobiology and ECM rigidity has also been associated with cancer cell chemoresistance [179]–[181]. Because we previously found decreased vimentin expression affected chordoma cell mechanobiology, we sought to further explore the effects on cellular processes associated with cancer progression.

Cancer cells, including chordoma, commonly co-express vimentin and cytokeratin IFs. This co-expression has been hypothesized to promote cell invasion and cancer metastasis [17]. Increased vimentin expression, associated with the EMT,

typically enhances cell motility and promotes cancer metastasis. For instance, the overexpression of vimentin has been connected to tumor metastasis in a variety of cancers such as melanoma [15], prostate carcinoma [19], breast cancer [17], and hepatocellular carcinoma [18]. Similarly, decreased vimentin expression has been found to reduce cell migration and invasion in cancerous and non-cancerous cells alike [10], [12], [85], [103]. Due primarily to its association with increased metastasis, vimentin expression is associated with poor cancer prognosis [104]. The role of cytokeratin expression in cell migration is less clear than that of vimentin and appears to be cancer type-specific. Knockdown of cytokeratins 8 or 18 decreased cell migration and invasion in non-small lung cancer and oral squamous cell carcinoma [9], [84], but increased cell migration and invasion in liver hepatocellular carcinoma cells [11]. Additionally, the overexpression of cytokeratins 8 and 18 have been associated with increased migration in melanoma cells [16], but reduced cell invasion in breast cancer cells [102].

IFs have also been suggested to play a role in cancer cell resistance to traditional cytotoxic chemotherapeutic drugs, such as cisplatin and paclitaxel. Cisplatin induces apoptosis through its direct binding to DNA, and paclitaxel inhibits cell division through its specific binding to microtubules. In non-small cell lung cancer and gastric cancer cells, EMT suppression, characterized by decreased vimentin expression, was found to increase cell sensitivity to cisplatin [20], [22]. Cisplatin sensitivity was also increased in epithelial cancer and nasopharyngeal carcinoma cells following the knockdown of cytokeratins 8 and 18 [11], [21]. Similarly, knockdown of cytokeratin 18 enhanced paclitaxel-induced apoptosis in non-small cell lung cancer cells [84].

However, decreased expression of cytokeratins 8 and 18 have also been associated with poor prognosis in breast and colorectal cancer [108], [109]. While increased expression of both vimentin and cytokeratin-8 have been found to contribute to cancer cell resistance to chemotherapy, their roles in chordoma chemoresistance have not yet been reported.

Chordoma progression is commonly associated with the expression of various genes, including brachyury (T), SHH, and N-cadherin, that are consistently identified in chordomas. Both SHH and brachyury play essential roles in embryonic development, regulating notochord formation and patterning of the axial skeleton and neural tube. However, following embryonic development, overexpression of SHH and brachyury have been associated with tumor formation and progression [124], [125]. It is theorized that the reactivation of SHH in notochordal remnants could cause a malignant transformation [182]. Because of the high, consistent expression of brachyury in chordoma tumors, and its significant contribution to chordoma pathogenesis, brachyury has been identified as a diagnostic marker and is actively being researched in clinical trials as a therapeutic target for chordoma [52], [55], [69], [183]. Increased expression of brachyury, SHH, and N-cadherin have all been connected to EMT [125]–[130], increased vimentin expression, and enhanced chordoma cell proliferation, migration, and invasion [184].

In this study, we examined the involvement of vimentin and cytokeratin-8 expression in chordoma cell migration, invasion, gene expression, and chemoresistance. Similar to our previous studies, we accomplished this using RNAi to knockdown vimentin and cytokeratin-8 expression in the human chordoma cell line

(MUG-Chor1). Our findings suggest that both vimentin and cytokeratin-8 IFs contribute to chordoma cell migration, but only vimentin, and not cytokeratin-8, IFs are essential for chordoma cell invasion. Further, we found vimentin knockdown resulted in decreased SHH expression in chordoma cells cultured on rigid substrates. Our data also suggests increased vimentin expression may contribute to chordoma chemoresistance.

5.2 Materials and Methods

5.2.1 Cell Culture

Similar to previous studies, MUG-Chor1 chordoma cells (ATCC Cat# CRL-3219, RRID:CVCL_9277) were cultured in Iscove's Modified Dulbecco's Medium: Roswell Park Memorial Institute 1640 Medium (4:1) (Gibco/Thermo Fisher Scientific) supplemented with 10% FBS (Gibco/Thermo Fisher) and 1% Penicillin-Streptomycin (Gibco/Thermo Fisher). Media was exchanged every 2-3 days and cells were cultured at 37°C, 5% CO_2.

5.2.2 Transfection of siRNA

To decrease vimentin and cytokeratin-8 expression, chordoma cells were transfected with siRNA, as previously described. Cells were plated at a density of 10,000 cells/cm2 onto TCTP coated with rat tail type I collagen (Advanced BioMatrix). The following day, cells were transfected with Silencer Select Pre-designed siRNA (Ambion/Thermo Fisher) targeting KRT8 (s7970), VIM (s14798), or Silencer Select Negative Control No. 1 siRNA (Ambion/Thermo Fisher) using Lipofectamine 2000

(Invitrogen/Thermo Fisher) diluted in reduced serum opti-MEM (Thermo Fisher) for a duration of 24h. Six days after transfection, cells were detached using 0.25% trypsin-EDTA (1x) and processed for the analysis of cell migration, transwell invasion, and viability. Fourteen days after transfection, cells were processed for the analysis of gene expression and viability.

5.2.3 Cell Migration

Control and vimentin and cytokeratin-8 knockdown cells were plated on bare, type I collagen-, or laminin-coated plastic (50-65 μg/ml) in 2 well silicone inserts (Ibidi). Cells were suspended in chordoma growth media at a concentration of $1x10^6$ cells/ml and 70 μl of the cell suspension was added per well of the insert. Following 24h of culture, culture inserts were removed, leaving a 500 μm cell-free gap between two confluent cell monolayers. For each sample, two (x,y) positions of the cell-free gap were randomly selected and imaged every 24h for 4 days under phase microscopy (100x magnification) using a Nipkow (spinning) disk-equipped Olympus IX81 microscope. In ImageJ, captured images were used to measure the area of the cell-free gap at each time point. For both (x,y) positions, the area of the cell-free gap was divided by its length to calculate the average gap width of each sample. For each time point, the average gap width was subtracted from the initial gap width to determine the total migration distance (μm). Instead of assuming inserts formed cell-free gaps of 500 μm in width, the average width of the initial cell-free gap was also calculated. The total migration distance for each time point was normalized by the initial gap width and an average of the two (x,y) positions was calculated. At least three independent

experiments were performed for each group and data are reported as the average ± SEM.

5.2.4 Cell Invasion

Corning BioCoat Angiogenesis Systems (Corning, Corning, NY, USA) were utilized for the analysis of cell invasion. These systems consist of a Corning Fluoroblok 24-multiwell insert plate with 3 µm pore size Polyethylene Terephtalate (PET) membranes that were pre-coated with Corning Matrigel® Matrix. The uniform Matrigel coating occludes the PET membrane pores and blocks non-invasive cells. Control and knockdown cells were re-suspended in serum-free growth media (2.0×10^5 cells/ml) and added to the top chamber of the plates onto the Matrigel-coated inserts (50,000 cells/insert). Growth media containing 10% FBS was then added as a chemoattractant through a sample port to the bottom chamber of the plate. Cells were incubated for 48 hours at 37°C, 5% CO_2. After 24 hours, an additional 250 µl/insert of serum-free media was added to the top chambers to ensure complete hydration over the 48-hour incubation period.

To visualize live, invaded cells at the 48-hour time-point, inserts were stained with calcein AM (Invitrogen/Thermo Fisher) and the nuclear counterstain Hoechst 33342 (Invitrogen/Thermo Fisher Scientific). Because the Corning Fluoroblok membrane is designed to block the passage of light from 490-700 nm, we were able to specifically detect the fluorescence of cells that had passed through the membrane using a Nikon Ti2-E Inverted Automated Microscope. Fluorescence images were captured (x200 magnification) across the entire surface area of each insert with a tile-

scan and images were subsequently stitched together to visualize all of the invaded cells/insert. Calcein AM-stained cells were counted using NIS-Elements Software and the total number of invaded cells/insert was quantified. Four separate samples were examined for each cell type and data are reported as the average ± SEM.

5.2.5 Collagen Gel Preparation

Six days after transfection, cells were detached using 0.25% trypsin-EDTA (1x) and seeded on top of or embedded within type I collagen gels for an additional 8 days of culture. Collagen pre-gel solutions were prepared by mixing 9 parts of 4 mg/ml rat tail type I collagen (Advanced BioMatrix) with 1-part neutralization solution (Advanced Biomatrix). For 2D culture, pre-gel solutions (1 ml) were added to 6-well tissue culture-treated plates and incubated for 1 hour at 37°C to promote gelation. The final gel thickness was estimated to be approximately 1 mm. Cells were plated on top of gels at a density of 10,000 cells/cm^2. For 3D culture, cells suspended in chordoma growth media were mixed into collagen pre-gel solutions for final cell and collagen concentrations of 1x10^6 cells/ml and 2.7 mg/ml, respectively. Collagen solutions containing cells were added to 48 well plates (125 µl/well) and allowed to incubate for 20 minutes at 37°C. Once gels had formed, 500 µl of chordoma growth media was added on top of each gel. After 8 days of culture, corresponding to 14 days post-transfection, cells were processed for gene expression analysis.

5.2.6 Gene Expression

As previously described, RNA isolation was performed using phenol-chloroform extraction. Cells were lysed with TRIzol (Ambion/Thermo Fisher Scientific) and RNA was precipitated from the resulting lysate using chloroform and isopropanol. To quantify expression of VIM, KRT8, T, SHH, CDH2, and 18S (Table 3.1), reverse transcribed RNA samples underwent qRT-PCR (MyiQ System, BioRad) using SsoFast EvaGreen Supermix (BioRad, Hercules, CA, USA). Using 18S as a housekeeping gene, relative quantitation of qRT-PCR data was performed using the $\Delta\Delta C_t$ method. Briefly, ΔC_t values were computed by subtracting C_t values of the 18S control gene from those of each gene of interest (i.e., $\Delta C_{t\,SHH} = C_{t\,SHH} - C_{t\,18S}$). For each gene of interest, $\Delta\Delta C_t$ values were computed by subtracting ΔC_t values of the reference sample (e.g. cells transfected with negative control siRNA), from ΔC_t values of cells transfected with siRNA targeting either VIM or KRT8 ($\Delta\Delta C_{t\,SHH;VIM\,siRNA} = \Delta C_{t\,SHH;VIM\,siRNA} - \Delta C_{t\,SHH;NC\,siRNA}$). Using $\Delta\Delta C_t$ values, relative changes in mRNA levels (fold difference) were expressed through the exponential relation: $2^{-\Delta\Delta Ct}$. Technical replicates for each sample, along with appropriate no RT and no template controls, were performed in triplicate. Data collected over three independent cell transfections (n=3) for each of the siRNA groups are reported as the average of the range of the fold difference, which incorporates the standard deviation of the $\Delta\Delta C_t$ value [142], [143].

5.2.7 Western Blotting

For protein extraction, cells were detached from culture surfaces using 0.25% trypsin-EDTA (Gibco/Thermo Fisher) and re-suspended in a lysis buffer supplemented with a 1:100 concentration of protease inhibitor cocktail (Thermo Fisher), as previously described. Protein concentrations were determined using a modified Lowry assay with a Folin-Phenol color reaction detected by a ND-1000 Spectrophotometer. For SDS-Page, protein extracts were mixed (1:1) with a loading buffer (13% (v/v) Tris-HCl, 20% (v/v) glycerol, 4.6% (w/v) SDS, 0.02% (w/v) bromophenol blue, 200 mM dithiothreitol) and subsequently loaded (8µg of protein per sample) into pre-cast Criterion Tris-HCl gels (BioRad). Proteins were electrophoretically transferred to polyvinylidene fluoride membranes and detected using rabbit IgG anti-vimentin polyclonal (Abcam) and mouse IgG1 anti-cytokeratin-8 [M20] (Abcam) antibodies in combination with Vectastain ABC-AmP for chromogenic detection. GAPDH, detected with a rabbit IgG anti-GAPDH [EPR16884] (Abcam) antibody, was used as a loading control. Semi-quantitative analysis was performed using ImageJ (https://imagej.nih.gov/ij/, RRID:SCR_003070) to determine vimentin and cytokeratin-8 band intensities normalized to GAPDH. Protein expression levels are reported as experimental relative to cells transfected with negative control siRNA ± SEM.

5.2.8 Immunofluorescence

Immunofluorescence was used to verify IF knockdown and visualize cytoskeletal proteins following cell treatment with the chemotherapy agent cisplatin.

As previously described, cells were fixed with 4% PFA, permeabilized using 0.1% Triton X-100, and labelled with rabbit IgG anti-vimentin [SP20] (Thermo Fisher Scientific) or mouse IgG1 anti-cytokeratin-8 [M20] (Abcam) antibodies. A biotinylated (anti-rabbit IgG) secondary antibody (Vector Laboratories) was used in combination with Texas Red-labelled streptavidin (Vector Laboratories) to visualize vimentin. An Alexa Fluor 594-conjugated (anti-mouse IgG) secondary antibody (Thermo Fisher Scientific) was used to visualize cytokeratin-8. Cells were stained with Alexa Fluor 488 Phalloidin (Invitrogen/Thermo Fisher Scientific) to visualize F-actin, and DAPI (Invitrogen/Thermo Fisher Scientific) was used as a nuclear counterstain. A Nipkow (spinning) disk-equipped Olympus IX81 microscope was used to capture images at x100 magnification. Confocal fluorescence images were taken at x600 magnification and Z-stacks (1 μm slices) were projected into a single image for analysis.

5.2.9 Polyacrylamide Gel Preparation

PA gels corresponding to stiffnesses of 1 kPa (3% acrylamide + 0.2% bis acrylamide) and 13 kPa (8% acrylamide + 0.2% bis acrylamide) were prepared on glass coverslips (12-15mm). The stiffness of gels formed with these acrylamide to bis-acrylamide ratios has previously been confirmed using DMA and AFM [159], [160]. As previously described, glass coverslips were coated with 0.1M NaOH, air dried, coated with 3-amino-propyltrimethoxysilane, and fixed with 0.5% glutaraldehyde in PBS. Pre-gel solutions were added onto activated glass coverslips and distributed evenly across the surface by placing a coverslip of equivalent size on top of the solution. Gel polymerization was initiated with 10% ammonium persulfate and catalyzed with

TEMED. After 30 minutes, the top coverslip was removed and polymerized gels were treated with sulfo-SANPAH for the chemical crosslinking of laminin (MilliporeSigma) to the gel surface.

5.2.10 Chemotherapy Drug Sensitivity

The effects of IF protein knockdown and substrate stiffness on the sensitivity of chordoma cells to standard chemotherapeutic agents were examined *in vitro* using an alamarBlue® cell viability assay (Thermo Fisher Scientific). Thirteen days after transfection, vimentin knockdown cells were transferred to 24- or 48-well tissue culture-treated plates. For substrate stiffness analysis, non-transfected chordoma cells were plated on BME gels, laminin-coated PA gels (1, 13kPa), and laminin-coated glass. Laminin-rich BME gels were formed by dispensing unpolymerized BME (Trevigen) onto 12-15 mm diameter glass coverslips (~60 µl/cm^2) and incubating for 30 minutes at 37C. Laminin-coated glass substrates were prepared by absorbing laminin (65 µg/ml) from EHS murine sarcoma basement membrane (MilliporeSigma) onto glass coverslips (12-15mm). Cells were cultured overnight to promote cell attachment before treatment with 20 µM cisplatin (Selleck Chemicals, Houston, TX, USA) or 5 µM paclitaxel (Selleck Chemicals). Due to the interference of serum with the alamarBlue cell viability reagent, drugs were diluted in reduced-serum media (2% FBS). Untreated or DMSO-treated reduced-serum media was added to cells to serve as controls for cisplatin and paclitaxel, respectively. After two or five days of treatment, the alamarBlue cell viability reagent was added to cells. Following 24h incubation with alamarBlue, corresponding to three or six day incubations with chemotherapeutic

drugs, plates were analyzed using a SpectraMax® M5 Microplate Reader (Molecular Devices, San Jose, CA, USA). Increased incubation time with alamarBlue allowed for the detection of small differences in cell viability. Relative fluorescence unit (RFU) values of samples containing the same media, but no cells, were subtracted from cell samples to calculate corrected RFU values. The percent cell survival was determined using the following equation: [(corrected average RFU of treated cells / corrected average RFU of untreated cells) x 100]. Data are reported as the average ± SEM.

5.2.11 Statistical Analysis

Statistical analyses were completed using SPSS (http://www-03.ibm.com/software/products/en/spss-statistics/, RRID:SCR_002865) and statistical significance was set to ($\alpha = 0.05$). One-sample t-tests were used to compare the relative expression of cytokeratin-8 and vimentin, as measured by Western blot, in siVIM- and siKRT8-cells to that of siNEG-cells. One-sample t-tests were also used to compare the percent cell survival of cells treated with cytotoxic drugs to the percent cell survival of untreated cells (100%). Two-sample t-tests were used to compare gene expression of siVIM- and siKRT8-cells to siNEG-cells. For all other studies, Kruskal-Wallis followed by Mann-Whitney U tests for independent samples were performed.

5.3 Results

5.3.1 Knockdown of Vimentin and Cytokeratin-8 Decreases Chordoma Cell Migration

Modified wound healing assays, utilizing 2 well inserts with a defined cell-free gap, were performed to investigate the involvement of vimentin and cytokeratin-8 IFs

in chordoma cell migration. Because chordoma cells were found to migrate at a slow rate, cell-free gaps were examined over 96h. On bare and collagen-coated plastic, siVIM and siKRT8 cell migration was decreased compared to siNEG-cells (Figure 5.1a, b). Significant differences were observed at 48, 72, and 96h on bare plastic and at 48h on collagen (Figure 5.1a, b). Differences in migration were not observed between cell types on laminin-coated plastic (Figure 5.1c). Compared to other substrates, cell migration was overall decreased on laminin.

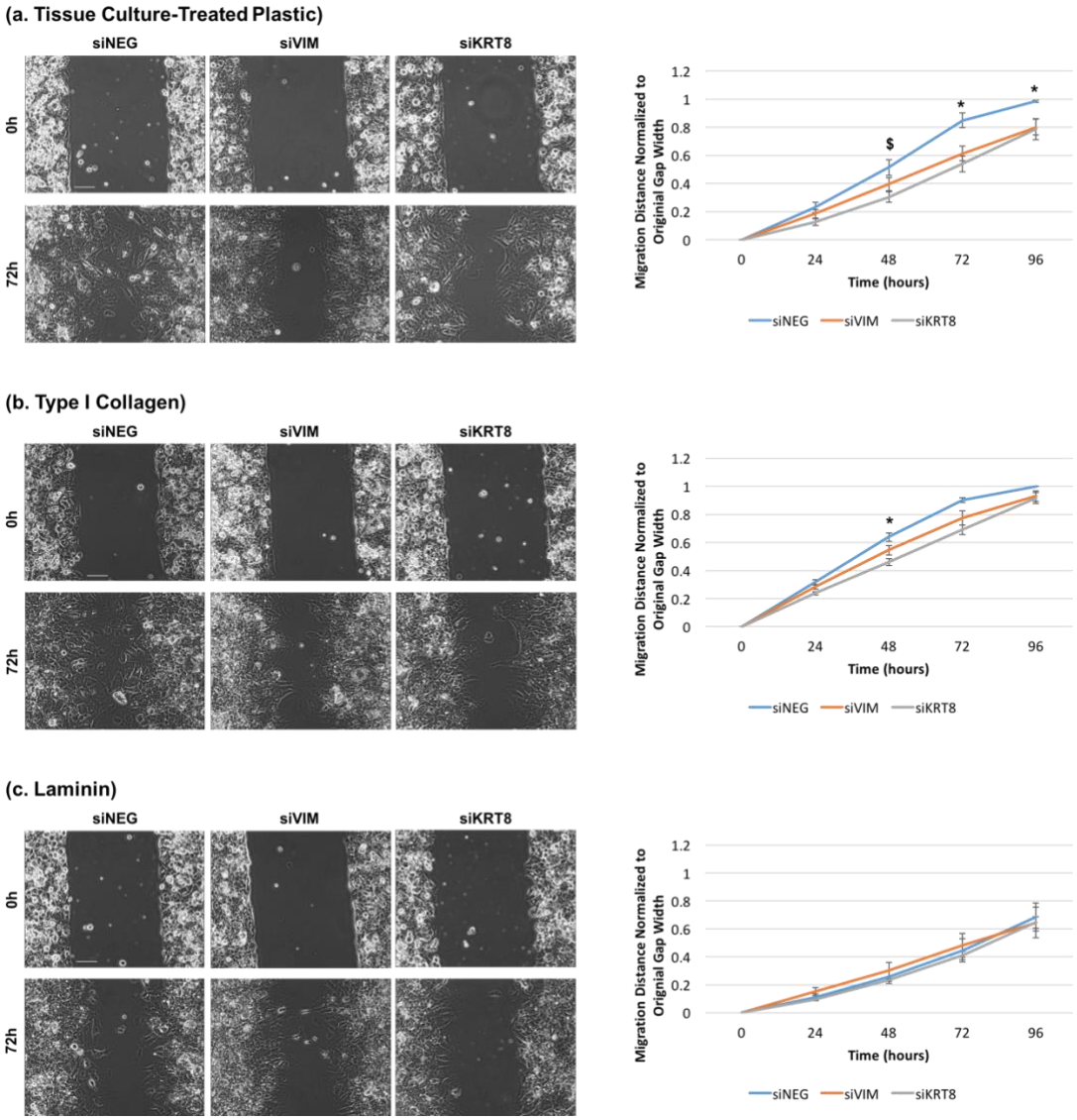

Figure 5.1: The effect of vimentin and cytokeratin-8 knockdown on chordoma cell migration in 2D. (a), (b), and (c) Representative phase images of siNEG-, siVIM-, and siKRT8-cells on bare, type I collagen-, and laminin-coated plastic at 0 and 72 hours after removing cell divider. Scale bars: 100 µm. Cell migration normalized to cell-free gap at 0h reported as the daily average ± SEM. $p < 0.05$: * relative to siVIM- and siKRT8-cells; $ relative to siKRT8-cells.

5.3.2 Chordoma Cell Invasion is Dependent on Vimentin Intermediate Filaments

The invasive behavior of chordoma cells with vimentin and cytokeratin-8 RNAi was analyzed using Corning Fluoroblok 24-multiwell insert plates with Corning

Matrigel® Matrix pre-coated PET membranes (3 µm pores). Similar to cell migration in 2D culture, significantly fewer siVIM-cells invaded through the Matrigel membrane compared to siNEG-cells (Figure 5.2a, b, d). In contrast, the number of invaded siKRT8-cells was not statistically different from the number of invaded siNEG-cells (Figure 5.2a, c, d). While markedly more siKRT8-cells invaded compared to siVIM-cells, these differences were not statistically different (Figure 5.2b, c, d).

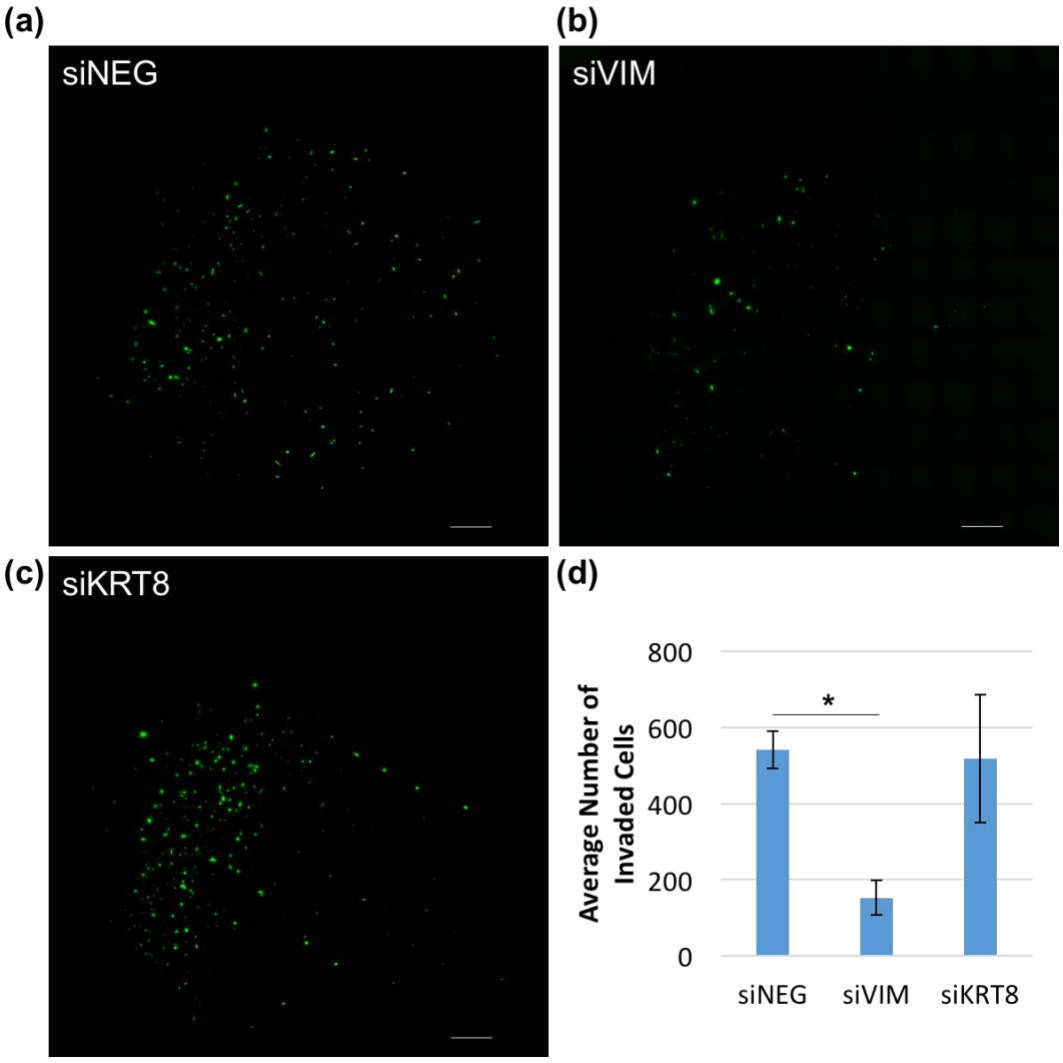

Figure 5.2: The effect of vimentin and cytokeratin-8 knockdown on chordoma cell invasion. Representative fluorescence images of (a) siNEG-, (b) siVIM-, and (c) siKRT8-cells stained

with calcein-AM that have invaded through 3 µm pore-PET membranes coated with Matrigel. Scale bars: 500 µm; (d) The number of invaded siNEG-, siVIM-, and siKRT8-cells per insert after 48h of culture reported as the average ± SEM. *$p < 0.05$.

5.3.3 Vimentin Knockdown via RNAi is Stable in Chordoma Cells over Fourteen Days of Culture

To mitigate cellular side effects from the transfection process, such as decreased cell proliferation, and to allow for potential changes in the cell phenotype following IF protein knockdown, we chose to increase the culture time of siRNA-transfected cells prior to processing. Similar to analyses on day six (Chapter 3.3.3), when cells were examined fourteen days after transfection, chordoma cells transfected with siRNA targeting VIM (siVIM) exhibited significant decreases in vimentin expression. In contrast, cytokeratin-8 expression was not significantly different in siKRT8-transfected cells relative to siNEG-transfected cells examined fourteen days after transfection (Figure 5.3a). Through semi-quantitative analysis of western blotting, an approximate 50% decrease in vimentin expression was measured in siVIM-transfected cells compared to siNEG-transfected cells (Figure 5.3a). Decreased vimentin expression was also visualized by immunofluorescence (Figure 5.3b) and quantified by qRT-PCR (Figure 5.4).

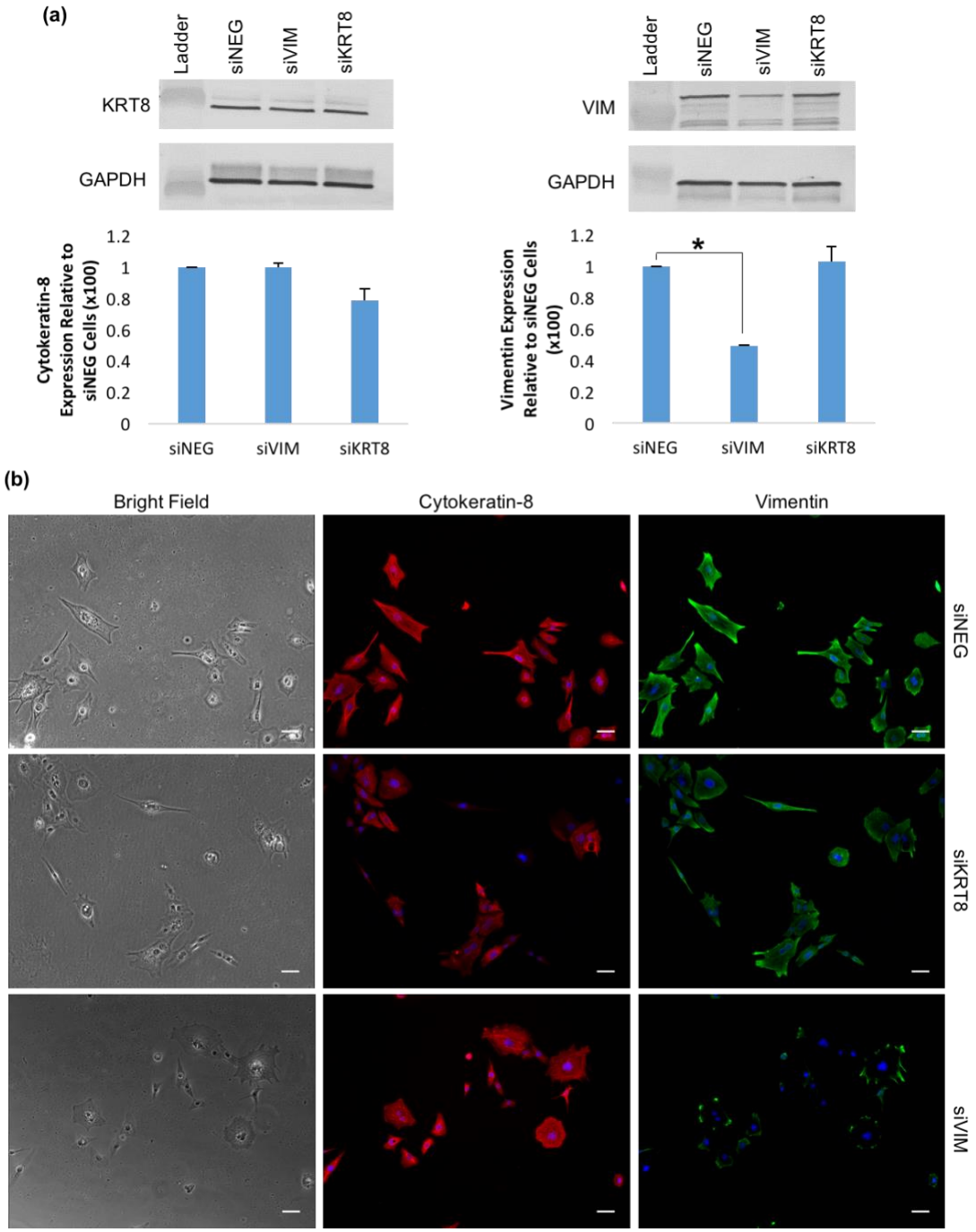

Figure 5.3: Characterization of cytokeratin-8 and vimentin knockdown in chordoma cells fourteen days after transfection with siRNA. (a) Western blot of siKRT8- and siVIM-transfected cells analyzed relative to siNEG-transfected cells. Data is reported as the average ± SEM. *p< 0.05, relative to siNEG-cells. KRT8 and VIM band intensities normalized to

GAPDH; (b) Representative bright field and fluorescence images of siNEG-, siKRT8- and siVIM-transfected cells. Cytokeratin-8 (red) and vimentin (green). Scale bars: 50 μm.

5.3.4 Knockdown of Vimentin Decreases Sonic Hedgehog Expression in Chordoma Cells on Rigid Substrates

The expression of phenotypic genes, previously examined six days after siRNA transfection (Chapter 3.3.5), was re-examined fourteen days after siRNA transfection. Gene expression was examined of cells in 2D (on type I collagen-coated plastic and type I collagen gels) and 3D (embedded in type I collagen gels) culture. Both knockdown and control cells were cultured on the same substrate for comparison. On type I collagen-coated plastic, SHH expression was significantly decreased in siVIM-cells relative to siNEG-cells (Figure 5.4a). This effect was dependent on culture condition, as SHH expression was not decreased in siVIM-cells relative to siNEG-cells when cells were cultured on top of or embedded within type I collagen gels (Figure 5.4b, c). Cytokeratin-8 expression returned to levels comparable to siNEG control at fourteen days, indicating knockdown was transient. Not surprisingly, chordoma cell gene expression was not significantly different between siKRT8- and siNEG-cells.

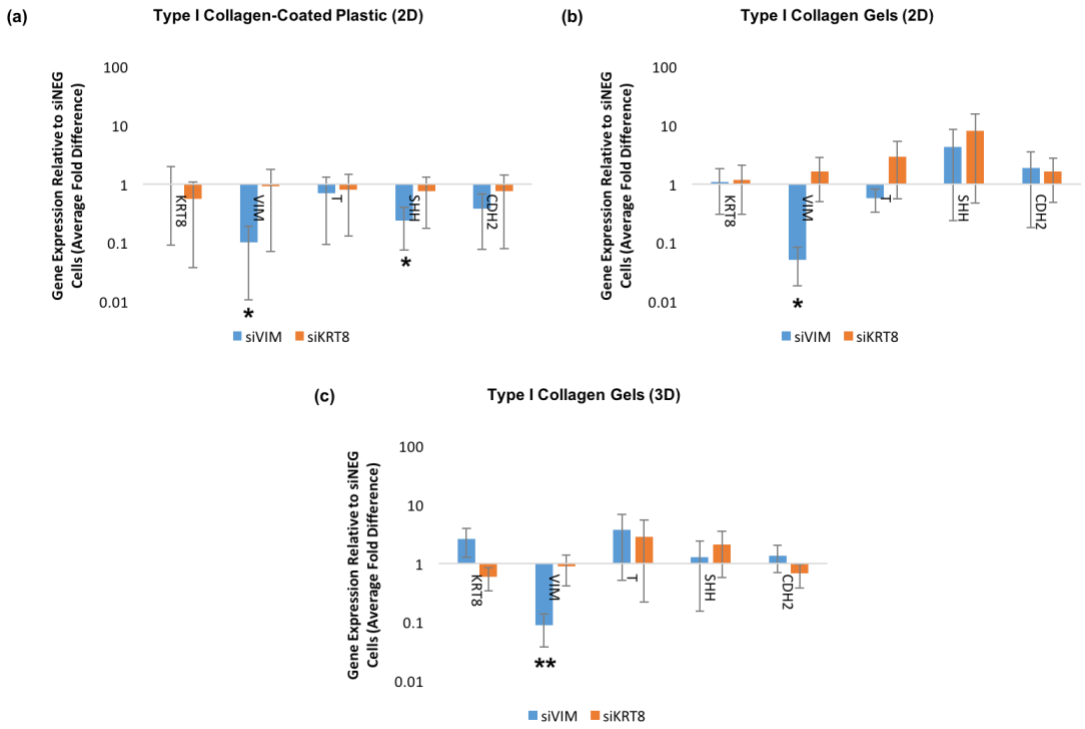

Figure 5.4: The effect of vimentin knockdown in chordoma cells on their expression of phenotypic genes. Gene expression of cells processed for analysis fourteen days after transfection with siRNA. siKRT8- and siVIM-transfected cells analyzed relative to siNEG-transfected cells cultured (a) in 2D on plastic coated with type I collagen; (b) in 2D on type I collagen gels; (c) in 3D in type I collagen gels. *p< 0.05 and **p<0.01, relative to siNEG-cells.

5.3.5 Vimentin Expression May Contribute to Chordoma Cell Resistance to Chemotherapeutic Agents

To improve our understanding of the relationship between IFs and the response of chordoma cells to cytotoxic chemotherapeutic agents, we examined the intensity and organization of vimentin and cytokeratin-8 IFs in chordoma cells treated with cisplatin via immunostaining and fluorescence imaging. We observed increased fluorescence intensity of vimentin in cisplatin-treated chordoma cells compared to untreated chordoma cells (Figure 5.5). Cisplatin treatment did not noticeably affect the

fluorescence intensity of cytokeratin-8, but appeared to induce changes in cytokeratin-8 IF organization. In cisplatin-treated cells, cytokeratin-8 was commonly observed to be concentrated at the cell nucleus (Figure 5.5).

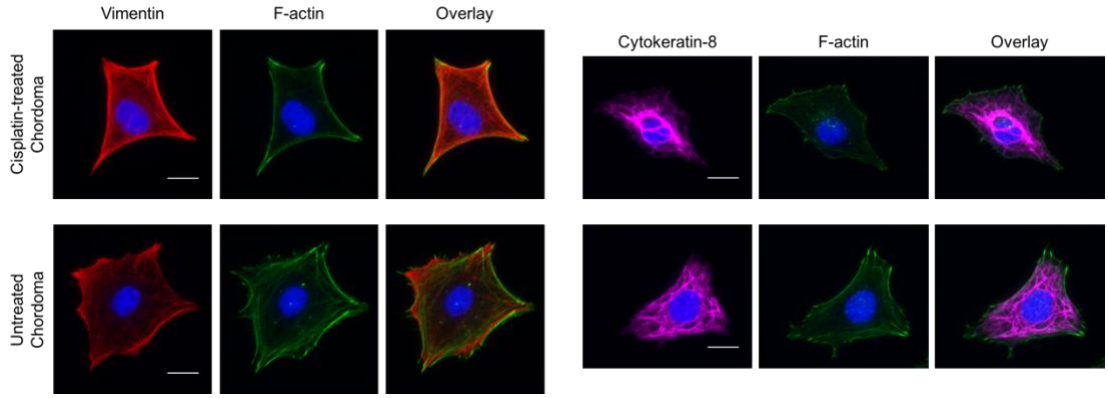

Figure 5.5: The effect of cisplatin treatment on vimentin and cytokeratin-8 intermediate filament networks. (a) Representative fluorescence images of cisplatin-treated chordoma cells labeled for F-actin (green), vimentin (red), and cytokeratin-8 (magenta). Scale bars: 15 µm.

To determine the potential involvement of IF integrity in chordoma cell chemoresistance to traditional cytotoxic chemotherapy drugs, we analyzed the viability of day fourteen vimentin knockdown cells treated with cisplatin. As a positive control, we included a parallel group of vimentin knockdown cells treated with paclitaxel, which induces cytotoxicity through cytoskeletal disruption, to serve as a gold standard. We did not include siKRT8-cells because knockdown was not sustained through 14 days. Following three days of treatment with both cisplatin and paclitaxel, the average percent cell survival of siNEG-cells tended to be greater (~7%) than that of siVIM-cells (Figure 5.6a). However, these trends were not statistically significant. Similar

trends were found when the duration of cisplatin and paclitaxel treatment was increased from three to six days (Figure 5.6b).

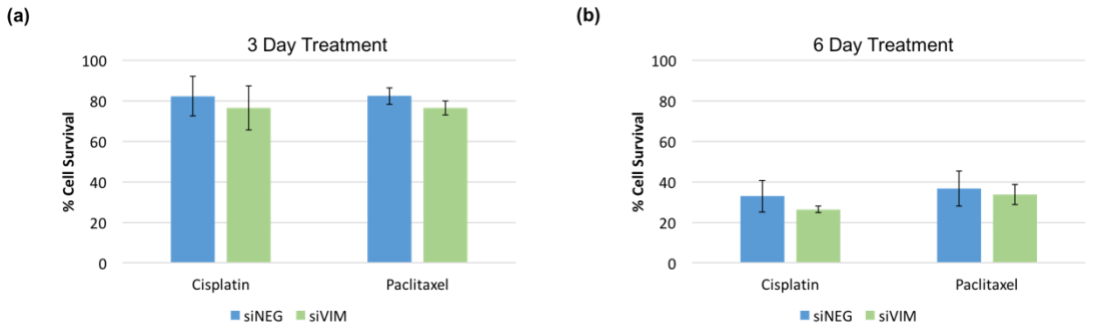

Figure 5.6: The relationship between vimentin intermediate filament integrity and chordoma cell response to cytotoxic chemotherapy drugs. (a) The percent cell survival of siNEG- and siVIM-cells treated with 20 µM cisplatin or 5 µM paclitaxel for 3 days. Data are reported as the average ± SEM; (b) The percent cell survival of siNEG- and siVIM-cells treated with 20 µM cisplatin or 5 µM paclitaxel for 6 days. Data are reported as the average ± SEM.

5.3.6 Substrate Stiffness Modulation Does Not Affect Chordoma Cell Resistance to Chemotherapeutic Agents

To further investigate the relationship between mechanical cues and chordoma cell chemoresistance, we cultured chordoma cells on substrates of variable stiffness and analyzed cell viability following treatment with cisplatin. As previously described (Chapter 4.3.1), we found chordoma cell area was significantly increased (Figure 5.7a) and cell circularity was significantly decreased (Figure 5.7b) on stiff (glass, 13 kPa PA gels) compared to soft (BME gels, 1 kPa PA gels) substrates. Despite significant differences in cell morphology, the sensitivity of chordoma cells to cisplatin was not affected by substrate stiffness. Following treatment with cisplatin, the percent cell

survivals of cells on soft substrates (BME, 1 kPA PA gels) were not statistically different than those of cells on stiff substrates (13 kPa PA gels, glass) (Figure 5.7c).

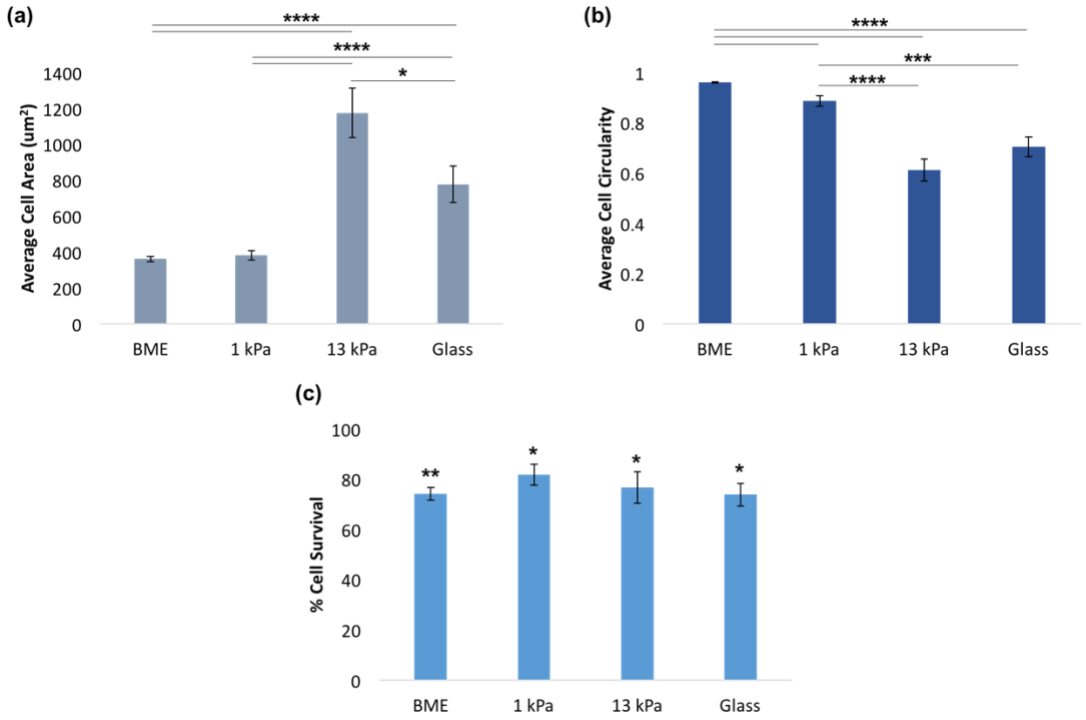

Figure 5.7: The effect of substrate stiffness on chordoma cell morphology and response to cisplatin. (a) The average cell area of chordoma cells cultured on BME gels, 1 and 13 kPa PA gels, and glass substrates reported as the average ± SEM. *p<0.05; ****p<0.0001; (b) The average cell circularity of chordoma cells cultured on BME gels, 1 and 13 kPa PA gels, and glass substrates reported as the average ± SEM. ***p<0.001; ****p<0.0001; (c) The percent cell survival of chordoma cells cultured on different substrates treated with 20 µM cisplatin reported as the average ± SEM. *p<0.05 and **p<0.01: relative to untreated cells on the same substrate.

5.4 Discussion

Patients diagnosed with chordoma are typically given a poor prognosis, due to high recurrence rates and treatment difficulties [172], [173]. Because chordomas grow near vital structures, such as the brainstem and spinal cord, total surgical resection is

difficult and often impossible. Radiation therapy and chemotherapy have also proven ineffective treatments, as chordomas are resistant to both [1], [66], [174]. Currently no systemic drugs are approved by the FDA for treatment of chordoma. Presumably due to its rarity, few studies of chordoma have been performed at the molecular level. However, such studies are necessary to identify and improve our understanding of factors that contribute to chordoma formation and progression. Ultimately, this knowledge may assist in the development of effective treatments.

IFs, both vimentin and cytokeratins, have individually been found to play roles in cell migration, invasion, and chemoresistance and their co-expression is suggested to promote a malignant cell phenotype [17]. Additionally, EMT, characterized by increased vimentin expression, is associated with cancer metastasis and poor prognosis [15], [18], [19], [104]. However, the roles of vimentin and cytokeratin IFs in chordoma cell motility and chemoresistance have not been reported. Results of this study reveal that vimentin expression may contribute to chordoma progression. Specifically, decreased vimentin expression in chordoma cells inhibited cell migration, invasion, and decreased the expression of the chordoma biomarker, SHH. Our results also suggest that vimentin expression may play a role in chordoma chemoresistance.

The roles of vimentin and cytokeratin-8 IFs in chordoma cell migration in 2D were investigated using a modified wound healing assay. Similar to previous reports [184], [185] we observed chordoma cells to migrate at a slow rate and therefore examined cell migration over a four-day period. On bare and collagen-coated plastic, we found migration was significantly decreased in vimentin and cytokeratin-8 knockdown cells. Our results are consistent with reports on the effects of vimentin and

cytokeratin knockdown in other types of cancer cells. Down-regulation of vimentin has been found to decrease cell migration in cells that express only vimentin IFs, such as fibroblasts, in addition to cells that co-express vimentin and cytokeratin IFs, such as colon cancer cells [10], [12]. Similarly, down-regulation of cytokeratins 8 or 18 decreased cell migration, without modulating vimentin expression, in non-small lung cancer and oral squamous cell carcinoma [9], [84]. Collectively, these data strongly suggest that both vimentin and cytokeratin IFs play a role in chordoma cell migration.

We observed the migration of all cell types was inhibited on laminin-coated substrates compared to bare and collagen-coated substrates. Immunohistological examination has previously revealed expression of both laminins and type I collagen in chordomas [186]. Type I collagen has been found to be the predominant collagenous protein within chordomas [186], and cell proliferation has previously been shown to increase in chordoma cell lines cultured on type I collagen substrates [68]. The differences we observed in chordoma cell migration when cultured on different substrate proteins may be attributed to differences in the expression levels of collagen- and laminin-binding integrins. The density and distribution of laminin versus type I collagen across the cell culture surface may also be different, despite our use of similar protein concentrations. Both integrin and ligand density can affect cell migration, where intermediate expression levels and cell-substrate adhesions supports maximum migration [187].

Cell invasion assays were completed to determine the potential effects of vimentin and cytokeratin-8 knockdown on cell migration through a physical barrier of ECM proteins. In addition to cell motility, cell invasion requires proteolysis, enabling

cells to pass through the basement membrane and ECM. Tumor cells that have acquired the ability to invade the surrounding tissues tend to progress to intravasation, which ultimately leads to cancer metastasis. For our studies, we utilized Corning Fluoroblok 24-multiwell insert plates with PET membranes (3 μm pores). To serve as a barrier and occlude pores, membranes were coated with Corning Matrigel Matrix, a basement membrane preparation derived from EHS mouse sarcoma. Matrigel is composed of laminin, collagen IV, heparin sulfate proteoglycans, entactin/nidogen, and a variety of growth factors. As expected, we found significantly fewer chordoma cells invaded through the Matrigel matrix when vimentin expression was decreased. This result is consistent with previous reports of decreased cell invasion in vimentin-deficient cells [12] and the correlation between tumor metastasis and vimentin overexpression [15], [17]–[19]. Despite decreased cell migration in 2D, we did not observe any differences in cell invasion as a result of cytokeratin-8 knockdown. Cell migration and invasion were found to be uncoupled in other cell types. For example, pre-EMT rat prostate cancer cells were more migratory than their post-EMT counterpart, but the opposite trend was observed for cell invasion [188]. Post-EMT, but not pre-EMT, cells were vimentin positive. Consistent with our results, this suggests vimentin IFs, rather than cytokeratin IFs, play a more prominent role in chordoma cell invasion.

Invasive cancer cells have previously been characterized as being more deformable than non-invasive cells [189], likely aiding in their ability to penetrate through small spaces. Consequently, cell deformability is emerging as a biomarker for malignant cells [115], [190]. Our vimentin knockdown chordoma cells have proven to be inconsistent with this relationship between cell deformability and invasiveness. We

found both chordoma cell stiffness (Chapter 4.3.4) and invasion to be significantly decreased in cells with decreased vimentin expression. Therefore, in addition to cell deformability, we suggest vimentin expression should be taken into account when examining and characterizing cancer cells.

We found siRNA-mediated vimentin knockdown was maintained for two weeks. Following siRNA transfection, we consistently observed little to no cell proliferation within the first week of culture. We hypothesize that decreased cell proliferation is the primary reason for stable vimentin knockdown, as previous reports show that siRNA-mediated protein knockdown can last 3-4 weeks in non-dividing cells [191]. Examining the effect of vimentin knockdown on chordoma phenotypic gene expression, we found that siVIM-cells exhibited significant downregulation of SHH expression relative to control, siNEG-cells 14 days after transfection on type I collagen coated plastic. A positive correlation between SHH and vimentin expression has previously been demonstrated in other cell types. For instance, increased expression of SHH upregulated vimentin in pancreatic cancer cells [130]. Similarly, activation of the SHH signaling pathway has been found to promote EMT, where vimentin is a key mesenchymal marker [126], [127], [130]. Increased expression of SHH has been associated with tumor formation and progression in various cancers and is believed to play a role in the malignant transformation of notochordal remnants [124], [182].

Interestingly, differences in SHH expression were not detected between siVIM- and siNEG-cells cultured on top of (2D) or embedded within (3D) type I collagen gels. Substrate rigidity and its effect on cell proliferation and SHH signaling may be responsible for the differences in SHH expression we observed between collagen-

coated plastic and collagen gels. Cancer cell proliferation, associated with SHH signaling [192], [193], often increases with increasing substrate stiffness [194]. It has also been shown that the expression of Gil2, a mediator of SHH signaling, was upregulated in breast cancer cells on rigid compared to compliant substrates [195]. In contrast to the stable knockdown of vimentin over a fourteen-day period, cytokeratin-8 knockdown was transient in siKRT8-cells. Therefore, we were unable to determine the effect of long-term cytokeratin-8 knockdown on the expression of phenotypic genes.

Finally, we investigated the involvement of IFs in chordoma cell resistance to the commonly used chemotherapeutic agents, cisplatin and paclitaxel. Cisplatin's reported mechanism of action is through DNA binding and initiation of apoptosis. Paclitaxel inhibits cell division through specific binding to and stabilization of microtubules. Previous studies have demonstrated increased cisplatin and paclitaxel sensitivity in vimentin- and cytokeratin-deficient cancer cells; however, the mechanisms are not fully understood. Cytokeratin expression has been associated with apoptotic resistance in both normal and malignant epithelial cells [196], [197], presumably providing specific resistance to the apoptotic effect of TNFα via moderation of TNFα-mediated NF-κB activity [11], [196]. Vimentin IFs have been shown to interact with proteins, such as phosphorylated Erk (pErk) MAP kinases [198], involved in cell signaling pathways critical in cell proliferation and apoptosis. To gain a better understanding of the potential relationship between cytotoxic drug treatment and IF integrity, we visualized the cytoskeleton of chordoma cells treated with cisplatin. Compared to untreated cells, cytokeratin-8 IFs tended to localize around the

cell nucleus in cisplatin-treated cells. The cytoskeleton, including cytokeratin IFs, has previously been shown to collapse and aggregate around the nucleus in cells treated with cisplatin [199]. Collapse of the cytoskeletal network was only partially reversible when cells were allowed to recover in drug-free growth media, suggesting cisplatin may target other cellular components in addition to DNA [199]. We also observed an increase in vimentin fluorescence intensity in chordoma cells treated with cisplatin. Others have reported that cisplatin treatment increases vimentin expression and migration in residual cancer cells [200]. Therefore, supplementing chemotherapy with molecules targeting the EMT pathway may reduce tumor recurrence.

To further explore potential interactions between IF integrity and chemoresistance, we examined the viability of day fourteen vimentin knockdown cells treated with cisplatin and paclitaxel. Cytokeratin-8 knockdown cells were not included in these analyses due to transient knockdown. We chose to increase the length of cell culture time between siRNA transfection and cisplatin/ paclitaxel treatment to promote potential cell phenotypic changes initiated by vimentin knockdown and give cells sufficient time to recover from the transfection process, which appeared to encourage chemoresistance. For instance, when cells were examined only six days after siRNA transfection, nearly 90% of transfected (siNEG) cells survived cisplatin treatment, compared to approximately 70% cell survival in non-transfected chordoma cells. When treated with cisplatin and paclitaxel, we consistently observed vimentin knockdown cells to have decreased cell survival compared to control cells; however, these differences were not statistically significant. In agreement, EMT suppression and resulting decreased vimentin expression, increased the sensitivity of non-small cell

lung cancer and gastric cancer cells to cisplatin [20], [22]. These results suggest that vimentin overexpression may contribute to chordoma chemoresistance and targeting vimentin or EMT pathways may increase chordoma cell sensitivity to cytotoxic agents.

We also examined the effects of substrate stiffness on the chordoma cell response to chemotherapy. To do this, we generated substrates of varying stiffness (BME gels, 1 and 13 kPa laminin-coated PA gels, and laminin-coated glass) and treated chordoma cells adhered to these substrates with cisplatin. Consistent with our previous observations (Chapter 4.3.1), we found untreated chordoma cells were significantly more spread, measured by increased cell area and decreased circularity, when cultured on stiffer substrates. Despite changes in cell morphology, we did not find that chordoma cells were more or less sensitive to cisplatin when substrate stiffness was altered. Similar to our findings, pancreatic cancer cells treated with gemcitabine, a cytotoxic drug that incorporates into DNA and RNA, exhibited changes in vimentin expression and their resistance was not affected by substrate rigidity [179]. However, other groups have observed that increasing or decreasing substrate stiffness can promote cell resistance to chemotherapy drugs. For instance, hepatocellular carcinoma cells were more resistant to cisplatin when cultured on stiffer (12 vs. 1 kPa) PA gels [201], and breast cancer cells were more resistant to cisplatin and paclitaxel when cultured on softer PDMS substrates [202]. Because the effects of substrate stiffness on chemoresistance are commonly attributed to EMT, the changes we observed in vimentin and cytokeratin-8 IFs following cisplatin treatment may explain the similar chemo-response of chordoma cells across all substrates. Future comparisons of IF integrity and protein expression levels in cisplatin-treated chordoma cells on soft versus

stiff substrates may improve our understanding of this relationship. Examining additional chemotherapy drugs with different mechanisms of action may also provide further insight.

5.5 Conclusion

Results of this study demonstrate that chordoma cell migration and invasion depend on vimentin IFs. The role of vimentin IFs in cancer cell motility and resulting metastasis is commonly accepted, and this is the first study to confirm this role in chordoma cells. Chordoma cell migration was also dependent on cytokeratin-8 IFs. However, knockdown of cytokeratin-8 IFs did not prevent chordoma cell invasion. We also observed decreased SHH expression in chordoma cells lacking vimentin, further supporting the involvement of vimentin IFs in chordoma progression. A positive correlation between vimentin and SHH expression has been observed in other cancers and SHH expression is commonly associated with tumor formation and progression. Finally, our results suggest that overexpression of vimentin may encourage chordoma cell resistance to cytotoxic chemotherapy drugs. Overall, chordoma cells expressing vimentin were associated with a more malignant and metastatic cell phenotype. Currently, chordomas are often associated with a poor prognosis because they are difficult to treat and have a propensity for recurrence. Elucidating biological factors that encourage chordoma progression and chemoresistance is essential for the development of effective treatments.

Chapter 6: Conclusions and Future Work

The overall goal of this work was to determine the functional roles of vimentin and cytokeratin IFs in the mechanobiology and progression of chordoma. Normal cell functioning is dependent on the cytoskeleton. Most cell processes, such as cell division, mechanotransduction, and migration, are attributed to microtubules and actin microfilaments, while the roles of IFs are often overlooked. In fact, IFs were initially believed to be static networks that only served a structural role. More recent evidence supports the involvement of IFs in cell mechanical properties and processes; however, the functional roles of IFs remain unclear.

Co-expression of vimentin and cytokeratin IFs has been reported in a variety of different types of cancer cells, indicating a hybrid cell phenotype that has not fully completed EMT or vice versa. The ability of cells to maintain a hybrid phenotype, expressing features of both mesenchymal (vimentin) and epithelial (cytokeratin) origin, may promote a more aggressive malignancy [23]. However, the mechanisms responsible for the reported increase in malignant behaviors of cells in partial EMT is unknown and may be elucidated through the examination of vimentin and cytokeratin IFs. To investigate this, we decreased vimentin and cytokeratin-8 expression in chordoma cells using RNAi and examined the resulting effects on cell phenotype, mechanobiology, invasive behavior, and chemoresistance (Figure 6.1).

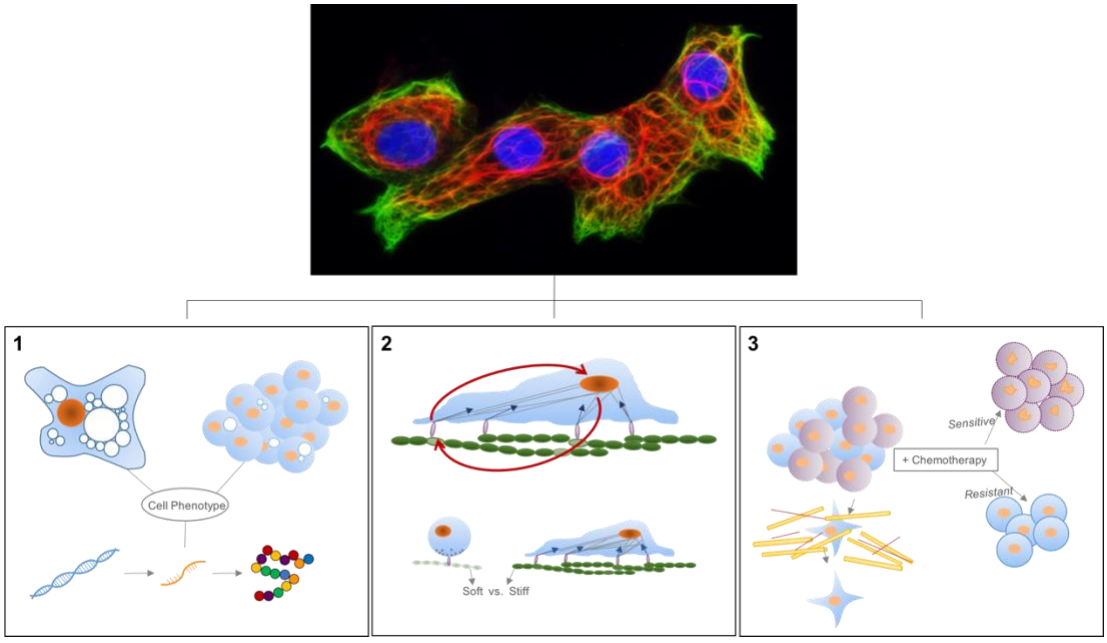

Figure 6.1: Schematic of the objectives of the three aims completed in this work. Using RNAi, the effects of cytokeratin-8 and vimentin knockdown on the phenotype (Aim 1), mechanobiology (Aim 2), and characteristic malignant behaviors (Aim 3) of chordoma cells was investigated. Fluorescence image of chordoma cells: vimentin = green; cytokeratin-8 = red.

6.1 Cytosolic Vacuoles of Chordoma Cells Are Dependent on Cytokeratin-8 Intermediate Filaments

The first objective of this work was to determine the phenotypic changes of chordoma cells following vimentin and cytokeratin-8 knockdown. Optimal knockdown was achieved six days after transfection with siRNA, and was verified at the mRNA level, using qRT-PCR, and the protein level, using western blotting and immunofluorescence. Vimentin and cytokeratin-8 knockdown cells were specifically examined for their tendency to organize in dense cell clusters, the presence of cytosolic vacuoles, and their expression of genes characteristically expressed in notochordal and chordoma cells. In the mature NP, NCs tend to transition into chondrocyte-like cells,

which is marked by decreased cytokeratin-8 expression and increased vimentin expression [44], [48]. Therefore, we hypothesized that decreasing cytokeratin-8 expression in chordoma cells, which originate from notochordal remnants [52], would stimulate other characteristic developmental changes such as a loss of cytosolic vacuoles and decreased cell clustering. Surprisingly, knockdown of cytokeratin-8 did not affect chordoma cell clustering or the expression of the notochordal markers T brachyury, SHH, or N-cadherin. These results were also consistent for vimentin knockdown cells. However, cytokeratin-8 knockdown did reduce the number of cytosolic vacuoles per cell compared to control and vimentin knockdown cells.

In support, we also observed cytokeratin-8 IFs organized immediately around chordoma cell vacuoles. This peri-vacuolar relationship was not observed for other cytoskeletal elements including vimentin. Further, we found disruption of the IF network with acrylamide significantly decreased the number of cytosolic vacuoles in chordoma cells. Although vacuole loss was also observed as a result of F-actin disruption with cytochalasin-D and microtubule disruption with nocodazole, vacuole loss was the greatest in cells treated with acrylamide. Together, these results suggest that IFs, specifically those containing cytokeratin-8 proteins, are critical for the vacuolation of chordoma cells.

Further work needs to be completed to elucidate the mechanisms in which cytokeratin-8 IFs contribute to chordoma cell vacuolation. Due to the gradual process of IF protein knockdown, we were unable to determine the change in the number of vacuoles for a particular cell as a direct result of knockdown. Consequently, it is not clear if more vacuoles were lost or less vacuoles were formed in cells with decreased

cytokeratin-8 expression. Additional studies of the involvement of cytokeratin-8 IFs in notochord morphogenesis would provide clarity of how cytokeratin-8 may participate in vacuologenesis. While chordomas are commonly identified and distinguished from other tumors by their vacuoles, the significance of chordoma cells maintaining cytosolic vacuoles is unknown. The identification of cytokeratin-8 IFs as a critical component for the existence of cytosolic vacuoles could assist future studies aimed to characterize the contents and functions of chordoma cell vacuoles.

6.2 Chordoma Cell Mechanosensing, Traction Forces, and Stiffness Are Dependent on Vimentin Intermediate Filaments

Our second objective was to determine the roles of vimentin and cytokeratin-8 IFs in chordoma cell mechanobiology, as mechanical cues are essential determinants of cell functions and are often used as cancer biomarkers. Using vimentin and cytokeratin-8 knockdown cells characterized in our first study, we examined cell stiffness, traction forces, and sensitivity to substrate stiffness. Brillouin microscopy was used to directly measure cell longitudinal modulus and subsequently determine cell stiffness. We found the longitudinal modulus of vimentin knockdown cells was significantly decreased compared to control and cytokeratin-8 knockdown cells, indicating vimentin IFs contribute to chordoma cell stiffness. While cell stiffness has predominately been attributed to F-actin, previous reports have also found vimentin IFs contribute to cell stiffness [4], [8], [85], [170]. Interestingly, metastatic cells have been found to be more deformable than their non-metastatic counterparts, and deformability is increasingly being used as a cancer biomarker [115], [189], [190]. If cell stiffness

was used as a cancer biomarker in our study, vimentin knockdown cells would be categorized as more metastatic. This is contradicting to the generally accepted correlation between vimentin expression and metastasis.

Using traction force microscopy, we determined vimentin knockdown also affected chordoma cell traction forces. Specifically, we found chordoma cells with decreased vimentin expression exerted significantly greater traction forces than control and cytokeratin-8 knockdown cells. Because these differences were not maintained when cells were treated with blebbistatin, a myosin II inhibitor, we postulate greater traction forces in vimentin knockdown cells were a result of F-actin over compensation. This relationship between vimentin knockdown, actin stress fiber assembly, and increased traction forces has previously been observed in osteosarcoma cells [6].

Finally, we found vimentin knockdown disrupted chordoma cell sensitivity to substrate stiffness. To examine cell mechanosensitivity, cell area and circularity were measured of knockdown cells cultured on PA gels of variable stiffness. Typically, cell spread area increases with increasing substrate stiffness [165]. This behavior was confirmed in control cells and was not affected by cytokeratin-8 knockdown. In contrast, vimentin knockdown cells cultured on soft (0.42kPa), Col-PA gels exhibited significant cell spreading. This result contradicts previous reports of vimentin knockdown reducing cell spreading [166], [167]. It is possible that residual vimentin, and its strong association with cell protrusions and focal adhesions, is contributing to the increased spreading of vimentin knockdown cells. Overall, our findings suggest that vimentin IFs contribute to chordoma cell mechanobiology to a greater extent than cytokeratin-8 IFs. The ability of cells to probe and respond to the mechanical properties

of their surrounding ECM is critical for proper cell function. Therefore, we predicted chordoma cell behaviors such as cell migration and invasion will be dependent on vimentin expression.

Additional studies could be completed to further understand the implicated role of vimentin IFs in chordoma cell stiffness, traction forces, and mechanosensitivity. In this work we measured the longitudinal moduli and traction forces of cells cultured on 5 kPa PA gels. Because we determined vimentin knockdown dysregulated chordoma cell sensitivity to substrate stiffness, it would be interesting to examine how decreased vimentin expression affects cell stiffness and traction forces across a range of substrate stiffness. The ability of cells to sense and respond to the mechanical properties of their surrounding ECM, typically through mirrored increases in cell stiffness and traction forces, may be dependent on vimentin expression. The localization of residual vimentin in vimentin knockdown cells to the cell periphery, particularly within cell protrusions, may be a factor contributing to the results we observed in this study. To differentiate the effects of decreased vimentin expression from those of residual vimentin localization, complete ablation of vimentin is required.

6.3 Vimentin Expression is Associated with Metastatic Behaviors in Chordoma Cells

The third and final objective of this work was to improve our understanding of how vimentin and cytokeratin-8 IFs are involved in cell behaviors that promote the progression of chordoma. Based on the observed effects of vimentin knockdown on chordoma cell stiffness and mechanosensitivity, we predicted vimentin knockdown would also disrupt cell migration and invasion. Similar to our first two studies, we

generated vimentin and cytokeratin-8 knockdown cells via RNAi. Using these knockdown cells, we analyzed cell migration in 2D culture, cell invasion through an ECM-like barrier, gene expression of chordoma biomarkers, and cell sensitivity to traditional cytotoxic chemotherapeutics. Similar to previous reports [9], [10], [12], [84], we observed decreased cell migration as a result of both vimentin and cytokeratin-8 knockdown. For vimentin knockdown cells, this effect on cell motility was translated to cell invasion, which was also significantly decreased. Interestingly, chordoma cell invasion was not affected by decreased cytokeratin-8 expression. These results are consistent with previous reports that reveal migration and invasion are uncoupled [188], and vimentin expression is positively correlated with cancer metastasis [15], [17]–[19].

Although short-term (processed for analysis six days after transfection with siRNA) vimentin and cytokeratin-8 knockdown cells did not exhibit changes in gene expression of chordoma biomarkers, we found long-term (processed for analysis fourteen days after transfection with siRNA) vimentin knockdown resulted in decreased SHH expression. In contrast to vimentin knockdown, cytokeratin-8 knockdown was transient and therefore the effects of long-term cytokeratin-8 knockdown on biomarker expression could not be determined. Expression of SHH has been associated with tumor formation and progression in other cancers, and the reactivation of SHH in notochordal remnants is believed to stimulate a malignant transformation [124], [130], [182]. Therefore, our results suggest that vimentin expression promotes a malignant and metastatic cell phenotype.

Our final analysis was focused on determining the potential involvement of IFs in the resistance of chordoma cells to cytotoxic chemotherapy drugs. Expression of both vimentin and cytokeratin-8, in addition to cell mechanobiology, has previously been associated with cancer cell chemoresistance [11], [20]–[22], [84], [179]. Analysis of vimentin knockdown cells suggests that decreased vimentin expression could potentially increase the efficiency of cisplatin and paclitaxel in treating chordoma. Through immunofluorescence, we observed the fluorescence intensity of vimentin IFs to be greater in chordoma cells treated with cisplatin compared to untreated chordoma cells. This suggests that chemotherapy may encourage vimentin expression and cancer metastasis in residual cells [200]. In combination with chemotherapy, vimentin could be utilized as a molecular target to increase cell sensitivity and prevent tumor recurrence.

Further studies need to be completed to form a more comprehensive understanding of the relationship between IFs, substrate stiffness, and migration. To complement our analysis of 2D cell migration on plastic substrates, the migration of knockdown chordoma cells could be analyzed on softer substrates such as type I collagen gels. Gels with a stiffness gradient could also be designed to investigate the roles of vimentin and cytokeratin-8 IFs in chordoma cell durotaxis. Future studies should also explore the role of vimentin and cytokeratin-8 IFs in chordoma cell proliferation, which could further improve our understanding of chordoma progression and chemoresistance, as rapidly dividing cells tend to be more responsive to cytotoxic drugs. While initial findings suggest that decreasing vimentin expression increases the sensitivity of chordoma cells to cytotoxic chemotherapeutics, additional studies need

to be completed to confirm these results. In addition to examining chordoma cell chemoresistance in monolayer culture, a more physiologically relevant culture system should be designed and utilized to better understand how these effects may translate *in vivo*. Compared to monolayer cell culture, cells in 3D culture tend to proliferate slower, and as a result will probably respond differently to cytotoxic drug treatment. Therefore, it is necessary to also examine the effects of administering chemotherapeutics to vimentin knockdown chordoma cells embedded within a 3D scaffold composed of proteins characteristic of chordoma, such as type I collagen.

6.4 Concluding Remarks

Our results suggest that vimentin and cytokeratin-8 IFs have specific functional roles in chordoma cells. While cytokeratin-8 expression was essential for the presence of cytosolic vacuoles, vimentin expression was essential for cell mechanosensing of substrate stiffness and contributed to cell stiffness. Presumably due to its greater contribution to chordoma cell mechanobiology, vimentin expression was also essential for chordoma cell invasion, the expression of the chordoma biomarker sonic hedgehog, and was associated with increased cell resistance to cisplatin and paclitaxel. For the first time, these results elucidate roles of vimentin and cytokeratin-8 IFs in chordoma cell mechanobiology and suggest a correlation between vimentin expression and malignant behaviors in chordoma cells.

Overall, this work shows IFs are essential, dynamic components of the cytoskeleton and – similar to microtubules and actin microfilaments – are critical for normal cell functioning. More specifically, our findings improve our knowledge of IFs in cancer, revealing the dependence of cell mechanics and motility on IFs. The

progression of cancer is influenced by changes in the biomechanical properties of cells and their surrounding environment. Identifying cellular components that play key roles in these processes and are uniquely or overexpressed in cancer is necessary for the development of effective targeted cancer therapies.

Appendix A: Phenotype of Rat Nucleus Pulposus Cells: Effects of the Extracellular Environment and a Comparison to Chordoma Cells

Prior to focusing on chordoma cells, I primarily worked with NP cells isolated from rat caudal IVDs. As the NP and chordoma are both derived from the embryonic notochord, I chose to include this work. Included here is a study examining the effects of the extracellular environment on the morphology of NP cells, in addition to a phenotypic comparison of rat NP and human chordoma cells.

A.1 Introduction

The NP tissue of the IVD is generally considered to be populated by two major cell types: NCs (immature NP cells) and chondrocyte-like cells. As humans age, NCs, characterized by their large size and abundant cytosolic vacuoles, tend to be replaced and/or supplanted by chondrocyte-like cells. The cellular transition from NCs to mature NP cells coincides with age-associated changes in the NP ECM such as decreases in water and proteoglycan content [44], [119], [100], [120] and increased tissue stiffness [158], ultimately impairing the tissue's ability to behave hydrostatically and withstand compression [203]. As a result, the IVD becomes more susceptible to disc degeneration and resulting low back pain [121], [122].

Because cells of the NP are responsible for the synthesis of a functional ECM, the cellular transition observed with aging is believed to be involved in the progression of disc degeneration [49], [50]. Changes in cell morphology have been shown to play a role in the NP cellular transition. For instance, previous studies of rat NP cells in vitro show that a rounded cell morphology corresponded to maintenance of notochordal gene

expression [142]. Therefore, our objective was to investigate the role of extracellular cues in governing morphological changes in NP cells. In this study, we examined the morphological consequences of culturing NP cells on collagen substrates of different stiffness and configuration. In order to implement a well-controlled, systematic approach, we utilized type I collagen thin films (CTFs), a 2-D platform for cell culture developed by the National Institute of Standards and Technology. We were able to manipulate the stiffness of CTFs through dehydration, where dehydrated TFs ($3x10^{-2}$ N/m ± $2x10^{-2}$ N/m) are stiffer than hydrated TFs ($3x10^{-3}$ N/m ± 2x10-3 N/m) [204]. We found that NP cells cultured on hydrated CTFs had significantly smaller cell areas, corresponding to more circular morphologies, compared to NP cells on dehydrated CTFs, absorbed collagen molecules, and TCTP. That dehydrated CTFs, adsorbed collagen, and TCTP yielded similar results suggests that collagen stiffness, rather than collagen configuration, has a dominant effect on NP cell morphology.

Further, we compared the phenotype of rat NP cells to that of human chordoma cells derived from the MUG-Chor1 cell line that was utilized in this dissertation. Characteristic of NCs, both cell types contained cytosolic vacuoles and co-expressed cytokeratin and vimentin IFs. However, the vimentin IF network appeared to be more prominent in chordoma cells than in rat NP cells.

A.2 Materials and Methods

A.2.1 Nucleus Pulposus Tissue Harvest and Cell Isolation

NP tissue was harvested from caudal discs of adult Sprague-Dawley rats after euthanasia, and digested sequentially in 4 mg/ml pronase for 1 hour and 0.25 mg/ml

type II collagenase overnight. All procedures were approved by the Institutional Animal Care & Use Committee.

A.2.2 Collagen Thin Film Preparation

Type I collagen solutions consisting of 87.5% 1x DPBS (Sigma-Aldrich), 10% 3 mg/ml bovine type I collagen (Advanced Biomatrix), 1.25% 0.1N NaOH, and 1.25% 10x DPBS (Sigma-Aldrich) were prepared and incubated in six-well non-tissue culture-treated polystyrene plates (1-2 ml/well) overnight. Surfaces were then rinsed with PBS, followed by deionized water, and sprayed briefly with inert nitrogen gas to form CTFs. PBS was added immediately to hydrated CTFs, whereas dehydrated TFs were dried for 24 hours before the addition of PBS.

A.2.3 Cell Culture

Immediately following isolation, NP cells were seeded at a density of 3,000 cells/cm^2 on either hydrated type I CTFs, dehydrated type I CTFs, absorbed type I collagen (50 μg/ml) molecules, or TCTP. NP cells were cultured in α-MEM supplemented with 2% FBS (Gibco/Thermo Fisher) and 1% Penicillin-Streptomycin (Gibco/Thermo Fisher). MUG-Chor1 chordoma cells (ATCC Cat# CRL-3219, RRID:CVCL_9277) were cultured in Iscove's Modified Dulbecco's Medium: Roswell Park Memorial Institute 1640 Medium (4:1) (Gibco/Thermo Fisher Scientific) supplemented with 10% FBS (Gibco/Thermo Fisher) and 1% Penicillin-Streptomycin (Gibco/Thermo Fisher). Complete media exchange was completed every 2-3 days and cells were cultured at 37°C, 5% CO_2.

A.2.4 Morphological Analysis

NP cells were fixed on either day 3 or day 7 of culture in 4% PFA, permeabilized with 0.1% Triton-X in PBS, and blocked for non-specific binding using 1.5% normal goat serum (NGS) in PBS. Cells were then incubated with 2.5% Alexa Fluor® 594 Phalloidin (Molecular Probes, Eugene, OR) to stain the actin cytoskeleton and DAPI (Molecular Probes) used as a nuclear counterstain. Cells were imaged at x100 magnification with a Nipkow (spinning) disk-equipped Olympus IX81 microscope, and Image J was used to measure the area and perimeter of each cell with a single nucleus. Shape factor, a measure of cell circularity, was calculated for each cell: $SF = (4\pi * \text{cell area}) / (\text{cell perimeter})^2$. A shape factor closer to one indicates a more circular cell.

A.2.5 Immunofluorescence

Immunofluorescence was used to visualize IFs in NP and chordoma cells. As previously described, cells were fixed with 4% PFA, permeabilized using 0.1% Triton X-100, and blocked for non-specific binding using 1.5% NGS. For vimentin, rat NP and human chordoma cells were labelled with rabbit IgG anti-vimentin polyclonal (Abcam) and rabbit IgG anti-vimentin [SP20] (Thermo Fisher Scientific) antibodies, respectively. A biotinylated (anti-rabbit IgG) secondary antibody (Vector Laboratories) was used in combination with FITC-labelled streptavidin (Vector Laboratories) to visualize vimentin. For cytokeratins, rat NP and human chordoma cells were labelled with a mouse IgG1 anti-cytokeratin 8+18+19 [2A4] (Abcam) antibody. An Alexa Fluor

594-conjugated (anti-mouse IgG) secondary antibody (Thermo Fisher Scientific) was used to visualize cytokeratins 8, 18, and 19. DAPI (Invitrogen/Thermo Fisher Scientific) was used as a nuclear counterstain. Confocal fluorescence images were captured at x600 magnification using a Nipkow (spinning) disk-equipped Olympus IX81 microscope and Z-stacks (1 μm slices) were projected into a single image.

A.2.6 Statistical Analysis

Statistical significance between time points was determined using a two-tailed t-test, while ANOVA with Tukey's post-hoc analysis was used to compare substrates within each time point. Due to unequal variances, cell area among substrates within time points were further analyzed for significance using Kruskal-Wallis and Mann-Whitney tests. For all analyses, critical significance levels were set to $\alpha = 0.05$. Average cell areas are reported as mean ± SEM.

A.3 Results

A.3.1 Substrate Stiffness Modulates Nucleus Pulposus Cell Morphology

NP cells seeded on hydrated CTFs had significantly smaller cell areas than NP cells seeded on dehydrated CTFs, adsorbed collagen, and TCTP (Figure A.1a, b). This result was observed on both days three and seven of cell culture. On day seven of culture, NP cells cultured on stiffer substrates (TCTP, absorbed collagen, dehydrated CTFs) became more spread with visible actin stress fibers (Figure A.1a). In contrast, NP cells on hydrated CTFs remained more rounded (Figure A.1a). Analyzing cell shape factor, statistical significance was found between hydrated CTFs and TCTP for

day three and between hydrated CTFs and all other surface types (TCTP, adsorbed collagen, and dehydrated CTFs) for day seven (Figure A.1c). Statistically significant differences were also found comparing day three and day seven data, where cells on day seven had larger cell areas and were more spread for all surface types.

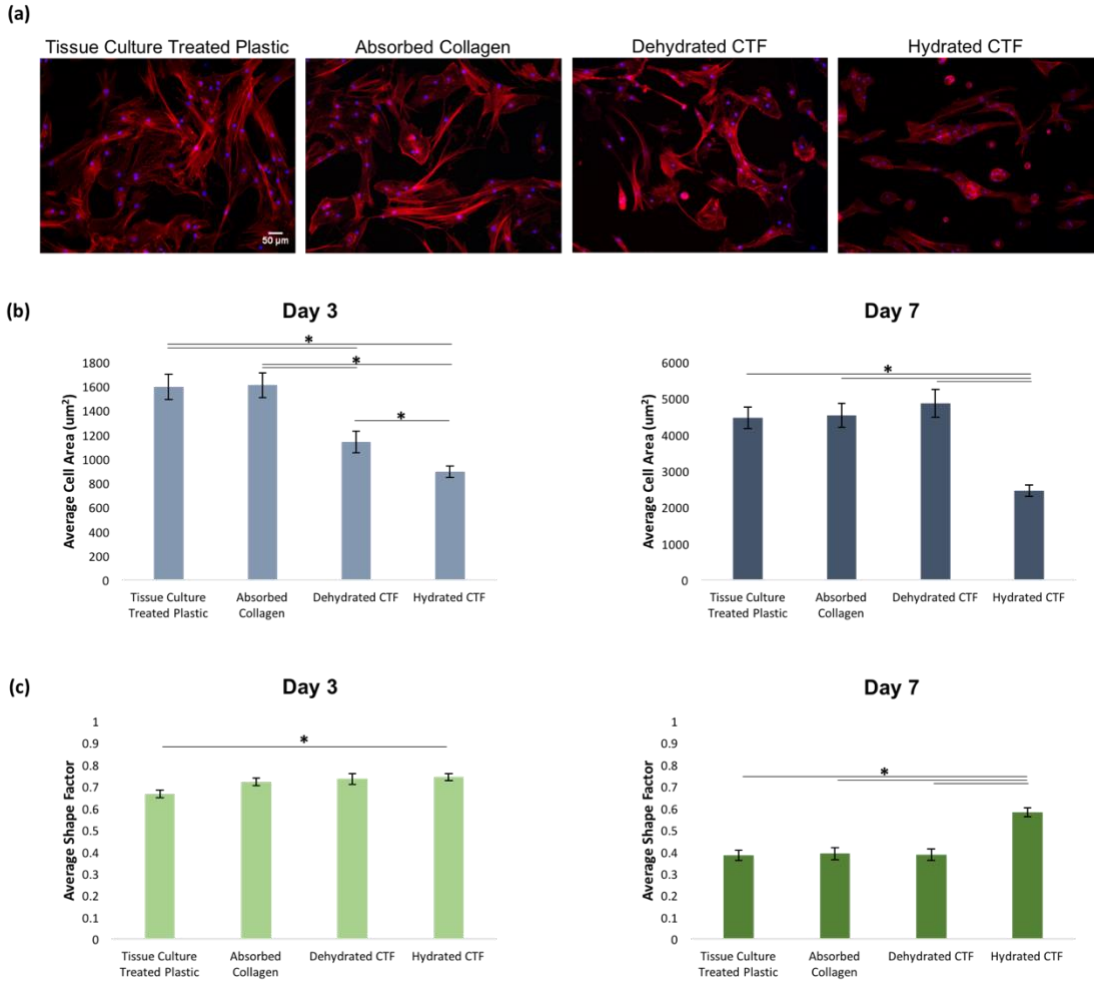

Figure A.1: The effect of type I collagen substrate configuration and stiffness on NP cell morphology. (a) Representative fluorescence images of NP cells cultured for seven days on TCTP, absorbed collagen, dehydrated CTFs, and hydrated CTFs. Stained for F-actin (red). Scale bars: 50 µm; NP cell (b) area and (c) shape factor on days 3 and 7 of culture on TCTP, absorbed collagen, dehydrated CTFs, and hydrated CTFs reported as average ± SEM. *$p < 0.05$.

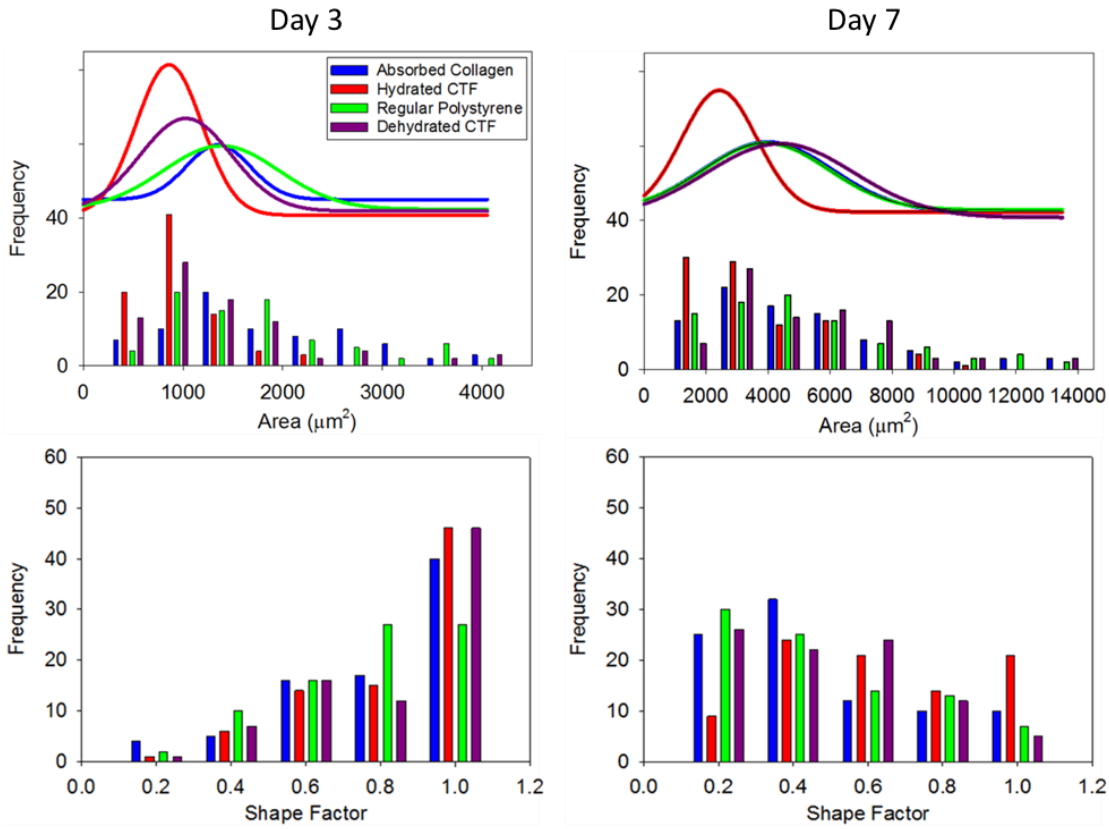

Figure A.2: Frequency distributions of day three and day seven NP cell area and shape factor data. Non-linear regression analysis was used to fit a Gaussian (4 parameter) curve to the data.

A.3.2 Rat Nucleus Pulposus and Human Chordoma Cells Contain Characteristic Features of Notochordal Cells

To verify and expand on previous studies characterizing the human chordoma cell line that we utilized for our studies, we compared the morphology and IFs of MUG-Chor1 chordoma cells to rat NP cells. Rats are one of the vertebrates that have been shown to maintain large, vacuolated NCs in their NP throughout life. Similar to rat NP cells, we observed human MUG-Chor1 chordoma cells contained cytosolic vacuoles (Figure A.3a). Visualizing their morphology, the chordoma cell line appeared to have

a heterogeneous cell population, with many fibroblast-like cells in addition to larger, vacuolated cells (Figure A.3c). With prolonged culture in monolayer, the number of vacuolated cells appeared to increase (Figure A.3c). Visualizing vimentin and cytokeratin (8, 18, 19) IFs via immunofluorescence, we observed positive cytokeratin IF staining in both rat NP and human chordoma cells (Figure A.3b). However, vimentin fluorescence was noticeably weaker in rat NP cells compared to chordoma cells (Figure A.3b). While a continuous vimentin IF network was observed throughout the cell body in chordoma cells, vimentin IFs were only detected at the periphery of NP cells (Figure A.3b).

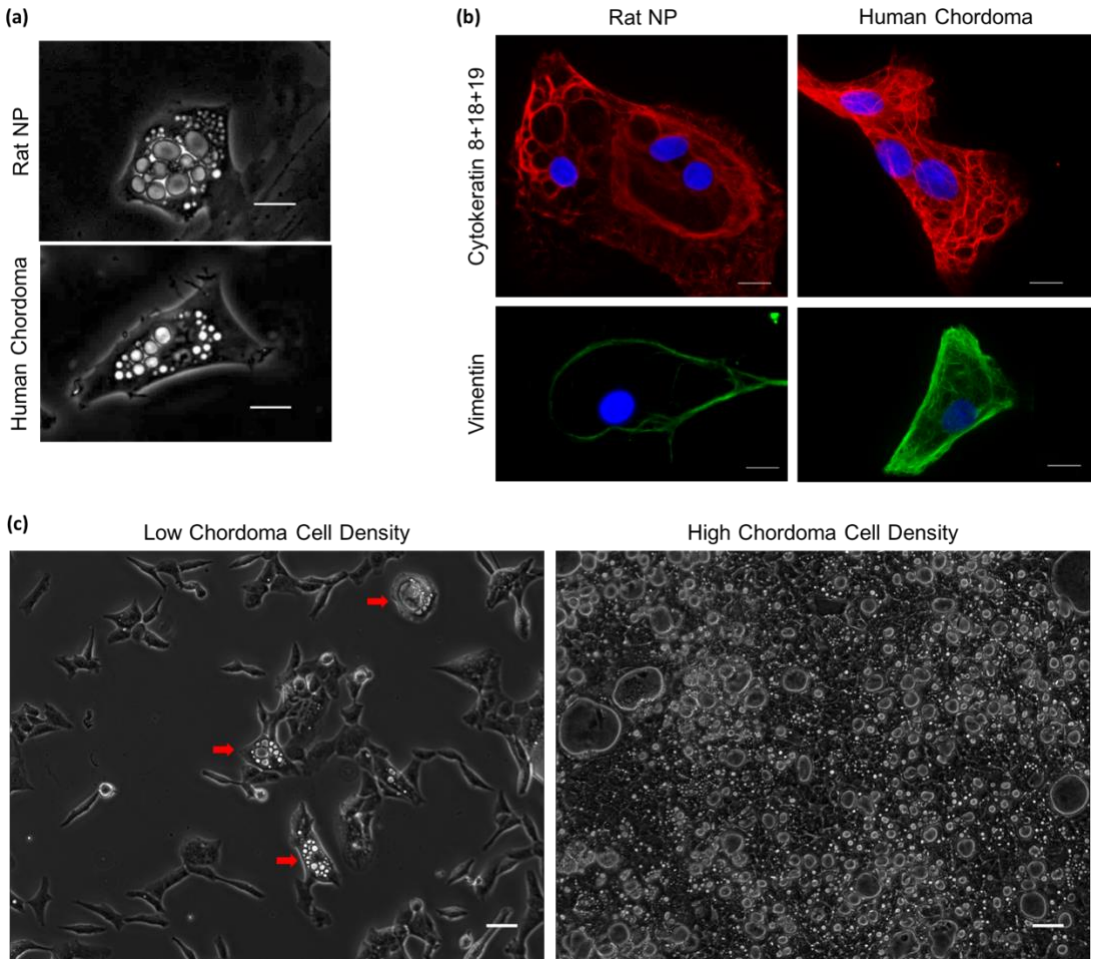

Figure A.3: Comparison of NP and chordoma cell phenotypes in monolayer culture. (a) Bright field images of a rat NP cell and a human chordoma cell showing cytosolic vacuoles. Scale bars: 25 µm; (b) Representative fluorescence images of rat NP cells and human chordoma cells. Cytokeratins 8, 18, 19 (red) and vimentin (green). Scale bars: 10 µm; (c) Representative bright field images of human chordoma cells in monolayer culture at low and high and cell densities. Red arrows indicate individual, vacuolated cells in low cell density culture. Scale bars: 50 µm.

A.4 Discussion

This study examines the role of type I collagen stiffness and configuration on NP cellular behavior. We specifically examined NP cell morphology (area and shape) to distinguish effects of various culturing conditions. Smaller cell areas and more rounded morphologies observed for NP cells seeded on hydrated type I CTFs are similar to previous studies of NP cells cultured in 3D alginate beads [142] and BME [144]. Comparing hydrated CTFs with dehydrated CTFs further supports the hypothesis that decreased substrate stiffness induces a more rounded morphology, as hydrated TFs have a stiffness of $3x10^{-3}$ N/m ± $2x10^{-3}$ N/m and dehydrated TFs have a stiffness of $3x10^{-2}$ N/m ± $2x10^{-2}$ N/m [204]. Studies by Rastogi et al. additionally found that notochordal gene expression was maintained in rat NP cells that exhibited a more rounded, less stretched morphology [142]. Collectively, this suggests that softer substrates should be used to maintain the NC phenotype *in vitro*.

The loss of NCs within the NP coincides with changes in the composition, such as decreased proteoglycan and water content [44], [119], [100], [120], and mechanical properties of the ECM [158]. Ultimately, these age-associated changes impair NP function and the IVD becomes more susceptible to degeneration [121], [122], [203]. Because NCs are believed to synthesize a more functional ECM than mature NP cells,

NCs are actively being researched for their tissue regeneration potential. Studies have found NC secretions were capable of stimulating the synthesis of proteoglycans, a critical component of the NP, in mature NP cells [205]–[207]. Additionally, NC conditioned media was found to drive human mesenchymal stem cell (hMSC) differentiation toward a young, NP-like phenotype [208]. Understanding factors involved in maintaining the NC phenotype is essential for the development of NC-based therapies targeting disc degeneration.

We additionally compared the phenotype of rat NP cells to human chordoma cells. Similar to the NP, malignant chordomas are believed to originate from remnants of the embryonic notochord [33], [55]. However, the mechanisms responsible for the malignant transformation of NCs are not fully understood. Characteristic of NCs, we found both rat NP and human chordoma cells contained cytosolic vacuoles and co-expressed vimentin and cytokeratin IFs. Interestingly, we observed via immunofluorescence a continuous vimentin IF network in chordoma cells, but not in NP cells. In NP cells, vimentin IFs were only observed in the cell periphery. This is supported by previous studies of cancer cells, where malignant and metastatic cells had increased vimentin expression compared to healthy cells [18], [19]. While our initial findings suggest that vimentin expression is increased in chordoma cells relative to NP cells, additional studies need to be completed to quantify vimentin gene and protein expression. Further comparison studies utilizing human, rather than rat, NP cells should also be completed. Elucidating molecular differences between healthy NC cells residing in the mature NP and malignant chordoma cells is critical for understanding the progression of chordoma.

Appendix B: Morphological Analysis of Chordoma Cells Measured with Brillouin Confocal Microscopy and Traction Force Microscopy

The morphology of the chordoma cells included in our studies examining cell stiffness (Chapter 4.3.4) and traction forces (Chapter 4.3.2) was analyzed by measuring cell spread area and circularity. This was accomplished by manually tracing individual cells in bright field images using ImageJ. We determined that the average cell area and circularity were not statistically different comparing siNEG-, siVIM-, and siKRT8-cells measured with Brillouin confocal microscopy (Figure B.1) or traction force microscopy (Figure B.2). This suggests that the increased cell spreading we observed in siVIM-cells on 5 kPa PA gels (Chapter 4.3.1) was not a contributing factor to the decreased cell stiffness (Chapter 4.3.4) and increased cell traction forces (Chapter 4.3.2) of siVIM-cells compared to siNEG- and siKRT8-cells.

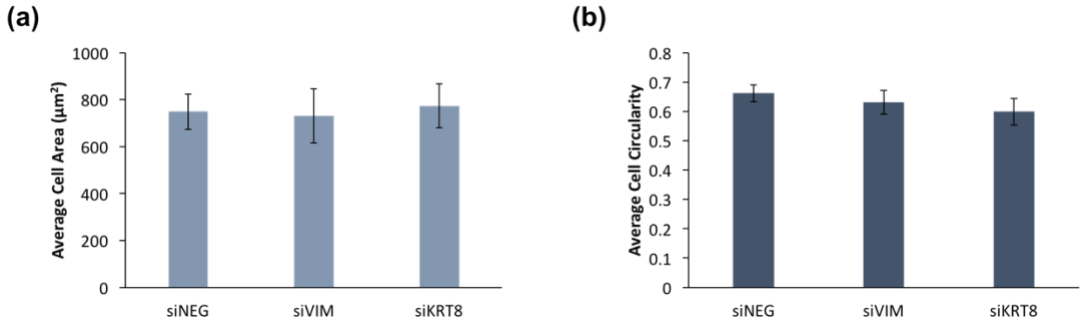

Figure B.1: Morphological analysis of knockdown chordoma cells measured with Brillouin confocal microscopy. Chordoma cell (a) area and (b) circularity reported as the average ± SEM.

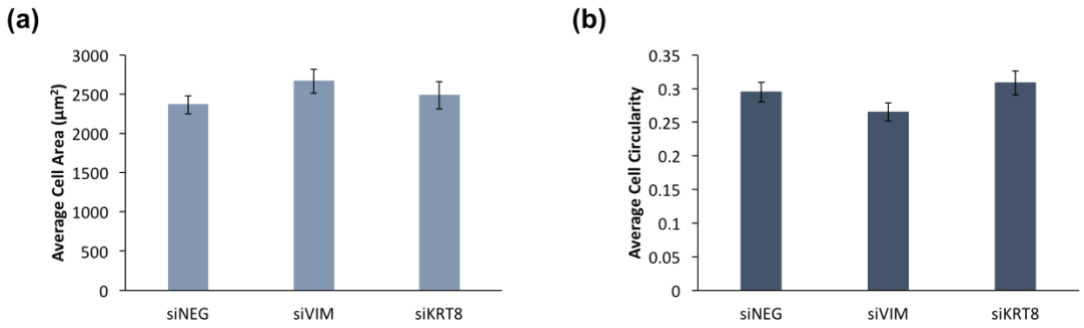

Figure B.2: Morphological analysis of knockdown chordoma cells examined with traction force microscopy. Chordoma cell (a) area and (b) circularity reported as the average ± SEM.

We further examined the correlation of cell spreading with cell stiffness and traction forces. We observed a positive correlation between cell circularity and cell stiffness (Figure B.3b) and a negative correlation between cell area and cell stiffness (Figure B.3a) for all cell types (siNEG, siVIM, and siKRT8). On the other hand, we did not observe any correlation between cell spreading with average (Figure B.4) or maximum (Figure B.5) cell traction forces.

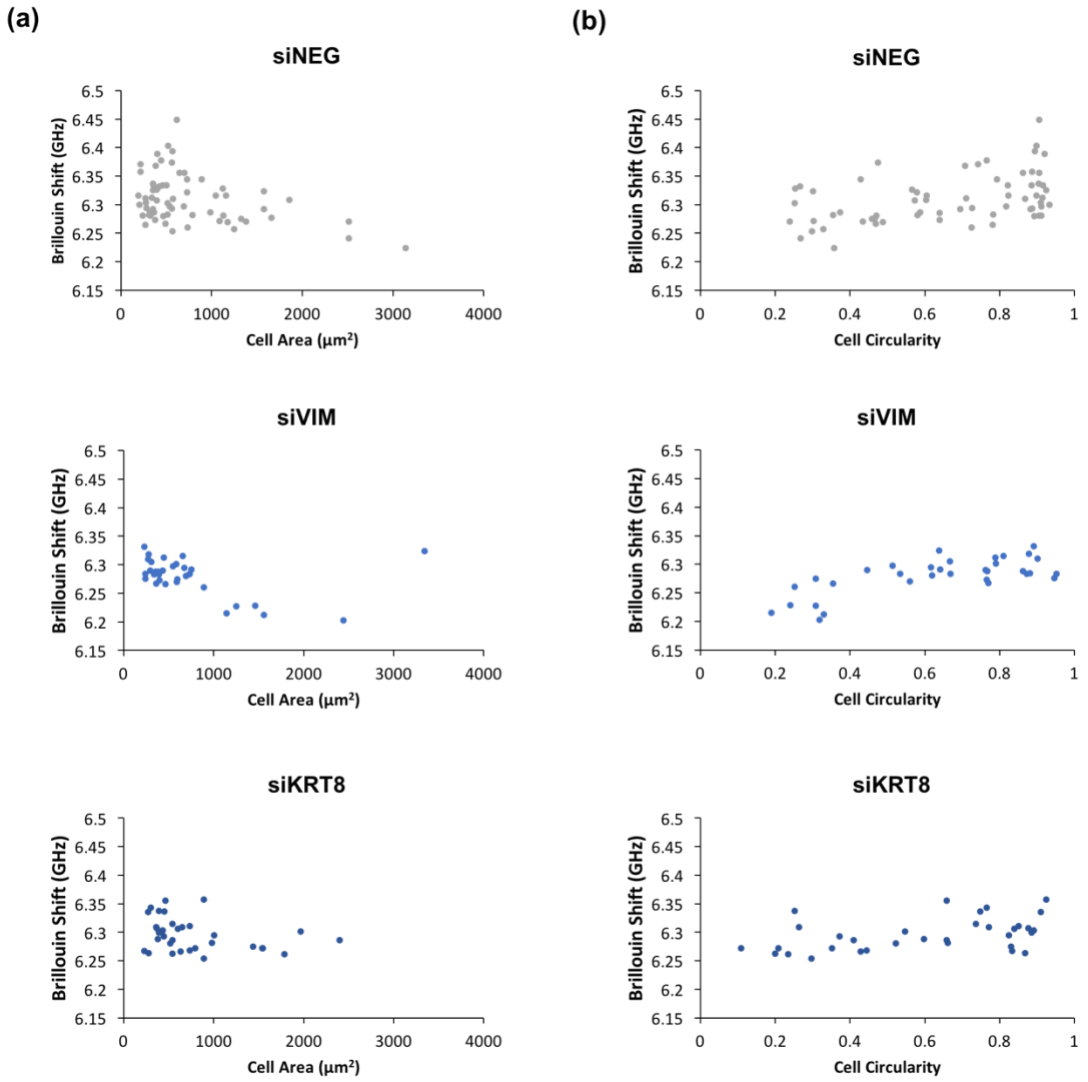

Figure B.3: Relationship between chordoma cell morphology and longitudinal modulus. Correlation of the measured Brillouin shift of chordoma cells with cell (a) area and (b) circularity.

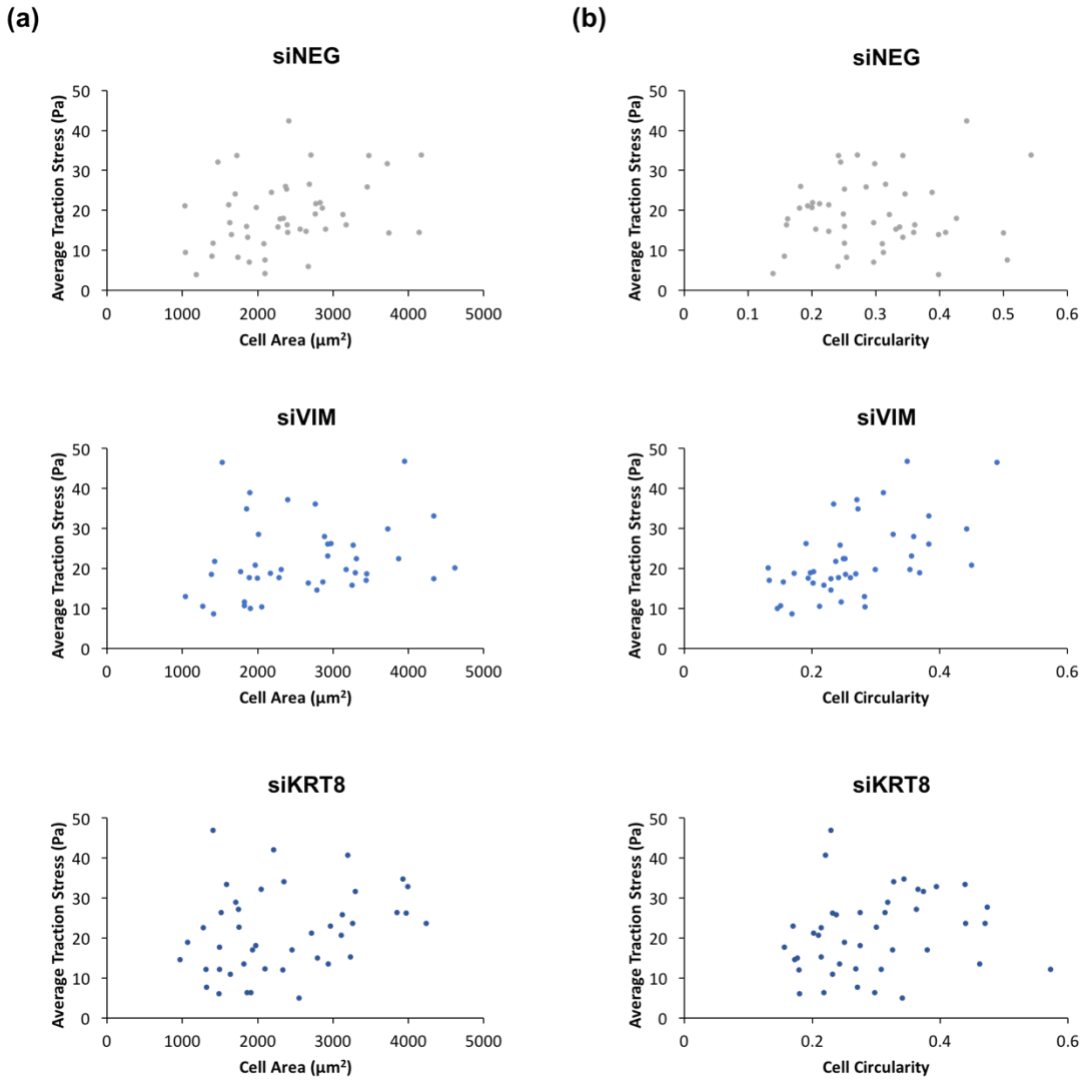

Figure B.4: Relationship between chordoma cell morphology and average traction forces. Correlation of the average traction stress with chordoma cell (a) area and (b) circularity.

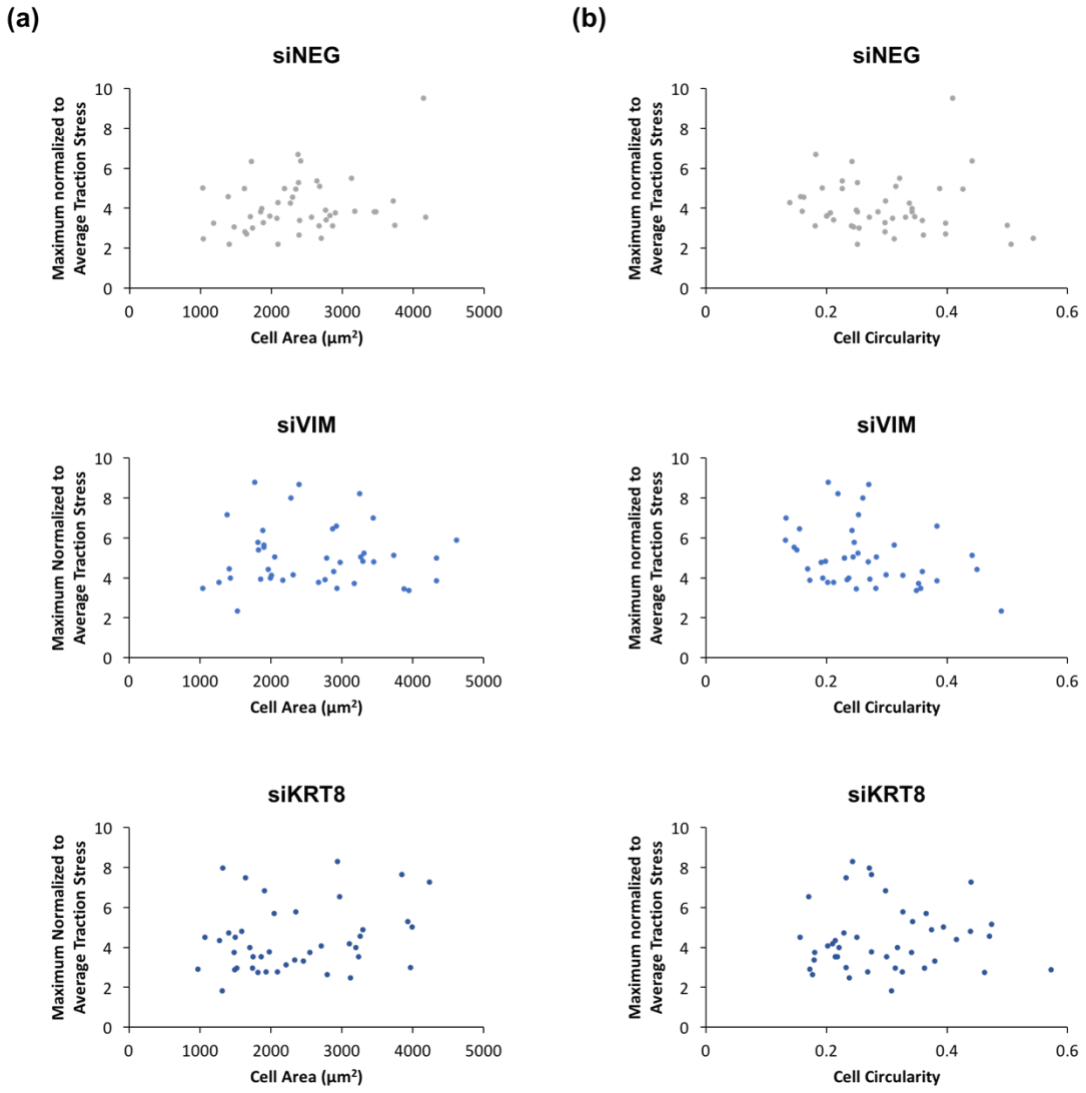

Figure B.5: Relationship between chordoma cell morphology and maximum traction forces. Correlation of the normalized maximum traction stress with chordoma cell (a) area and (b) circularity.

Bibliography

[1] R. Chugh, H. Tawbi, D. R. Lucas, J. S. Biermann, S. M. Schuetze, and L. H. Baker, "Chordoma: the nonsarcoma primary bone tumor," *The Oncologist*, vol. 12, no. 11, pp. 1344–1350, Nov. 2007.

[2] J. Roche, "The Epithelial-to-Mesenchymal Transition in Cancer," *Cancers*, vol. 10, no. 2, Feb. 2018.

[3] J. A. Käs, A. Fritsch, K. Seltmann, and T. Magin, "Keratins Significantly Contribute to Cell Stiffness and Impact Invasive Behavior," *Biophys. J.*, vol. 106, no. 2, pp. 574a-575a, Jan. 2014.

[4] N. Wang and D. Stamenović, "Contribution of intermediate filaments to cell stiffness, stiffening, and growth," *Am. J. Physiol. Cell Physiol.*, vol. 279, no. 1, pp. C188-194, Jul. 2000.

[5] S. Fujiwara, K. Ohashi, T. Mashiko, H. Kondo, K. Mizuno, and Y.-L. Wang, "Interplay between Solo and keratin filaments is crucial for mechanical force–induced stress fiber reinforcement," *Mol. Biol. Cell*, vol. 27, no. 6, pp. 954–966, Jan. 2016.

[6] Y. Jiu *et al.*, "Vimentin intermediate filaments control actin stress fiber assembly through GEF-H1 and RhoA," *J. Cell Sci.*, vol. 130, no. 5, pp. 892–902, 01 2017.

[7] F. Bordeleau, M.-E. M. Lapierre, Y. Sheng, and N. Marceau, "Keratin 8/18 Regulation of Cell Stiffness-Extracellular Matrix Interplay through Modulation of Rho-Mediated Actin Cytoskeleton Dynamics," *PLOS ONE*, vol. 7, no. 6, p. e38780, Jun. 2012.

[8] M. G. Mendez, D. Restle, and P. A. Janmey, "Vimentin enhances cell elastic behavior and protects against compressive stress," *Biophys. J.*, vol. 107, no. 2, pp. 314–323, Jul. 2014.

[9] H. Alam, S. T. Kundu, S. N. Dalal, and M. M. Vaidya, "Loss of keratins 8 and 18 leads to alterations in α6β4-integrin-mediated signalling and decreased neoplastic progression in an oral-tumour-derived cell line," *J Cell Sci*, vol. 124, no. 12, pp. 2096–2106, Jun. 2011.

[10] B. Eckes *et al.*, "Impaired wound healing in embryonic and adult mice lacking vimentin," *J. Cell Sci.*, vol. 113 (Pt 13), pp. 2455–2462, Jul. 2000.

[11] A.-M. Fortier, E. Asselin, and M. Cadrin, "Keratin 8 and 18 loss in epithelial cancer cells increases collective cell migration and cisplatin sensitivity through

claudin1 up-regulation," *J. Biol. Chem.*, vol. 288, no. 16, pp. 11555–11571, Apr. 2013.

[12] L. McInroy and A. Määttä, "Down-regulation of vimentin expression inhibits carcinoma cell migration and adhesion," *Biochem. Biophys. Res. Commun.*, vol. 360, no. 1, pp. 109–114, Aug. 2007.

[13] F.-C. Chang, C.-T. Tsao, A. Lin, M. Zhang, S. L. Levengood, and M. Zhang, "PEG-Chitosan Hydrogel with Tunable Stiffness for Study of Drug Response of Breast Cancer Cells," *Polymers*, vol. 8, no. 4, p. 112, Mar. 2016.

[14] M. J. Paszek *et al.*, "Tensional homeostasis and the malignant phenotype," *Cancer Cell*, vol. 8, no. 3, pp. 241–254, Sep. 2005.

[15] A. Ben-Ze'ev and A. Raz, "Relationship between the Organization and Synthesis of Vimentin and the Metastatic Capability of B16 Melanoma Cells," *Cancer Res.*, vol. 45, no. 6, pp. 2632–2641, Jun. 1985.

[16] Y. W. Chu, E. A. Seftor, L. H. Romer, and M. J. Hendrix, "Experimental coexpression of vimentin and keratin intermediate filaments in human melanoma cells augments motility," *Am. J. Pathol.*, vol. 148, no. 1, pp. 63–69, Jan. 1996.

[17] M. J. Hendrix, E. A. Seftor, R. E. Seftor, and K. T. Trevor, "Experimental co-expression of vimentin and keratin intermediate filaments in human breast cancer cells results in phenotypic interconversion and increased invasive behavior.," *Am. J. Pathol.*, vol. 150, no. 2, pp. 483–495, Feb. 1997.

[18] L. Hu *et al.*, "Association of Vimentin overexpression and hepatocellular carcinoma metastasis," *Oncogene*, vol. 23, no. 1, pp. 298–302, Jan. 2004.

[19] S. H. Lang *et al.*, "Enhanced expression of vimentin in motile prostate cell lines and in poorly differentiated and metastatic prostate carcinoma," *The Prostate*, vol. 52, no. 4, pp. 253–263, Sep. 2002.

[20] L.-L. Wang, X.-H. Zhang, X. Zhang, and J.-K. Chu, "MiR-30a increases cisplatin sensitivity of gastric cancer cells through suppressing epithelial-to-mesenchymal transition (EMT)," *Eur. Rev. Med. Pharmacol. Sci.*, vol. 20, no. 9, pp. 1733–1739, 2016.

[21] Y. Wang, Q.-Y. He, S.-W. Tsao, Y.-H. Cheung, A. Wong, and J.-F. Chiu, "Cytokeratin 8 silencing in human nasopharyngeal carcinoma cells leads to cisplatin sensitization," *Cancer Lett.*, vol. 265, no. 2, pp. 188–196, Jul. 2008.

[22] G. Xu *et al.*, "Cisplatin sensitivity is enhanced in non-small cell lung cancer cells by regulating epithelial-mesenchymal transition through inhibition of eukaryotic translation initiation factor 5A2," *BMC Pulm. Med.*, vol. 14, Nov. 2014.

[23] M. K. Jolly *et al.*, "Implications of the Hybrid Epithelial/Mesenchymal Phenotype in Metastasis," *Front. Oncol.*, vol. 5, Jul. 2015.

[24] K. Ellis, J. Bagwell, and M. Bagnat, "Notochord vacuoles are lysosome-related organelles that function in axis and spine morphogenesis," *J. Cell Biol.*, vol. 200, no. 5, pp. 667–679, Mar. 2013.

[25] T. J. Koob and J. H. Long, "The Vertebrate Body Axis: Evolution and Mechanical Function," *Am. Zool.*, vol. 40, no. 1, pp. 1–018, Feb. 2000.

[26] D. L. Stemple, "Structure and function of the notochord: an essential organ for chordate development," *Development*, vol. 132, no. 11, pp. 2503–2512, Jun. 2005.

[27] D. S. Adams, R. Keller, and M. A. Koehl, "The mechanics of notochord elongation, straightening and stiffening in the embryo of Xenopus laevis," *Dev. Camb. Engl.*, vol. 110, no. 1, pp. 115–130, Sep. 1990.

[28] B. G. Herrmann and A. Kispert, "The T genes in embryogenesis," *Trends Genet. TIG*, vol. 10, no. 8, pp. 280–286, Aug. 1994.

[29] P. Smits and V. Lefebvre, "Sox5 and Sox6 are required for notochord extracellular matrix sheath formation, notochord cell survival and development of the nucleus pulposus of intervertebral discs," *Development*, vol. 130, no. 6, pp. 1135–1148, Mar. 2003.

[30] C. Chiang *et al.*, "Cyclopia and defective axial patterning in mice lacking Sonic hedgehog gene function," *Nature*, vol. 383, no. 6599, pp. 407–413, Oct. 1996.

[31] J. A. McMahon, S. Takada, L. B. Zimmerman, C.-M. Fan, R. M. Harland, and A. P. McMahon, "Noggin-mediated antagonism of BMP signaling is required for growth and patterning of the neural tube and somite," *Genes Dev.*, vol. 12, no. 10, pp. 1438–1452, May 1998.

[32] A. Peacock, "Observations on the pre-natal development of the intervertebral disc in man," *J. Anat.*, vol. 85, no. Pt 3, pp. 260-274.4, Jul. 1951.

[33] M. R. McCann, O. J. Tamplin, J. Rossant, and C. A. Séguin, "Tracing notochord-derived cells using a Noto-cre mouse: implications for intervertebral disc development," *Dis. Model. Mech.*, vol. 5, no. 1, pp. 73–82, Jan. 2012.

[34] C. J. Hunter, J. R. Matyas, and N. A. Duncan, "Cytomorphology of notochordal and chondrocytic cells from the nucleus pulposus: a species comparison," *J. Anat.*, vol. 205, no. 5, pp. 357–362, Nov. 2004.

[35] J. J. Trout, J. A. Buckwalter, K. C. Moore, and S. K. Landas, “Ultrastructure of the human intervertebral disc. I. Changes in notochordal cells with age,” *Tissue Cell*, vol. 14, no. 2, pp. 359–369, 1982.

[36] J. J. Trout, J. A. Buckwalter, and K. C. Moore, “Ultrastructure of the human intervertebral disc: II. Cells of the nucleus pulposus,” *Anat. Rec.*, vol. 204, no. 4, pp. 307–314, Dec. 1982.

[37] U. E. Pazzaglia, J. R. Salisbury, and P. D. Byers, “Development and involution of the notochord in the human spine.,” *J. R. Soc. Med.*, vol. 82, no. 7, pp. 413–415, Jul. 1989.

[38] C. J. Hunter, J. R. Matyas, and N. A. Duncan, “The functional significance of cell clusters in the notochordal nucleus pulposus: survival and signaling in the canine intervertebral disc,” *Spine*, vol. 29, no. 10, pp. 1099–1104, May 2004.

[39] B. A. Maldonado and T. R. Oegema, “Initial characterization of the metabolism of intervertebral disc cells encapsulated in microspheres,” *J. Orthop. Res.*, vol. 10, no. 5, pp. 677–690, Sep. 1992.

[40] C. J. Hunter, J. R. Matyas, and N. A. Duncan, “The three-dimensional architecture of the notochordal nucleus pulposus: novel observations on cell structures in the canine intervertebral disc,” *J. Anat.*, vol. 202, no. 3, pp. 279–291, Mar. 2003.

[41] A. Gilson, M. Dreger, and J. P. Urban, “Differential expression level of cytokeratin 8 in cells of the bovine nucleus pulposus complicates the search for specific intervertebral disc cell markers,” *Arthritis Res. Ther.*, vol. 12, no. 1, p. R24, 2010.

[42] J. Chen, W. Yan, and L. A. Setton, “Molecular phenotypes of notochordal cells purified from immature nucleus pulposus,” *Eur. Spine J.*, vol. 15, no. Suppl 3, pp. 303–311, Aug. 2006.

[43] C. j. Hunter, J. r. Matyas, and N. a. Duncan, “The Notochordal Cell in the Nucleus Pulposus: A Review in the Context of Tissue Engineering,” *Tissue Eng.*, vol. 9, no. 4, pp. 667–677, Aug. 2003.

[44] T. Saggese, P. Redey, and S. R. McGlashan, “Same-species phenotypic comparison of notochordal and mature nucleus pulposus cells,” *Eur. Spine J.*, vol. 24, no. 9, pp. 1976–1985, Dec. 2014.

[45] X. Tang, L. Jing, and J. Chen, “Changes in the Molecular Phenotype of Nucleus Pulposus Cells with Intervertebral Disc Aging,” *PLoS ONE*, vol. 7, no. 12, Dec. 2012.

[46] F. Lv, V. Y. L. Leung, S. Huang, Y. Huang, Y. Sun, and K. M. C. Cheung, “In search of nucleus pulposus-specific molecular markers,” *Rheumatology*, vol. 53, no. 4, pp. 600–610, Apr. 2014.

[47] M. V. Risbud *et al.*, “Defining the Phenotype of Young Healthy Nucleus Pulposus Cells: Recommendations of the Spine Research Interest Group at the 2014 Annual ORS Meeting,” *J. Orthop. Res. Off. Publ. Orthop. Res. Soc.*, vol. 33, no. 3, pp. 283–293, Mar. 2015.

[48] P. Stosiek, M. Kasper, and U. Karsten, “Expression of cytokeratin and vimentin in nucleus pulposus cells,” *Differentiation*, vol. 39, no. 1, pp. 78–81, Nov. 1988.

[49] Z. Sun *et al.*, “Down-regulated CK8 expression in human intervertebral disc degeneration,” *Int. J. Med. Sci.*, vol. 10, no. 8, pp. 948–956, 2013.

[50] B. M. Minogue, S. M. Richardson, L. A. Zeef, A. J. Freemont, and J. A. Hoyland, “Transcriptional profiling of bovine intervertebral disc cells: implications for identification of normal and degenerate human intervertebral disc cell phenotypes,” *Arthritis Res. Ther.*, vol. 12, no. 1, p. R22, 2010.

[51] F. Wang, F. Cai, R. Shi, X.-H. Wang, and X.-T. Wu, “Aging and age related stresses: a senescence mechanism of intervertebral disc degeneration,” *Osteoarthritis Cartilage*, vol. 24, no. 3, pp. 398–408, Mar. 2016.

[52] S. Vujovic *et al.*, “Brachyury, a crucial regulator of notochordal development, is a novel biomarker for chordomas,” *J. Pathol.*, vol. 209, no. 2, pp. 157–165, Jun. 2006.

[53] J. Bjornsson, L. E. Wold, M. J. Ebersold, and E. R. Laws, “Chordoma of the mobile spine. A clinicopathologic analysis of 40 patients,” *Cancer*, vol. 71, no. 3, pp. 735–740, Feb. 1993.

[54] C. Youssef, S. Aoun, J. R. Moreno, and C. A. Bagley, “Recent advances in understanding and managing chordomas,” *F1000Research*, vol. 5, p. 2902, Dec. 2016.

[55] S. Gulluoglu, O. Turksoy, A. Kuskucu, U. Ture, and O. F. Bayrak, “The molecular aspects of chordoma,” *Neurosurg. Rev.*, vol. 39, no. 2, pp. 185–196, Apr. 2016.

[56] J. R. Salisbury, “[Embryology and pathology of the human notochord],” *Ann. Pathol.*, vol. 21, no. 6, pp. 479–488, Dec. 2001.

[57] N. Presneau *et al.*, “Role of the transcription factor T (brachyury) in the pathogenesis of sporadic chordoma: a genetic and functional-based study,” *J. Pathol.*, vol. 223, no. 3, pp. 327–335, Feb. 2011.

[58] I. O. Karikari *et al.*, "Molecular characterization of chordoma xenografts generated from a novel primary chordoma cell source and two chordoma cell lines," *J. Neurosurg. Spine*, vol. 21, no. 3, pp. 386–393, Sep. 2014.

[59] K.-S. Choi, M. J. Cohn, and B. D. Harfe, "Identification of Nucleus Pulposus Precursor Cells and Notochordal Remnants in the Mouse: Implications for Disk Degeneration and Chordoma Formation," *Dev. Dyn. Off. Publ. Am. Assoc. Anat.*, vol. 237, no. 12, pp. 3953–3958, Dec. 2008.

[60] J. R. Salisbury and P. G. Isaacson, "Demonstration of cytokeratins and an epithelial membrane antigen in chordomas and human fetal notochord," *Am. J. Surg. Pathol.*, vol. 9, no. 11, pp. 791–797, Nov. 1985.

[61] B. J. O'Hara, A. Paetau, and M. Miettinen, "Keratin subsets and monoclonal antibody HBME-1 in chordoma: immunohistochemical differential diagnosis between tumors simulating chordoma," *Hum. Pathol.*, vol. 29, no. 2, pp. 119–126, Feb. 1998.

[62] S. Brüderlein *et al.*, "Molecular Characterization of Putative Chordoma Cell Lines, Molecular Characterization of Putative Chordoma Cell Lines," *Sarcoma Sarcoma*, vol. 2010, 2010, p. e630129, Dec. 2010.

[63] B. Rinner *et al.*, "Establishment and detailed functional and molecular genetic characterisation of a novel sacral chordoma cell line, MUG-Chor1," *Int. J. Oncol.*, vol. 40, no. 2, pp. 443–451, Feb. 2012.

[64] N. Fujita *et al.*, "A chordoma-derived cell line U-CH1-N recapitulates the biological properties of notochordal nucleus pulposus cells," *J. Orthop. Res. Off. Publ. Orthop. Res. Soc.*, Jun. 2016.

[65] S. Boriani *et al.*, "Chordoma of the mobile spine: fifty years of experience," *Spine*, vol. 31, no. 4, pp. 493–503, Feb. 2006.

[66] O. F. Bayrak *et al.*, "The effects of chemotherapeutic agents on differentiated chordoma cells," *J. Neurosurg. Spine*, vol. 15, no. 6, pp. 620–624, Dec. 2011.

[67] J. Schwab *et al.*, "Combination of PI3K/mTOR inhibition demonstrates efficacy in human chordoma," *Anticancer Res.*, vol. 29, no. 6, pp. 1867–1871, Jun. 2009.

[68] C. Yang *et al.*, "Characterization and Analysis of Human Chordoma Cell Lines," *Spine*, vol. 35, no. 13, pp. 1257–1264, Jun. 2010.

[69] C. R. Heery *et al.*, "Phase I Trial of a Yeast-Based Therapeutic Cancer Vaccine (GI-6301) Targeting the Transcription Factor Brachyury," *Cancer Immunol. Res.*, vol. 3, no. 11, pp. 1248–1256, Nov. 2015.

[70] K. Sugimoto, T. Hayata, and M. Asashima, “XBtg2 is required for notochord differentiation during early Xenopus development,” *Dev. Growth Differ.*, vol. 47, no. 7, pp. 435–443, Sep. 2005.

[71] C. J. Hunter, S. Bianchi, P. Cheng, and K. Muldrew, “Osmoregulatory Function of Large Vacuoles Found in Notochordal Cells of the Intervertebral Disc,” *Mol. Cell. Biomech. MCB*, vol. 4, no. 4, pp. 227–237, Dec. 2007.

[72] M. V. Risbud *et al.*, “Defining the phenotype of young healthy nucleus pulposus cells: Recommendations of the Spine Research Interest Group at the 2014 annual ORS meeting,” *J. Orthop. Res.*, vol. 33, no. 3, pp. 283–293, Mar. 2015.

[73] B. M. Minogue, S. M. Richardson, L. A. H. Zeef, A. J. Freemont, and J. A. Hoyland, “Characterization of the human nucleus pulposus cell phenotype and evaluation of novel marker gene expression to define adult stem cell differentiation,” *Arthritis Rheum.*, vol. 62, no. 12, pp. 3695–3705, Dec. 2010.

[74] G. M. Cooper, “Intermediate Filaments,” *Cell Mol. Approach 2nd Ed.*, 2000.

[75] E. J. Blain, “Involvement of the cytoskeletal elements in articular cartilage homeostasis and pathology,” *Int. J. Exp. Pathol.*, vol. 90, no. 1, pp. 1–15, Feb. 2009.

[76] M. D’Alessandro, D. Russell, S. M. Morley, A. M. Davies, and E. B. Lane, “Keratin mutations of epidermolysis bullosa simplex alter the kinetics of stress response to osmotic shock,” *J. Cell Sci.*, vol. 115, no. Pt 22, pp. 4341–4351, Nov. 2002.

[77] S. Sivaramakrishnan, J. V. DeGiulio, L. Lorand, R. D. Goldman, and K. M. Ridge, “Micromechanical properties of keratin intermediate filament networks,” *Proc. Natl. Acad. Sci. U. S. A.*, vol. 105, no. 3, pp. 889–894, Jan. 2008.

[78] L. Ramms *et al.*, “Keratins as the main component for the mechanical integrity of keratinocytes,” *Proc. Natl. Acad. Sci. U. S. A.*, vol. 110, no. 46, pp. 18513–18518, Nov. 2013.

[79] P. A. Coulombe and P. Wong, “Cytoplasmic intermediate filaments revealed as dynamic and multipurpose scaffolds,” *Nat. Cell Biol.*, vol. 6, no. 8, pp. 699–706, Aug. 2004.

[80] R. Vassar, P. A. Coulombe, L. Degenstein, K. Albers, and E. Fuchs, “Mutant keratin expression in transgenic mice causes marked abnormalities resembling a human genetic skin disease,” *Cell*, vol. 64, no. 2, pp. 365–380, Jan. 1991.

[81] M. Gregor *et al.*, "Mechanosensing through focal adhesion-anchored intermediate filaments," *FASEB J. Off. Publ. Fed. Am. Soc. Exp. Biol.*, vol. 28, no. 2, pp. 715–729, Feb. 2014.

[82] P. M. Schiffers *et al.*, "Altered flow-induced arterial remodeling in vimentin-deficient mice," *Arterioscler. Thromb. Vasc. Biol.*, vol. 20, no. 3, pp. 611–616, Mar. 2000.

[83] A.-M. Fortier, E. Asselin, and M. Cadrin, "Keratin 8 and 18 Loss in Epithelial Cancer Cells Increases Collective Cell Migration and Cisplatin Sensitivity through Claudin1 Up-regulation," *J. Biol. Chem.*, vol. 288, no. 16, pp. 11555–11571, Apr. 2013.

[84] B. Zhang *et al.*, "Cytokeratin 18 knockdown decreases cell migration and increases chemosensitivity in non-small cell lung cancer," *J. Cancer Res. Clin. Oncol.*, vol. 142, no. 12, pp. 2479–2487, Dec. 2016.

[85] B. Eckes *et al.*, "Impaired mechanical stability, migration and contractile capacity in vimentin-deficient fibroblasts," *J. Cell Sci.*, vol. 111, no. 13, pp. 1897–1907, Jul. 1998.

[86] J. E. Eriksson *et al.*, "Introducing intermediate filaments: from discovery to disease," *J. Clin. Invest.*, vol. 119, no. 7, pp. 1763–1771, Jul. 2009.

[87] D. R. Haudenschild *et al.*, "Vimentin contributes to changes in chondrocyte stiffness in osteoarthritis," *J. Orthop. Res.*, vol. 29, no. 1, pp. 20–25, Jan. 2011.

[88] B. T. Helfand *et al.*, "Vimentin organization modulates the formation of lamellipodia," *Mol. Biol. Cell*, vol. 22, no. 8, pp. 1274–1289, Apr. 2011.

[89] J. T. Thaiparambil *et al.*, "Withaferin A inhibits breast cancer invasion and metastasis at sub-cytotoxic doses by inducing vimentin disassembly and serine 56 phosphorylation," *Int. J. Cancer*, vol. 129, no. 11, pp. 2744–2755, Dec. 2011.

[90] C. Velez-delValle, M. Marsch-Moreno, F. Castro-Muñozledo, I. J. Galván-Mendoza, and W. Kuri-Harcuch, "Epithelial cell migration requires the interaction between the vimentin and keratin intermediate filaments," *Sci. Rep.*, vol. 6, p. 24389, Apr. 2016.

[91] M. G. Mendez, S.-I. Kojima, and R. D. Goldman, "Vimentin induces changes in cell shape, motility, and adhesion during the epithelial to mesenchymal transition," *FASEB J. Off. Publ. Fed. Am. Soc. Exp. Biol.*, vol. 24, no. 6, pp. 1838–1851, Jun. 2010.

[92] M. Tijsterman and R. H. A. Plasterk, "Dicers at RISC: The Mechanism of RNAi," *Cell*, vol. 117, no. 1, pp. 1–3, Apr. 2004.

[93] D. M. Dykxhoorn, C. D. Novina, and P. A. Sharp, “Killing the messenger: short RNAs that silence gene expression,” *Nat. Rev. Mol. Cell Biol.*, vol. 4, no. 6, pp. 457–467, Jun. 2003.

[94] M. L. Bobbin and J. J. Rossi, “RNA Interference (RNAi)-Based Therapeutics: Delivering on the Promise?,” *Annu. Rev. Pharmacol. Toxicol.*, vol. 56, no. 1, pp. 103–122, 2016.

[95] C. Morrison, “Alnylam prepares to land first RNAi drug approval,” *Nature Reviews Drug Discovery*, 28-Feb-2018. [Online]. Available: https://www-nature-com.proxy-um.researchport.umd.edu/articles/nrd.2018.20. [Accessed: 05-May-2018].

[96] F. C. Ramaekers, D. Haag, A. Kant, O. Moesker, P. H. Jap, and G. P. Vooijs, “Coexpression of keratin- and vimentin-type intermediate filaments in human metastatic carcinoma cells,” *Proc. Natl. Acad. Sci. U. S. A.*, vol. 80, no. 9, pp. 2618–2622, May 1983.

[97] C. M. Coffin, P. E. Swanson, M. R. Wick, and L. P. Dehner, “An immunohistochemical comparison of chordoma with renal cell carcinoma, colorectal adenocarcinoma, and myxopapillary ependymoma: a potential diagnostic dilemma in the diminutive biopsy,” *Mod. Pathol. Off. J. U. S. Can. Acad. Pathol. Inc*, vol. 6, no. 5, pp. 531–538, Sep. 1993.

[98] E. B. Lane, B. L. M. Hogan, M. Kurkinen, and J. I. Garrels, “Co-expression of vimentin and cytokeratins in parietal endoderm cells of early mouse embryo,” *Nature*, vol. 303, no. 5919, pp. 701–704, Jun. 1983.

[99] M. Kasper and U. Karsten, “Coexpression of cytokeratin and vimentin in Rathke’s cysts of the human pituitary gland,” *Cell Tissue Res.*, vol. 253, no. 2, pp. 419–424, Aug. 1988.

[100] J. Antoniou *et al.*, “The human lumbar intervertebral disc: evidence for changes in the biosynthesis and denaturation of the extracellular matrix with growth, maturation, ageing, and degeneration.,” *J. Clin. Invest.*, vol. 98, no. 4, pp. 996–1003, Aug. 1996.

[101] J. A. Buckwalter, “Aging and degeneration of the human intervertebral disc,” *Spine*, vol. 20, no. 11, pp. 1307–1314, Jun. 1995.

[102] H. Bühler and G. Schaller, “Transfection of keratin 18 gene in human breast cancer cells causes induction of adhesion proteins and dramatic regression of malignancy in vitro and in vivo,” *Mol. Cancer Res. MCR*, vol. 3, no. 7, pp. 365–371, Jul. 2005.

[103] M. Nieminen, T. Henttinen, M. Merinen, F. Marttila-Ichihara, J. E. Eriksson, and S. Jalkanen, "Vimentin function in lymphocyte adhesion and transcellular migration," *Nat. Cell Biol.*, vol. 8, no. 2, pp. 156–162, Feb. 2006.

[104] N. Yamashita *et al.*, "Vimentin as a poor prognostic factor for triple-negative breast cancer," *J. Cancer Res. Clin. Oncol.*, vol. 139, no. 5, pp. 739–746, May 2013.

[105] T. Fillies *et al.*, "Cytokeratin 8/18 expression indicates a poor prognosis in squamous cell carcinomas of the oral cavity," *BMC Cancer*, vol. 6, p. 10, Jan. 2006.

[106] T. Makino *et al.*, "Cytokeratins 18 and 8 are poor prognostic markers in patients with squamous cell carcinoma of the oesophagus," *Br. J. Cancer*, vol. 101, no. 8, pp. 1298–1306, Oct. 2009.

[107] Y. Messai *et al.*, "Cytokeratin 18 expression pattern correlates with renal cell carcinoma progression: relationship with Snail," *Int. J. Oncol.*, vol. 36, no. 5, pp. 1145–1154, May 2010.

[108] T. Knösel, V. Emde, K. Schlüns, P. M. Schlag, M. Dietel, and I. Petersen, "Cytokeratin profiles identify diagnostic signatures in colorectal cancer using multiplex analysis of tissue microarrays," *Cell. Oncol. Off. J. Int. Soc. Cell. Oncol.*, vol. 28, no. 4, pp. 167–175, 2006.

[109] U. Woelfle, G. Sauter, S. Santjer, R. Brakenhoff, and K. Pantel, "Down-regulated expression of cytokeratin 18 promotes progression of human breast cancer," *Clin. Cancer Res. Off. J. Am. Assoc. Cancer Res.*, vol. 10, no. 8, pp. 2670–2674, Apr. 2004.

[110] K. R. Levental *et al.*, "Matrix Crosslinking Forces Tumor Progression by Enhancing Integrin signaling," *Cell*, vol. 139, no. 5, pp. 891–906, Nov. 2009.

[111] P. Lu, V. M. Weaver, and Z. Werb, "The extracellular matrix: A dynamic niche in cancer progression," *J Cell Biol*, vol. 196, no. 4, pp. 395–406, Feb. 2012.

[112] M. Bignon *et al.*, "Lysyl oxidase-like protein-2 regulates sprouting angiogenesis and type IV collagen assembly in the endothelial basement membrane," *Blood*, vol. 118, no. 14, pp. 3979–3989, Oct. 2011.

[113] M. A. Wozniak, R. Desai, P. A. Solski, C. J. Der, and P. J. Keely, "ROCK-generated contractility regulates breast epithelial cell differentiation in response to the physical properties of a three-dimensional collagen matrix," *J. Cell Biol.*, vol. 163, no. 3, pp. 583–595, Nov. 2003.

[114] S. E. Cross, Y.-S. Jin, J. Rao, and J. K. Gimzewski, “Nanomechanical analysis of cells from cancer patients,” *Nat. Nanotechnol.*, vol. 2, no. 12, pp. 780–783, Dec. 2007.

[115] J. Guck *et al.*, “Optical deformability as an inherent cell marker for testing malignant transformation and metastatic competence,” *Biophys. J.*, vol. 88, no. 5, pp. 3689–3698, May 2005.

[116] Z. Li *et al.*, “Cellular traction forces: a useful parameter in cancer research,” *Nanoscale*, vol. 9, no. 48, pp. 19039–19044, Dec. 2017.

[117] V. Peschetola *et al.*, “Time-dependent traction force microscopy for cancer cells as a measure of invasiveness,” *Cytoskelet. Hoboken NJ*, vol. 70, no. 4, pp. 201–214, Apr. 2013.

[118] G. Zhang, M. Long, Z.-Z. Wu, and W.-Q. Yu, “Mechanical properties of hepatocellular carcinoma cells,” *World J. Gastroenterol.*, vol. 8, no. 2, pp. 243–246, Apr. 2002.

[119] R. H. Pearce, B. J. Grimmer, and M. E. Adams, “Degeneration and the chemical composition of the human lumbar intervertebral disc,” *J. Orthop. Res. Off. Publ. Orthop. Res. Soc.*, vol. 5, no. 2, pp. 198–205, 1987.

[120] T. Miyazaki, S. Kobayashi, K. Takeno, A. Meir, J. Urban, and H. Baba, “A Phenotypic Comparison of Proteoglycan Production of Intervertebral Disc Cells Isolated from Rats, Rabbits, and Bovine Tails; Which Animal Model is Most Suitable to Study Tissue Engineering and Biological Repair of Human Disc Disorders?,” *Tissue Eng. Part A*, vol. 15, no. 12, pp. 3835–3846, Aug. 2009.

[121] M. A. Adams, P. Lama, U. Zehra, and P. Dolan, “Why do some intervertebral discs degenerate, when others (in the same spine) do not?,” *Clin. Anat.*, vol. 28, no. 2, pp. 195–204, Mar. 2015.

[122] K. Luoma, H. Riihimäki, R. Luukkonen, R. Raininko, E. Viikari-Juntura, and A. Lamminen, “Low back pain in relation to lumbar disc degeneration,” *Spine*, vol. 25, no. 4, pp. 487–492, Feb. 2000.

[123] F. Wang *et al.*, “Formation, function, and exhaustion of notochordal cytoplasmic vacuoles within intervertebral disc: current understanding and speculation,” *Oncotarget*, vol. 8, no. 34, pp. 57800–57812, Aug. 2017.

[124] N. S. Chari and T. J. McDonnell, “The sonic hedgehog signaling network in development and neoplasia,” *Adv. Anat. Pathol.*, vol. 14, no. 5, pp. 344–352, Sep. 2007.

[125] M. Roselli *et al.*, "Brachyury, a driver of the epithelial-mesenchymal transition, is overexpressed in human lung tumors: an opportunity for novel interventions against lung cancer," *Clin. Cancer Res. Off. J. Am. Assoc. Cancer Res.*, vol. 18, no. 14, pp. 3868–3879, Jul. 2012.

[126] Y. Bai *et al.*, "Sonic hedgehog-mediated epithelial-mesenchymal transition in renal tubulointerstitial fibrosis," *Int. J. Mol. Med.*, vol. 37, no. 5, pp. 1317–1327, May 2016.

[127] H. M. Behnsawy *et al.*, "Possible Role of Sonic Hedgehog and Epithelial-Mesenchymal Transition in Renal Cell Cancer Progression," *Korean J. Urol.*, vol. 54, no. 8, pp. 547–554, Aug. 2013.

[128] S. Nakajima *et al.*, "N-cadherin expression and epithelial-mesenchymal transition in pancreatic carcinoma," *Clin. Cancer Res. Off. J. Am. Assoc. Cancer Res.*, vol. 10, no. 12 Pt 1, pp. 4125–4133, Jun. 2004.

[129] W. Song and G. C. Gobe, "Understanding Molecular Pathways and Targets of Brachyury in Epithelial-mesenchymal Transition (EMT) in Human Cancers," *Curr. Cancer Drug Targets*, vol. 16, no. 7, pp. 586–593, 2016.

[130] X. Xu *et al.*, "Sonic Hedgehog-Gli1 Signaling Pathway Regulates the Epithelial Mesenchymal Transition (EMT) by Mediating a New Target Gene, S100A4, in Pancreatic Cancer Cells," *PLoS ONE*, vol. 9, no. 7, Jul. 2014.

[131] N. Kanaji, S. Bandoh, J. Fujita, T. Ishii, T. Ishida, and A. Kubo, "Compensation of type I and type II cytokeratin pools in lung cancer," *Lung Cancer*, vol. 55, no. 3, pp. 295–302, Mar. 2007.

[132] A. Ben-Ze'ev, "Differential control of cytokeratins and vimentin synthesis by cell-cell contact and cell spreading in cultured epithelial cells," *J. Cell Biol.*, vol. 99, no. 4 Pt 1, pp. 1424–1433, Oct. 1984.

[133] D. Tsuruta and J. C. R. Jones, "The vimentin cytoskeleton regulates focal contact size and adhesion of endothelial cells subjected to shear stress," *J. Cell Sci.*, vol. 116, no. 24, pp. 4977–4984, Dec. 2003.

[134] J. Uttam *et al.*, "The genetic basis of epidermolysis bullosa simplex with mottled pigmentation," *Proc. Natl. Acad. Sci.*, vol. 93, no. 17, pp. 9079–9084, Aug. 1996.

[135] M. Potokar *et al.*, "Cytoskeleton and vesicle mobility in astrocytes," *Traffic Cph. Den.*, vol. 8, no. 1, pp. 12–20, Jan. 2007.

[136] Y. Kumar and R. H. Valdivia, “Actin and intermediate filaments stabilize the Chlamydia trachomatis vacuole by forming dynamic structural scaffolds,” *Cell Host Microbe*, vol. 4, no. 2, pp. 159–169, Aug. 2008.

[137] H. K. Truchan, C. L. Cockburn, L. J. May, L. VieBrock, and J. A. Carlyon, “Anaplasma phagocytophilum-Occupied Vacuole Interactions with the Host Cell Cytoskeleton,” *Vet. Sci.*, vol. 3, no. 3, p. 25, Sep. 2016.

[138] J. Ibarrondo *et al.*, “Close association of the alpha subunits of Gq and G11 G proteins with actin filaments in WRK1 cells: relation to G protein-mediated phospholipase C activation.,” *Proc. Natl. Acad. Sci. U. S. A.*, vol. 92, no. 18, pp. 8413–8417, Aug. 1995.

[139] J. Swanson, A. Bushnell, and S. C. Silverstein, “Tubular lysosome morphology and distribution within macrophages depend on the integrity of cytoplasmic microtubules,” *Proc. Natl. Acad. Sci. U. S. A.*, vol. 84, no. 7, pp. 1921–1925, Apr. 1987.

[140] W. R. Trickey, T. P. Vail, and F. Guilak, “The role of the cytoskeleton in the viscoelastic properties of human articular chondrocytes,” *J. Orthop. Res.*, vol. 22, no. 1, pp. 131–139, Jan. 2004.

[141] Á. T. Vigfúsdóttir, C. Pasrija, P. I. Thakore, R. B. Schmidt, and A. H. Hsieh, “Role of Pericellular Matrix in Mesenchymal Stem Cell Deformation during Chondrogenic Differentiation,” *Cell. Mol. Bioeng.*, vol. 3, no. 4, pp. 387–397, Jul. 2010.

[142] A. Rastogi *et al.*, “Environmental regulation of notochordal gene expression in nucleus pulposus cells,” *J. Cell. Physiol.*, vol. 220, no. 3, pp. 698–705, Sep. 2009.

[143] K. J. Livak and T. D. Schmittgen, “Analysis of Relative Gene Expression Data Using Real-Time Quantitative PCR and the 2−ΔΔCT Method,” *Methods*, vol. 25, no. 4, pp. 402–408, Dec. 2001.

[144] C. L. Gilchrist, E. M. Darling, J. Chen, and L. A. Setton, “Extracellular Matrix Ligand and Stiffness Modulate Immature Nucleus Pulposus Cell-Cell Interactions,” *PLOS ONE*, vol. 6, no. 11, p. e27170, Nov. 2011.

[145] H. K. Kleinman, M. L. McGarvey, L. A. Liotta, P. G. Robey, K. Tryggvason, and G. R. Martin, “Isolation and characterization of type IV procollagen, laminin, and heparan sulfate proteoglycan from the EHS sarcoma,” *Biochemistry*, vol. 21, no. 24, pp. 6188–6193, Nov. 1982.

[146] N. Buisson *et al.*, "An adhesome comprising laminin, dystroglycan and myosin IIA is required during notochord development in Xenopus laevis," *Dev. Camb. Engl.*, vol. 141, no. 23, pp. 4569–4579, Dec. 2014.

[147] J. Shih and R. Keller, "Cell motility driving mediolateral intercalation in explants of Xenopus laevis," *Development*, vol. 116, no. 4, pp. 901–914, Dec. 1992.

[148] E. C. Dell'Angelica, C. Mullins, S. Caplan, and J. S. Bonifacino, "Lysosome-related organelles," *FASEB J. Off. Publ. Fed. Am. Soc. Exp. Biol.*, vol. 14, no. 10, pp. 1265–1278, Jul. 2000.

[149] H. K. Grønlien, C. Stock, M. S. Aihara, R. D. Allen, and Y. Naitoh, "Relationship between the membrane potential of the contractile vacuole complex and its osmoregulatory activity in Paramecium multimicronucleatum," *J. Exp. Biol.*, vol. 205, no. 20, pp. 3261–3270, Oct. 2002.

[150] C. Stock, H. K. Grønlien, R. D. Allen, and Y. Naitoh, "Osmoregulation in Paramecium: in situ ion gradients permit water to cascade through the cytosol to the contractile vacuole," *J. Cell Sci.*, vol. 115, no. Pt 11, pp. 2339–2348, Jun. 2002.

[151] T. Wassmer, M. Froissard, H. Plattner, R. Kissmehl, and J. Cohen, "The vacuolar proton-ATPase plays a major role in several membrane-bounded organelles in Paramecium," *J. Cell Sci.*, vol. 118, no. 13, pp. 2813–2825, Jul. 2005.

[152] A. Aplin, T. Jasionowski, D. L. Tuttle, S. E. Lenk, and W. A. Dunn, "Cytoskeletal elements are required for the formation and maturation of autophagic vacuoles," *J. Cell. Physiol.*, vol. 152, no. 3, pp. 458–466, Sep. 1992.

[153] L. Chang and R. D. Goldman, "Intermediate filaments mediate cytoskeletal crosstalk," *Nat. Rev. Mol. Cell Biol.*, vol. 5, no. 8, pp. 601–613, Aug. 2004.

[154] Y. H. Tee *et al.*, "Cellular chirality arising from the self-organization of the actin cytoskeleton," *Nat. Cell Biol.*, vol. 17, no. 4, pp. 445–457, Apr. 2015.

[155] M. M. P. Zegers, K. J. M. Zaal, S. C. D. van IJzendoorn, K. Klappe, and D. Hoekstra, "Actin Filaments and Microtubules are Involved in Different Membrane Traffic Pathways That Transport Sphingolipids to the Apical Surface of Polarized HepG2 Cells," *Mol. Biol. Cell*, vol. 9, no. 7, pp. 1939–1949, Jul. 1998.

[156] M. Schliwa, "Action of cytochalasin D on cytoskeletal networks," *J. Cell Biol.*, vol. 92, no. 1, pp. 79–91, Jan. 1982.

[157] E. Lehtonen, V. Stefanovic, and M. Saraga-Babic, “Changes in the expression of intermediate filaments and desmoplakins during development of human notochord,” *Differ. Res. Biol. Divers.*, vol. 59, no. 1, pp. 43–49, Jul. 1995.

[158] S. Umehara, S. Tadano, K. Abumi, K. Katagiri, K. Kaneda, and T. Ukai, “Effects of degeneration on the elastic modulus distribution in the lumbar intervertebral disc,” *Spine*, vol. 21, no. 7, pp. 811–819; discussion 820, Apr. 1996.

[159] L. L. Norman and H. Aranda-Espinoza, “Cortical Neuron Outgrowth is Insensitive to Substrate Stiffness,” *Cell. Mol. Bioeng.*, vol. 3, no. 4, pp. 398–414, Dec. 2010.

[160] K. M. Stroka and H. Aranda-Espinoza, “Neutrophils display biphasic relationship between migration and substrate stiffness,” *Cell Motil. Cytoskeleton*, vol. 66, no. 6, pp. 328–341, Jun. 2009.

[161] S. J. Han, Y. Oak, A. Groisman, and G. Danuser, “Traction microscopy to identify force modulation in subresolution adhesions,” *Nat. Methods*, vol. 12, no. 7, pp. 653–656, Jul. 2015.

[162] R. Barer and S. Tkaczyk, “Refractive Index of Concentrated Protein Solutions,” *Nature*, vol. 173, no. 4409, pp. 821–822, May 1954.

[163] G. Scarcelli *et al.*, “Noncontact three-dimensional mapping of intracellular hydro-mechanical properties by Brillouin microscopy,” *Nat. Methods*, vol. 12, no. 12, pp. 1132–1134, Dec. 2015.

[164] J. Zhang, X. A. Nou, H. Kim, and G. Scarcelli, “Brillouin flow cytometry for label-free mechanical phenotyping of the nucleus,” *Lab. Chip*, vol. 17, no. 4, pp. 663–670, Feb. 2017.

[165] D. E. Discher, P. Janmey, and Y. Wang, “Tissue Cells Feel and Respond to the Stiffness of Their Substrate,” *Science*, vol. 310, no. 5751, pp. 1139–1143, Nov. 2005.

[166] H. Kim, F. Nakamura, W. Lee, C. Hong, D. Pérez-Sala, and C. A. McCulloch, “Regulation of cell adhesion to collagen via β1 integrins is dependent on interactions of filamin A with vimentin and protein kinase C epsilon,” *Exp. Cell Res.*, vol. 316, no. 11, pp. 1829–1844, Jul. 2010.

[167] H. Kim, F. Nakamura, W. Lee, Y. Shifrin, P. Arora, and C. A. McCulloch, “Filamin A is required for vimentin-mediated cell adhesion and spreading,” *Am. J. Physiol.-Cell Physiol.*, vol. 298, no. 2, pp. C221–C236, Feb. 2010.

[168] W. W. Franke *et al.*, "Simultaneous expression of two different types of intermediate sized filaments in mouse keratinocytes proliferating in vitro," *Differ. Res. Biol. Divers.*, vol. 14, no. 1–2, pp. 35–50, 1979.

[169] I. A. Schafer, A. Shapiro, M. Kovach, C. Lang, and R. B. Fratianne, "The interaction of human papillary and reticular fibroblasts and human keratinocytes in the contraction of three-dimensional floating collagen lattices," *Exp. Cell Res.*, vol. 183, no. 1, pp. 112–125, Jul. 1989.

[170] M. Guo *et al.*, "The role of vimentin intermediate filaments in cortical and cytoplasmic mechanics," *Biophys. J.*, vol. 105, no. 7, pp. 1562–1568, Oct. 2013.

[171] K.-S. Delank, J. Kriegsmann, P. Drees, A. Eckardt, and P. Eysel, "Metastasizing chordoma of the lumbar spine," *Eur. Spine J.*, vol. 11, no. 2, pp. 167–171, Apr. 2002.

[172] D. Baratti *et al.*, "Chordoma: Natural History and Results in 28 Patients Treated at a Single Institution," *Ann. Surg. Oncol.*, vol. 10, no. 3, pp. 291–296, Apr. 2003.

[173] V. A. Young, K. M. Curtis, H. T. Temple, F. J. Eismont, T. F. DeLaney, and F. J. Hornicek, "Characteristics and Patterns of Metastatic Disease from Chordoma," *Sarcoma*, vol. 2015, 2015.

[174] C. Catton *et al.*, "Chordoma: long-term follow-up after radical photon irradiation," *Radiother. Oncol. J. Eur. Soc. Ther. Radiol. Oncol.*, vol. 41, no. 1, pp. 67–72, Oct. 1996.

[175] S. Rohatgi, N. H. Ramaiya, J. P. Jagannathan, S. A. Howard, A. B. Shinagare, and K. M. Krajewski, "Metastatic Chordoma: Report of the Two Cases and Review of the Literature," *Eurasian J. Med.*, vol. 47, no. 2, pp. 151–154, Jun. 2015.

[176] P. Bergh, L. G. Kindblom, B. Gunterberg, F. Remotti, W. Ryd, and J. M. Meis-Kindblom, "Prognostic factors in chordoma of the sacrum and mobile spine: a study of 39 patients," *Cancer*, vol. 88, no. 9, pp. 2122–2134, May 2000.

[177] T. Fischer, N. Wilharm, A. Hayn, and C. T. Mierke, "Matrix and cellular mechanical properties are the driving factors for facilitating human cancer cell motility into 3D engineered matrices," *Converg. Sci. Phys. Oncol.*, vol. 3, no. 4, p. 044003, 2017.

[178] J. D. Mih, A. Marinkovic, F. Liu, A. S. Sharif, and D. J. Tschumperlin, "Matrix stiffness reverses the effect of actomyosin tension on cell proliferation," *J. Cell Sci.*, vol. 125, no. Pt 24, pp. 5974–5983, Dec. 2012.

[179] A. J. Rice *et al.*, "Matrix stiffness induces epithelial-mesenchymal transition and promotes chemoresistance in pancreatic cancer cells," *Oncogenesis*, vol. 6, no. 7, p. e352, Jul. 2017.

[180] D. A. Senthebane *et al.*, "The Role of Tumor Microenvironment in Chemoresistance: To Survive, Keep Your Enemies Closer," *Int. J. Mol. Sci.*, vol. 18, no. 7, Jul. 2017.

[181] S. Sharma, C. Santiskulvong, J. Rao, J. K. Gimzewski, and O. Dorigo, "The role of Rho GTPase in cell stiffness and cisplatin resistance in ovarian cancer cells," *Integr. Biol. Quant. Biosci. Nano Macro*, vol. 6, no. 6, pp. 611–617, Jun. 2014.

[182] J. M. M. Cates, D. M. Itani, C. M. Coffin, and B. D. Harfe, "The sonic hedgehog pathway in chordoid tumours," *Histopathology*, vol. 56, no. 7, pp. 978–979, Jun. 2010.

[183] M. Miettinen, Z. Wang, J. Lasota, C. Heery, J. Schlom, and C. Palena, "Nuclear Brachyury Expression Is Consistent in Chordoma, Common in Germ Cell Tumors and Small Cell Carcinomas, and Rare in Other Carcinomas and Sarcomas: An Immunohistochemical Study of 5229 Cases," *Am. J. Surg. Pathol.*, vol. 39, no. 10, pp. 1305–1312, Oct. 2015.

[184] H. Zhang, K. Yang, T. Ren, Y. Huang, X. Tang, and W. Guo, "miR-16-5p inhibits chordoma cell proliferation, invasion and metastasis by targeting Smad3," *Cell Death Dis.*, vol. 9, no. 6, p. 680, Jun. 2018.

[185] E. Osaka *et al.*, "MicroRNA-1(miR-1) inhibits chordoma cell migration and invasion by targeting Slug," *J. Orthop. Res. Off. Publ. Orthop. Res. Soc.*, vol. 32, no. 8, pp. 1075–1082, Aug. 2014.

[186] Y. Ueda, Y. Oda, A. Kawashima, H. Tsuchiya, K. Tomita, and I. Nakanishi, "Collagenous and basement membrane proteins of chordoma: immunohistochemical analysis," *Histopathology*, vol. 21, no. 4, pp. 345–352, Oct. 1992.

[187] A. Huttenlocher and A. R. Horwitz, "Integrins in Cell Migration," *Cold Spring Harb. Perspect. Biol.*, vol. 3, no. 9, Sep. 2011.

[188] D. Schaeffer, J. A. Somarelli, G. Hanna, G. M. Palmer, and M. A. Garcia-Blanco, "Cellular Migration and Invasion Uncoupled: Increased Migration Is Not an Inexorable Consequence of Epithelial-to-Mesenchymal Transition," *Mol. Cell. Biol.*, vol. 34, no. 18, pp. 3486–3499, Sep. 2014.

[189] A. N. Ketene, E. M. Schmelz, P. C. Roberts, and M. Agah, "The effects of cancer progression on the viscoelasticity of ovarian cell cytoskeleton structures," *Nanomedicine Nanotechnol. Biol. Med.*, vol. 8, no. 1, pp. 93–102, Jan. 2012.

[190] W. Xu, R. Mezencev, B. Kim, L. Wang, J. McDonald, and T. Sulchek, "Cell Stiffness Is a Biomarker of the Metastatic Potential of Ovarian Cancer Cells," *PLOS ONE*, vol. 7, no. 10, p. e46609, Oct. 2012.

[191] D. W. Bartlett and M. E. Davis, "Insights into the kinetics of siRNA-mediated gene silencing from live-cell and live-animal bioluminescent imaging," *Nucleic Acids Res.*, vol. 34, no. 1, pp. 322–333, 2006.

[192] V. Dormoy *et al.*, "The sonic hedgehog signaling pathway is reactivated in human renal cell carcinoma and plays orchestral role in tumor growth," *Mol. Cancer*, vol. 8, p. 123, Dec. 2009.

[193] A. Hanna and L. A. Shevde, "Hedgehog signaling: modulation of cancer properies and tumor mircroenvironment," *Mol. Cancer*, vol. 15, Mar. 2016.

[194] R. W. Tilghman *et al.*, "Matrix Rigidity Regulates Cancer Cell Growth and Cellular Phenotype," *PLoS ONE*, vol. 5, no. 9, Sep. 2010.

[195] S. A. Guelcher and J. A. Sterling, "Contribution of Bone Tissue Modulus to Breast Cancer Metastasis to Bone," *Cancer Microenviron.*, vol. 4, no. 3, pp. 247–259, Jul. 2011.

[196] C. Caulin, C. F. Ware, T. M. Magin, and R. G. Oshima, "Keratin-Dependent, Epithelial Resistance to Tumor Necrosis Factor-Induced Apoptosis," *J. Cell Biol.*, vol. 149, no. 1, pp. 17–22, Apr. 2000.

[197] N.-O. Ku, P. Strnad, H. Bantel, and M. B. Omary, "Keratins: Biomarkers and modulators of apoptotic and necrotic cell death in the liver," *Hepatol. Baltim. Md*, vol. 64, no. 3, pp. 966–976, 2016.

[198] E. Perlson *et al.*, "Vimentin binding to phosphorylated Erk sterically hinders enzymatic dephosphorylation of the kinase," *J. Mol. Biol.*, vol. 364, no. 5, pp. 938–944, Dec. 2006.

[199] P. Köpf-Maier and S. K. Mühlhausen, "Changes in the cytoskeleton pattern of tumor cells by cisplatin in vitro," *Chem. Biol. Interact.*, vol. 82, no. 3, pp. 295–316, May 1992.

[200] A. Latifi *et al.*, "Cisplatin treatment of primary and metastatic epithelial ovarian carcinomas generates residual cells with mesenchymal stem cell-like profile," *J. Cell. Biochem.*, vol. 112, no. 10, pp. 2850–2864, Oct. 2011.

[201] J. Schrader *et al.*, "Matrix stiffness modulates proliferation, chemotherapeutic response, and dormancy in hepatocellular carcinoma cells," *Hepatol. Baltim. Md*, vol. 53, no. 4, pp. 1192–1205, Apr. 2011.

[202] J. Feng, Y. Tang, Y. Xu, Q. Sun, F. Liao, and D. Han, "Substrate stiffness influences the outcome of antitumor drug screening in vitro," *Clin. Hemorheol. Microcirc.*, vol. 55, no. 1, pp. 121–131, 2013.

[203] M. A. Adams, D. S. McNally, and P. Dolan, "'Stress' distributions inside intervertebral discs. The effects of age and degeneration," *J. Bone Joint Surg. Br.*, vol. 78, no. 6, pp. 965–972, Nov. 1996.

[204] D. P. McDaniel *et al.*, "The Stiffness of Collagen Fibrils Influences Vascular Smooth Muscle Cell Phenotype," *Biophys. J.*, vol. 92, no. 5, pp. 1759–1769, Mar. 2007.

[205] W. M. Erwin, K. Ashman, P. O'Donnel, and R. D. Inman, "Nucleus pulposus notochord cells secrete connective tissue growth factor and up-regulate proteoglycan expression by intervertebral disc chondrocytes," *Arthritis Rheum.*, vol. 54, no. 12, pp. 3859–3867, Dec. 2006.

[206] D. Purmessur, R. M. Schek, R. D. Abbott, B. A. Ballif, K. E. Godburn, and J. C. Iatridis, "Notochordal conditioned media from tissue increases proteoglycan accumulation and promotes a healthy nucleus pulposus phenotype in human mesenchymal stem cells," *Arthritis Res. Ther.*, vol. 13, no. 3, p. R81, 2011.

[207] B. Gantenbein, E. Calandriello, K. Wuertz-Kozak, L. M. Benneker, M. J. Keel, and S. C. Chan, "Activation of intervertebral disc cells by co-culture with notochordal cells, conditioned medium and hypoxia," *BMC Musculoskelet. Disord.*, vol. 15, p. 422, 2014.

[208] C. L. Korecki, J. M. Taboas, R. S. Tuan, and J. C. Iatridis, "Notochordal cell conditioned medium stimulates mesenchymal stem cell differentiation toward a young nucleus pulposus phenotype," *Stem Cell Res. Ther.*, vol. 1, no. 2, p. 18, 2010.